


Spring 4-15-2017

# Cancer modeling: from optimal cell renewal to immunotherapy

CESAR L. ALVARADO

*University of New Mexico*

Follow this and additional works at: [https://digitalrepository.unm.edu/math\\_etds](https://digitalrepository.unm.edu/math_etds)

 Part of the [Applied Mathematics Commons](#), [Mathematics Commons](#), and the [Statistics and Probability Commons](#)

---

## Recommended Citation

ALVARADO, CESAR L.. "Cancer modeling: from optimal cell renewal to immunotherapy." (2017).  
[https://digitalrepository.unm.edu/math\\_etds/110](https://digitalrepository.unm.edu/math_etds/110)

This Dissertation is brought to you for free and open access by the Electronic Theses and Dissertations at UNM Digital Repository. It has been accepted for inclusion in Mathematics & Statistics ETDs by an authorized administrator of UNM Digital Repository. For more information, please contact [disc@unm.edu](mailto:disc@unm.edu).

Cesar Leonardo Alvarado Alvarado

---

*Candidate*

Mathematics and Statistics

---

*Department*

This dissertation is approved, and it is acceptable in quality and form for publication:

*Approved by the Dissertation Committee:*

Helen J. Wearing

---

Prof. Helen J. Wearing, Chair

Natalia Komarova

---

Prof. Natalia Komarova, Member

Jenz Lorenz

---

Prof. Jens Lorenz, Member

Gabriel Huerta

---

Prof. Gabriel Huerta, Member

# Cancer modeling: from optimal cell renewal to immunotherapy

by

**Cesar Leonardo Alvarado Alvarado**

B.Sc., Mathematics, National Pedagogical University Francisco  
Morazan, 2008

M.Sc., Mathematics, University of New Mexico, 2013

THESIS

Submitted in Partial Fulfillment of the  
Requirements for the Degree of

Doctor of Philosophy  
Mathematics

The University of New Mexico

Albuquerque, New Mexico

May, 2017

# Dedication

*To my wife Maryory, the joy of my heart, my late mother Adany, my dad Cesar, my auntie Magdalena, my siblings, Flor, Amanda, Rina, Geli, Jose, and Renan, and my nieces, Isa, Sofia, Zoe and Mia, for all their love and support, and for always believing in me.*

*“Mathematics is the most beautiful and most powerful creation of the human spirit”  
– Stefan Banach*

# Acknowledgments

I would like to thank my advisor, Professor Helen J. Wearing, for her support, patience, and valuable ideas that made this thesis possible. Thanks for being the best advisor and a fantastic human being.

I would also like to thank Professor Natalia Komarova, for allowing me to work on her project, and for her ideas and patience. This work would not have been possible without her contribution.

I am also grateful to the Wearing Lab: Michael, Larissa, Julie, Noah, Rosie, Will, and Pepper, for their feedback that made this thesis better.

I also want to thank Professor Gabriel Huerta and Professor Jens Lorenz for being part of my committee.

I am specially grateful to Dr. Adalid Gutierrez, thanks for always believing in me and for encouraging me to keep studying Mathematics.

I am also grateful to the National Pedagogical University Francisco Morazan, for their institutional support to get the Fulbright scholarship that allowed me to continue my graduate studies in the United States.

# **Cancer modeling: from optimal cell renewal to immunotherapy**

by

**Cesar Leonardo Alvarado Alvarado**

B.Sc., Mathematics, National Pedagogical University Francisco Morazan, 2008

M.Sc., Mathematics, University of New Mexico, 2013

Ph.D., Mathematics, University of New Mexico, 2017

## **Abstract**

Cancer is a disease caused by mutations in normal cells. According to the National Cancer Institute, in 2016, an estimated 1.6 million people were diagnosed and approximately 0.5 million people died from the disease in the United States. There are many factors that shape cancer at the cellular and organismal level, including genetic, immunological, and environmental components. In this thesis, we show how mathematical modeling can be used to provide insight into some of the key mechanisms underlying cancer dynamics. First, we use mathematical modeling to investigate optimal homeostatic cell renewal in tissues such as the small intestine with an emphasis on division patterns and tissue architecture. We find that the division patterns that delay the accumulation of mutations are strictly associated with the population sizes of the tissue. In particular, patterns with long chains of differentiation delay the time to observe a second-hit mutant, which is important given that for many cancers two mutations are enough to initiate a tumor. We also investigated homeostatic cell renewal under a selective pressure and find that hierarchically organized tissues act as suppressors of selection; we find that an architecture with a small number of stem cells and larger pools of transit amplifying cells and mature differentiated

cells, together with long chains of differentiation, form a robust evolutionary strategy to delay the time to observe a second-hit mutant when mutations acquire a fitness advantage or disadvantage. We also formulate a model of the immune response to cancer in the presence of costimulatory and inhibitory signals. We demonstrate that the coordination of such signals is crucial to initiate an effective immune response, and while immunotherapy has become a promising cancer treatment over the past decade, these results offer some explanations for why it can fail.

# Contents

<b>List of Figures</b>	<b>x</b>
<b>List of Tables</b>	<b>xiv</b>
<b>1 Introduction</b>	<b>1</b>
<b>2 Optimal homeostatic cell renewal</b>	<b>4</b>
2.1 Introduction . . . . .	4
2.2 Methods: ordinary differential equations and stochastic simulations . . . . .	9
2.2.1 Trees and their probabilities . . . . .	9
2.2.2 Chains of differentiation . . . . .	10
2.2.3 The expected number of mutants . . . . .	11
2.2.4 Stochastic simulations . . . . .	16
2.3 The role of proliferation rates and compartment sizes in mutant generation . . . . .	18
2.3.1 De-novo mutant generation . . . . .	19
2.3.2 Clonal dynamics of mutants . . . . .	20



*Contents*

2.3.3	The role of proliferation in mutant generation and dynamics . . . . .	23
2.3.4	The role of compartment sizes . . . . .	24
2.3.5	Stochastic simulations and a summary of trends . . . . .	25
2.3.6	Generation of two-hit mutants . . . . .	28
2.4	Discussion . . . . .	32
<b>3</b>	<b>Optimal homeostatic cell renewal under a selective pressure</b>	<b>37</b>
3.1	Introduction . . . . .	37
3.2	Methods . . . . .	40
3.3	Results . . . . .	41
3.3.1	The ODE approximation . . . . .	41
3.3.2	Fitness in a stochastic regime . . . . .	43
3.3.3	Fitness and second-hit mutants . . . . .	46
3.4	Discussion . . . . .	50
<b>4</b>	<b>A theoretical model of immune checkpoints</b>	<b>54</b>
4.1	Introduction . . . . .	54
4.2	Methods . . . . .	58
4.2.1	The Model . . . . .	58
4.2.2	Equilibria . . . . .	60
4.2.3	Initial conditions . . . . .	61
4.2.4	Sensitivity analysis . . . . .	61
4.3	Results . . . . .	63

*Contents*

4.3.1	Immune response dynamics at equilibrium . . . . .	63
4.3.2	Dynamics of immune responses as a function of negative and positive signals . . . . .	66
4.3.3	The role of initial conditions . . . . .	69
4.4	Assessing parameter uncertainty . . . . .	74
4.5	Discussion . . . . .	75
<b>5</b>	<b>Conclusions</b>	<b>79</b>
	<b>Appendices</b>	<b>81</b>
<b>A</b>	<b>Further analysis of the deterministic mutant dynamics</b>	<b>82</b>
<b>B</b>	<b>Comparison of the ODEs and stochastic simulations for large sys- tems</b>	<b>86</b>
<b>C</b>	<b>Further notes on the role of the compartment size</b>	<b>88</b>
<b>D</b>	<b>Further notes on tissue architecture, division patterns and fitness</b>	<b>93</b>
<b>E</b>	<b>Equilibria and stability for the immune response model</b>	<b>97</b>

# List of Figures

2.1	Symmetric divisions and division trees . . . . .	5
2.2	Chains of differentiations to replace $2^3$ cells . . . . .	11
2.3	Mean tree length and the mean number of compartments involved in the division trees . . . . .	12
2.4	The expected number of mutants from the ODE approximation for low and high proliferation probabilities . . . . .	17
2.5	The role of the proliferation rate on mutant generation and mutant dynamics . . . . .	20
2.6	Comparison of the mutant dynamics for different compartment size arrangements . . . . .	23
2.7	Mean number of mutants from 1000 stochastic simulations for increasing and constant architectures . . . . .	26
2.8	Distribution of the generation times to second mutation, obtained from 5000 stochastic simulations comparing increasing and constant architectures . . . . .	30
2.9	Distribution of the generation times to second mutation, obtained from stochastic simulations, in the case where $v$ depends on the compartment sizes . . . . .	31

*List of Figures*

3.1	The total number of mutants as a function of the fitness parameter $r$ , obtained from the ODE approximation for different values of the proliferation probability $v$ and two architectures . . . . .	44
3.2	The total number of mutants as a function of the proliferation probability $v$ , obtained from the ODE approximation for different values of the fitness parameter $r$ and two architectures . . . . .	45
3.3	Comparing small and high values of $v$ for increasing and constant architectures, and advantageous and disadvantageous mutants from 1000 stochastic simulations . . . . .	46
3.4	Comparing increasing and constant architectures for advantageous and disadvantageous one-hit mutants from 1000 stochastic simulations	47
3.5	Distribution of the time to observe a second mutation, obtained from 5000 stochastic simulations for advantageous and disadvantageous mutants . . . . .	48
3.6	Comparing the time to observe a second mutation for advantageous and disadvantageous mutants and decreasing architecture . . . . .	49
3.7	Comparing the time for a second mutation for small and high values of $v$ , for increasing and constant architectures when mutants are advantageous or disadvantageous . . . . .	50
4.1	A diagram showing the process of T cell activation and downregulation	57
4.2	Bifurcation diagrams illustrating the number of tumor cells at equilibrium as a function of negative and positive signals . . . . .	64
4.3	Bifurcation diagram of the number of tumor cells at equilibrium, as a function of the rate of antigen reception $s$ and the inhibitory signal $b_2$	65

*List of Figures*

4.4	The effect of increasing negative signals on the temporal dynamics of tumor and immune cells . . . . .	67
4.5	The first peak of tumor cells, the time to reach the first peak and the maximum peak of tumor cells as a function of the negative signals $b_1$ and $b_2$ . . . . .	68
4.6	Varying the initial tumor size . . . . .	70
4.7	Varying the initial number of loaded dendritic cells . . . . .	71
4.8	Varying the initial number of T cells . . . . .	73
4.9	Sensitivity analysis . . . . .	75
A.1	The total number of mutants as a function of the proliferation probability $v$ from the ODE approximation for 3 architectures . . . . .	83
A.2	The ODE mutant dynamics for 4 compartments, under two architectures	84
B.1	Comparison between the average number of mutants from 1000 stochastic simulations without replacement and the expected number of mutants predicted by the ODE approximation . . . . .	87
C.1	Comparison of mutant dynamics for two different compartment size arrangements when $v$ is a function of the compartment sizes . . . . .	89
C.2	Mean number of mutants from 1000 stochastic simulations comparing increasing and decreasing architectures . . . . .	91
C.3	Distribution of the time to observe a second mutation from 5000 stochastic simulations, comparing increasing and decreasing architectures . . . . .	92

*List of Figures*

D.1	The mean of the total number of mutants that occur in increasing versus decreasing architectures for different fitness values, based on 1000 stochastic simulations . . . . .	94
D.2	Distribution of the time to observe a second mutation, obtained from 5000 stochastic simulations comparing increasing and constant architectures, for advantageous and disadvantageous mutants . . . . .	95
D.3	Distribution of the time to observe a second mutation, obtained from 5000 stochastic simulations comparing increasing and decreasing architectures, for advantageous and disadvantageous mutants . . . . .	96

# List of Tables

4.1	Model parameters . . . . .	62
-----	----------------------------	----

# Chapter 1

## Introduction

Cancer is a major public health burden. According to the National Cancer Institute (NCI), in 2016, an estimated 1.6 million people were diagnosed and approximately 0.5 million people died from the disease in the United States. Cancer is produced by mutations in healthy cells. Normally, when cells become old or damaged, they die and are replaced by new cells, so that the tissue maintains its functionality. When cancer arises, cells proliferate uncontrolled, and eventually form tumors. Several factors at the organismal and cellular level can influence the development of cancer. Genetic, immunological and environmental components can all greatly influence cancer dynamics. In this thesis, we use mathematical modeling to gain insight into some of the mechanisms that play a crucial role in cancer dynamics.

This thesis consists of 5 chapters. In Chapters 2, 3, and 4, we develop the topics that form individual manuscripts, and in chapter 5, we present some general conclusions. In chapter 2 we study homeostatic cell renewal in hierarchically organized tissues such as the colon, the skin and the haematopoietic system, among others. In the bottom of the hierarchy, there are a small number of stem cells (SCs), which have almost an infinite replicative capacity. In intermediate positions of the hierarchy are transit amplifying cells (TACs), which have a limited replicative capacity, and in the



## *Chapter 1. Introduction*

top of the hierarchy are mature differentiated cells, which are constantly discarded and replaced to keep the tissue at constant numbers. This process of cell renewal triggers cascades or chains of differentiations that can greatly influence cancer dynamics. We propose a compartmental model of homeostatic cell renewal through a system of differential equations that predicts the expected number of mutants in each compartment of the hierarchy. We use the accumulation of one-hit mutants and the time to observe a second-hit mutant as measures for cancer risk. We focus on two key variables: the proliferation patterns and tissue architecture. Overall, we find that if the optimization task is to reduce the accumulation of one-hit mutants, in the long run, short chains of differentiation are better; on the other hand, if the optimization task is to delay the time to observe a second-hit, long chains of differentiation are preferred. A non-intuitive finding is that an architecture with larger populations in more primitive compartments delays the accumulation of mutations. The derivation of the ODEs was carried out by Dr. Natalia Komarova, while I performed most of the numerical experiments in this chapter under the guidance of Dr. Komarova and Dr. Helen Wearing.

In chapter 3, we extend the model proposed in chapter 2 by assigning a fitness advantage/disadvantage to mutants. In chapter 2 we assume that mutations are neutral, even though when cells divide it is very likely that they acquire a fitness advantage or disadvantage. It is widely accepted that tissues evolve to minimize cancer risk. The hierarchical organization of most tissues, the proliferation patterns for self-renewal, slow division rates, and the type of cell division are examples of how tissues attempt to minimize cancer risk [1–8]. In this context, the question is whether the tissues act as suppressors or amplifiers of selection, and under what conditions proliferation patterns and tissue architecture act as optimal evolutionary strategies to delay the accumulation of advantageous and disadvantageous mutants. We find that hierarchically organized tissues are suppressors of selection; in addition, we find that an increasing architecture (which has a small number of stem cells and larger

## *Chapter 1. Introduction*

number of mature cells) and long chains of differentiation, are a robust strategy to delay the time to observe a second-hit mutant, which can be translated into a lower risk of cancer.

In chapter 4, we model an immune response to cancer. In the last decade, immunotherapy, a treatment that uses the body's own immune system to attack cancer cells, has become a promising treatment to fight cancer. Despite its relative success, there are many factors that can lead to failure. In order to initiate an immune response, T cells need to receive antigen which is carried out by Antigen Presenting Cells (APCs), typically dendritic cells, and later, a costimulatory signal is activated so that T cells are ready to kill cancer cells. After activation of T cells, immune checkpoints (inhibitory signals) are activated which downregulate T cells. We propose a model described by a set of nonlinear differential equations that allows us to explore different types of immunotherapy treatments, and most importantly, we investigate scenarios under which immunotherapy can fail or succeed. Overall, if the inhibitory pathways are not successfully blocked, an immune response might not be sustained despite high rates of antigen presentation. In particular, if the immune checkpoints that activate after antigen presentation/reception are not blocked, stimulation of antigen presentation is no longer effective, indicating why treatments that stimulate antigen reception signaling could fail.

In conclusion, we use mathematical modeling to study homeostatic cell renewal that gives us a broader understanding of the role of tissue architecture, division patterns and selection, which are key factors that shape cancer dynamics in hierarchically organized tissues. We also propose a model of an immune response to cancer, which offers explanations of why some immunotherapy treatments can fail when the immune checkpoints are activated, despite large rates of antigen presentation.

# Chapter 2

## Optimal homeostatic cell renewal

### 2.1 Introduction

Many tissues in complex organisms are hierarchically organized, such as the human colon, the small intestine, the skin, and the haematopoietic system. Hierarchically organized tissues are renewed constantly by means of a balance of cell deaths and cell divisions. Understanding the mechanisms that regulate cell proliferation and differentiation patterns is key to explaining the robust nature of homeostasis [4]. Because of the imminent risk of mutation acquisition, tissue organization also plays an important role in preventing cancer [5–7, 9–13].

At the root of hierarchically organized tissues are a small number of stem cells (SCs), capable of both self renewal and differentiation into more specialized cells [14]. Downstream from SCs there are intermediate cells of increasing degrees of maturity, which can undergo a certain number of divisions. Finally, there are fully mature differentiated cells, which perform their function and are discarded and replenished through divisions of less differentiated cells. For instance, evidence suggests that on or near the bottom of the colon crypts and the small intestine crypts, there are

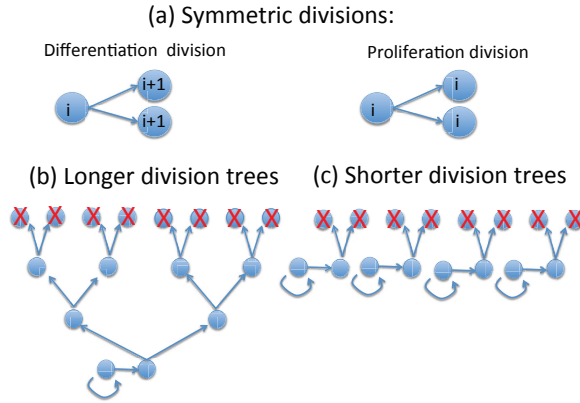


Figure 2.1: Schematics showing key concepts of the paper. (a) Two types of symmetric divisions: proliferations and differentiations. Each circle represents a cell, and  $i$  denotes the  $i$ th compartment, while  $i+1$  denotes the  $(i+1)$ th compartment. Panels (b) and (c) demonstrate the division chains that replenish 8 differentiated cells eliminated from the top compartment. Dead cells are denoted by X's and arrows show divisions. Cells are arranged in horizontal layers corresponding to compartments. Only the dividing cells are shown (for example, there may be more than 4 cells in the second to top compartment in panel (b)). In (b), the dead cells are replaced by a longer division tree, and in (c) by four shorter division trees.

between 4 – 6 SCs [15–17], and the remaining compartments are composed of transit amplifying cells (TACs) and finally mature differentiated cells that are discarded, so that the entire crypt is renewed every 2 – 7 days [18]. A similar situation occurs in the haematopoietic system, where a stem cell pool of about 400 cells is required to replenish a daily bone marrow output of about  $3.5 \times 10^{11}$  cells [19].

Stem cells are thought to be capable of symmetric or asymmetric divisions. Asymmetric divisions of a stem cell result in one daughter cell that is a stem cell and the other daughter cell that is a more differentiated cell. Symmetric divisions result in two identical daughter cells. The two types of symmetric divisions are illustrated in figure 2.1(a) in a more general context: differentiation divisions result in two offspring that are both more differentiated than the dividing cell, and proliferation divisions result in two offspring whose differentiation status is identical to that of the parent.

## *Chapter 2. Optimal homeostatic cell renewal*

Because experiments to track cell divisions and mutations are in general difficult, or not feasible in some hierarchically organized tissues, mathematical models have been used to understand cellular dynamics or homeostasis and mutations. In particular, the origin and development of colorectal cancer have been extensively studied. It has been demonstrated theoretically that mutations leading to colorectal cancer can originate in either the stem cell compartment or TACs [5, 9, 11, 20]. Computational models, such as virtual crypts, have helped to understand the process of self renewal in hierarchically organized tissues, for instance the organization of the colon [21–24]. Several studies have investigated tissue architecture with the goal of understanding its utility in protection against mutation accumulation. Traulsen, Werner and colleagues used mathematical models to study mutations in the haematopoietic system, and found theoretical evidence that tissue architecture and the process of self renewal were a protection mechanism against cancer [12, 13, 19, 25]. Rodriguez-Brenes et al. [6] proposed that an optimal tissue architecture that minimized the replication capacity of cells was one where the less differentiated cells had a larger rate of self-renewal. Shahriyari and Komarova [7] showed that having symmetric stem cell divisions (proliferations and differentiations) rather than asymmetric stem cell divisions minimized the risk of two-hit mutant generation. Dingli et al. [3] considered the question of mutation generation by stem cells and found that mutations that increased the probability of asymmetric replication could lead to rapid expansion of mutant stem cells in the absence of a selective fitness advantage. Pepper et al. [26] examined a tissue undergoing serial differentiation patterns originating with self-renewing somatic stem cells, continuing with several TACs differentiations, and showed that such patterns lowered the rate of somatic evolution. Paper [27] emphasizes the importance of spatial considerations in the modeling of stem cell hierarchies and division patterns.

Despite significant progress reported in the literature, there are still plenty of unanswered questions regarding tissue renewal and cancer development in hierarchically organized tissues. Particularly, the optimal mechanisms of self renewal and prolifera-

tion to maintain homeostasis is a crucial process which is far from being understood. To illustrate some of the questions we are interested in solving, consider a hierarchical tissue (such as the colon) where symmetric divisions are prevalent [28–31]. When mature differentiated cells are discarded, cells from the upstream compartment divide to replace the eliminated cells. This gives rise to a chain of differentiations, because the cells that differentiated and migrated from the upstream compartment also need to be replaced, in order to keep the tissue at homeostasis. Figure 2.1(b,c) schematically illustrates two opposite trends. Both panels depict 8 mature cells that are eliminated. These cells are replenished by 4 differentiation events, whereby cells from the neighboring compartment differentiate and migrate downstream to replace the dead cells. In figure 2.1(b), the 4 cells are, in turn, replenished by two differentiation events from the previous layer (representing a compartment in the hierarchy), leaving two cells to be replaced. This is done by a single differentiation event from the last layer, and the remaining cell is then replaced by a proliferation event from the same layer. These processes comprise a differentiation cascade, or a *differentiation chain*, which in this case included differentiation events in 3 consecutive compartments. A different scenario is shown in figure 2.1(c) where the 4 cells that differentiated and migrated from the second to top layer are all replaced by proliferation divisions of cells in the same layer. In this case we have 4 shorter differentiation chains which only include differentiation events in one compartment. As will be shown, a range of intermediate scenarios is possible.

Biologically, differentiation chains are shaped by a system of feedback loops determined by signals altering proliferation, differentiation, apoptosis, migration, and adhesion in both the stem cell compartment and the transit amplifying cells [4, 6, 32]. The proliferation and differentiation activity is a well controlled system to guarantee tissue homeostasis in hierarchically organized tissues, thus, changes in proliferation and differentiation patterns might be associated with an increased risk of cancer development, as found, for example, by Merrit et al. [33] in the context of colorectal cancer.

## *Chapter 2. Optimal homeostatic cell renewal*

Figure 2.1(b,c) suggests that in terms of tissue architecture, and in the presence of hierarchical lineages, there are multiple arrangements that are all, in principle, capable of maintaining balanced tissue turnover. Each arrangement preserves the number of cells in each compartment in the face of divisions triggered by cell deaths in the top compartment. Because each cell division is associated with a probability of harmful mutations, the question then becomes if there is a preferred strategy for a tissue to arrange its turnover and/or compartment sizes in order to minimize the number of mutants generated.

The goal of this work is to describe different differentiation/proliferation patterns and their effect on cancer generation in a hierarchically organized tissue. First, we derive analytical expressions for the expected number of mutants in each compartment, as a result of these chains of differentiation. This informs a deterministic approximation resulting in a set of differential equations describing mutant dynamics in different compartments. It turns out that this methodology can be further adapted to describe not only the approximately deterministic regime of large populations and large mutation rates, but a more relevant regime of small populations and small mutation rates. We investigate the dynamics of our model in different scenarios, focusing on different proliferation/differentiation probabilities and different compartment size arrangements. In addition, we perform stochastic simulations to study the accumulation of mutations in a stochastic regime. We describe both one-hit and two-hit mutant generation, and find the parameters that can be tuned to delay cancer initiation in hierarchically organized tissues.

## 2.2 Methods: ordinary differential equations and stochastic simulations

### 2.2.1 Trees and their probabilities

We start by formulating a metapopulation style model of stem cell lineages. Assume that there are  $n + 1$  compartments,  $C_0, \dots, C_n$ , with total constant cell numbers  $N_0, \dots, N_n$ . Inside individual compartments, we assume complete mixing, and the compartments are arranged linearly from the least mature,  $C_0$ , to the most mature,  $C_n$ . At each time step, we remove  $a_n = 2^n$  cells from compartment  $C_n$ . These cells must be replaced by  $2^n$  divisions in different compartments. Because cells in compartment  $C_n$  do not proliferate, there will be  $a_{n-1} = 2^{n-1}$  differentiation divisions in compartment  $C_{n-1}$ . Now,  $a_{n-1}$  cells in this compartment must be replaced, either by differentiation divisions from compartment  $C_{n-2}$  or by proliferation divisions from compartment  $C_{n-1}$ . Suppose there are  $a_{n-2}$  differentiations and  $a_{n-1} - 2a_{n-2}$  proliferations. Next,  $a_{n-2}$  cells from compartment  $C_{n-2}$  must be replaced. This process gives rise to a division tree, which is uniquely characterized by the numbers of differentiation divisions in each compartment:

$$\{a_{n-1}, \dots, a_0\}, \tag{2.1}$$

where  $a_{n-1} = 2^{n-1}$  and

$$0 \leq a_i \leq 2^i, i = 0, \dots, n - 1.$$

The number of proliferations in compartment  $C_i$  is given by  $a_i - 2a_{i-1}$ . The length of the tree is the number of compartments that have nonzero numbers of differentiation events, and it varies from 1 to  $n$ . Proliferation and differentiation events are assigned probabilistically, by means of the following process. Suppose  $a_i$  cells must be replaced in compartment  $C_i$ , that is, there are  $i$  openings to fill. Each cell is replaced by a proliferation division in this compartment with probability  $v_i$ . If the



number of remaining openings is odd, then an additional proliferation division happens, such that the number of remaining openings is even, and they are then filled by differentiation divisions from compartment  $C_{i-1}$ . This allows us to calculate the probability of a given tree defined by string (2.1). First we calculate the probability of having  $a_i$  differentiations in compartment  $C_i$  given that there are  $a_{i+1}$  differentiations in compartment  $C_{i+1}$ :

$$p(a_i) = \mathcal{C}_{a_{i+1}}^{2a_i} (1 - v_{i+1})^{2a_i} v_{i+1}^{a_{i+1} - 2a_i} + \mathcal{C}_{a_{i+1}}^{2a_i+1} (1 - v_{i+1})^{2a_i+1} v_{i+1}^{a_{i+1} - 2a_i - 1}, \quad 0 \leq i \leq n - 1,$$

where formally  $a_n = 2^n$  and we use the following notation for the binomial coefficients:

$$\mathcal{C}_n^k = \frac{n!}{k!(n-k)!}.$$

We then have the probability of string (2.1):

$$P(a_{n-1}, \dots, a_0) = \prod_{i=0}^{n-1} p(a_i).$$

In particular, since  $v_n = 0$ , we obtain that  $a_{n-1} = 2^{n-1}$  with certainty.

### 2.2.2 Chains of differentiation

The process previously described can be analyzed through division patterns or chains of differentiation of a given length. What are the possible patterns of replacement of  $2^n$  cells? For example, if  $n = 3$ , we have 5 possibilities to replace  $2^3$  cells as illustrated in figure 2.2. Figure 2.2(a) corresponds to 4 proliferation events in compartment  $C_2$  (4 differentiation chains of length one). Figures 2.2(b,c) represent one differentiation chain of length 2 and two differentiation chains of length 1. Figure 2.2(d) corresponds to 2 differentiation chains of length 2. In the last pattern, figure 2.2(e), we have one differentiation chain of length 3.

Decreasing the probability of proliferation,  $v$ , increases the mean length of proliferation trees, and shifts the divisions toward the stem cell compartment, see figure 2.3.

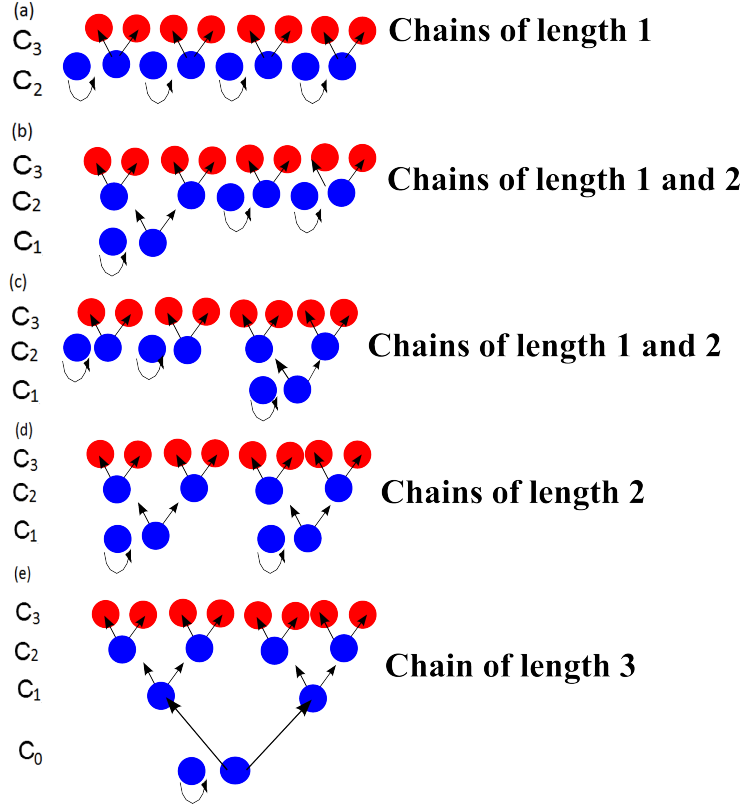


Figure 2.2: Possible patterns to replace  $2^3 = 8$  cells removed from compartment  $C_3$ . The cells in red correspond to 8 cells discarded in  $C_3$  and the blue cells are dividing cells (again, only dividing cells are shown, and the actual compartments contain more cells). (a) All 4 cells that differentiated out to replace 8 cells in  $C_3$  are replaced by 4 proliferation events in  $C_2$ . This pattern occurs with probability  $v^4$ . (b) and (c): 2 out of 4 cells that differentiated out from  $C_2$  are replaced by one differentiation event from  $C_1$  (followed by a proliferation in  $C_1$ ) and two cells in  $C_2$  are replaced by 2 proliferation events in  $C_2$ . The probability of each of these patterns is  $v^2(1 - v)^2$ . (d) The 4 cells that differentiated out from  $C_2$  are replaced by 2 differentiations  $C_1$ , followed by 2 proliferation events in  $C_2$ . The probability of this pattern is  $(1 - v)^4 v^2$ . (e) Similar to (d), except that the 2 cells in  $C_1$  are replaced by a differentiation from  $C_0$  followed by a proliferation event. This pattern occurs with probability  $(1 - v)^6$ .

### 2.2.3 The expected number of mutants

Let us suppose that in each compartment, the number of mutants is given by  $m_i$ ,  $0 \leq i \leq n$ . We would like to calculate the expected change in the number of mu-

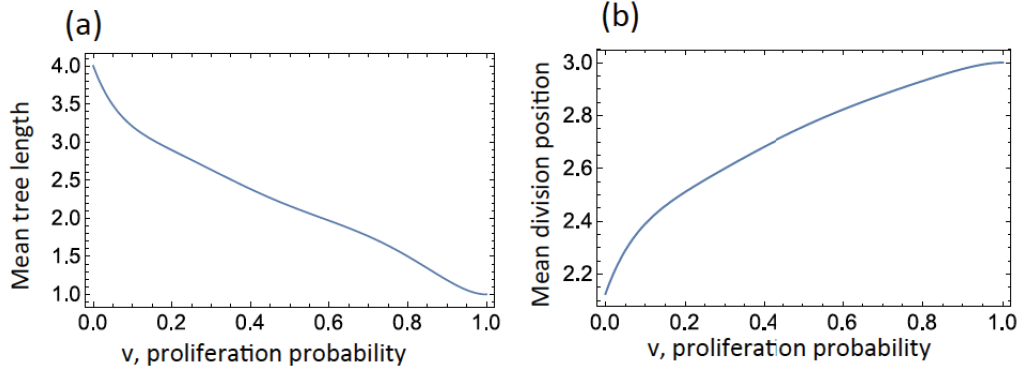


Figure 2.3: Properties of division trees as a function of  $v$ , the probability of proliferation in compartments  $1, \dots, n-1$ . (a) Mean tree length, defined as the mean number of compartments involved in the division trees. (b) Mean division position. For an individual tree, sequence (2.1), this is defined as  $2^{-n} \sum_{i=0}^n 2i(a_i - a_{i-1})$ ; plotted is the expectation of this quantity across all the trees. In this example,  $n = 4$ .

tants after  $2^n$  cells are removed in compartment  $C_n$ . To do this, let us determine the expected change in the number of mutants associated with a particular tree, string (2.1). This can be done by considering the change resulting from  $a_k$  differentiations from compartment  $C_k$  to compartment  $C_{k+1}$  and  $a_{k+1} - 2a_k$  proliferations in compartment  $C_{k+1}$ . These events will affect the numbers of mutants in compartments  $C_k$  and  $C_{k+1}$ .<sup>1</sup>

- (a) When  $a_k$  cells differentiate out of compartment  $C_k$ ,  $0 \leq k \leq n-1$ , with probability

$$P_i^{\text{diff}} = C_{a_k}^i \mu_k^i (1 - \mu_k)^{a_k - i},$$

$i$  of them may be mutants, where

$$\mu_k = \frac{m_k}{N_k},$$

<sup>1</sup>Note that in the equations in this section we used combinatorial expressions obtained from sampling with replacement. In the stochastic simulations below, sampling without replacement was used, but it was established that sampling with replacement led to similar results.

Chapter 2. Optimal homeostatic cell renewal

which is the probability to pick a mutant among  $N_k$  cells. In this case,  $i$  mutants are removed from compartment  $C_k$  and  $2i$  mutants are added to compartment  $C_{k+1}$ . Further, among the remaining  $a_k - i$  differentiations, there may be  $l$  mutations which will increase the number of mutants in compartment  $C_{k+1}$  by  $l$ . To calculate the corresponding probability, we note that  $a_k - i$  wild type cells differentiating in compartment  $C_k$  will produce  $2(a_k - i)$  offspring, each of which become mutants with probability  $u$ . Therefore,  $l$  mutants are generated with probability

$$P_{i,l}^{\text{diff}} = \mathcal{C}_{2(a_k-i)}^l u^l (1-u)^{2(a_k-i)-l}.$$

The total change in compartment  $C_{k+1}$  is then  $2i + l$ , the total change in compartment  $C_k$  is  $-i$ , and this happens with probability  $P_i^{\text{diff}} P_{i,l}^{\text{diff}}$ . These changes must be summed up for  $0 \leq i \leq a_k$  and  $0 \leq l \leq 2(a_k - i)$ .

- (b) When  $a_{k+1} - 2a_k$  cells proliferate in compartment  $C_{k+1}$ ,  $0 \leq k \leq n - 1$ , with probability

$$P_i^{\text{pro}} = \mathcal{C}_{a_{k+1}-2a_k}^i \mu_{k+1}^i (1 - \mu_{k+1})^{a_{k+1}-2a_k-i},$$

$i$  of them are mutants. This means that  $i$  new mutants are added to compartment  $C_{k+1}$ . The remaining  $a_{k+1} - 2a_k - i$  proliferating cells are wild type, and it is possible that  $l$  of the offspring are new mutants. This happens with probability

$$P_{i,l}^{\text{pro}} = \mathcal{C}_{2(a_{k+1}-2a_k-i)}^l u^l (1-u)^{2(a_{k+1}-2a_k-i)-l}.$$

The total change in compartment  $C_{k+1}$  is then given by  $i + l$  and happens with probability  $P_i^{\text{pro}} P_{i,l}^{\text{pro}}$ . Again, these changes must be summed up for  $0 \leq i \leq a_k$  and  $0 \leq l \leq 2(a_k - i)$ .

- (c) A special case is compartment  $C_0$ . Here,  $a_0$  cells will proliferate, and the number of mutants is calculated similar to (b).

Chapter 2. Optimal homeostatic cell renewal

- (d) Another special case is compartment  $C_n$ . Cells do not proliferate in this compartment, but  $2^n$  cells are removed, and we need to calculate the expected number of mutants removed, similar to  $P_i^{\text{diff}}$  in (a).

For each tree, the expected change in the number of mutants can be expressed as a vector whose components are obtained as the expected change in each compartment, as calculated in (a-d) above. These vectors must be added together, weighted with the probability of each tree. The resulting vector gives the time-derivatives of quantities  $m_0, \dots, m_n$ .

When  $a_k$  cells differentiate out of compartment  $C_k$ ,  $0 \leq a_k \leq n - 1$ , the expected gain of mutants in compartment  $C_{k+1}$  is given by

$$\alpha_{k+1}^{\text{diff}} = \sum_{i=0}^{a_k} \sum_{l=0}^{2(a_k-i)} (2i+l) P_i^{\text{diff}} P_{i,l}^{\text{diff}}.$$

When  $a_{k+1} - 2a_k$  cells proliferate in compartment  $C_{k+1}$ ,  $0 \leq k \leq n - 1$ , the expected gain of mutants in compartment  $C_{k+1}$  is

$$\alpha_{k+1}^{\text{pro}} = \sum_{i=0}^{a_k} \sum_{l=0}^{2(a_k-i)} (i+l) P_i^{\text{pro}} P_{i,l}^{\text{pro}}.$$

The compartment  $C_{k+1}$  loses mutants when  $a_{k+1}$  cells differentiate and migrate into compartment  $C_{k+2}$ , and the expected loss is

$$\beta_{k+1}^{\text{diff}} = \sum_{i=0}^{a_{k+1}} \sum_{l=0}^{2(a_{k+1}-i)} (2i+l) P_i^{\text{diff}} P_{i,l}^{\text{diff}}.$$

Thus the total change in the number of mutants in compartment  $C_{k+1}$  is

$$T_{k+1} = \alpha_{k+1}^{\text{diff}} + \alpha_{k+1}^{\text{pro}} - \beta_{k+1}^{\text{diff}}$$

The value  $T_{k+1}$  represents the expected number of mutants in compartment  $C_{k+1}$  produced by a single tree or chain of differentiation; because more than one tree could affect the expected number of mutants in each compartment, we need to sum

Chapter 2. Optimal homeostatic cell renewal

the contributions from all trees to compartment  $C_{k+1}$  weighted by their probability. This weighted sum defines the rate of change of the number of mutants in each compartment:

$$\dot{m}_k = \sum_{\text{All trees}} \text{Prob}^{\text{tree}} T_k^{\text{tree}}, \quad 0 \leq k \leq n. \quad (2.2)$$

For the simplest cases, we list the ODEs derived by computing the expected number of mutants produced by all possible chains of differentiation in each compartment. We will use the assumption that  $v_i = v$  for  $1 \leq i \leq n - 1$ , which has been assumed in other studies [5, 13, 19].

For the case  $n = 1$  we have

$$\begin{aligned} \dot{m}_1 &= u + \mu_0(1 - u) - \mu_1, \\ \dot{m}_0 &= 2u(1 - \mu_0). \end{aligned}$$

For  $n = 2$  we have

$$\begin{aligned} \dot{m}_2 &= 4(u + \mu_1(1 - u) - \mu_2), \\ \dot{m}_1 &= 2(1 - v)^2(u + \mu_0(1 - u) - \mu_1) + 4u(2 - v)v(1 - \mu_1), \\ \dot{m}_0 &= 2u(1 - v)^2(1 - \mu_0). \end{aligned}$$

For  $n = 3$  we have

$$\begin{aligned} \dot{m}_3 &= 8(u + \mu_2(1 - u) - \mu_3), \\ \dot{m}_2 &= 4[u(1 - \mu_1 + v(2 - 3v + 4v^2 - 2v^3))(1 + \mu_1 - 2\mu_2) \\ &\quad + (1 - v)^2(1 + 2v^2)(\mu_1 - \mu_2)], \\ \dot{m}_1 &= 2(1 - v)^6(u + \mu_0(1 - u) - \mu_1) + 4u(2 - v)(1 - v)^4v(1 - \mu_1) \\ &\quad + 4uv(2 - 3v + v^3)(1 - \mu_1), \\ \dot{m}_0 &= 2u(1 - v)^6(1 - \mu_0). \end{aligned} \quad (2.3)$$

$$(2.4)$$

## Chapter 2. Optimal homeostatic cell renewal

The  $n + 1$  linear ordinary differential equations derived here are applicable in the high mutation rate/large population limit ( $uN \gg 1$ ). The unique fixed point of the system, for all  $n$ , which is always stable, is

$$m_i = N_i, \quad 0 \leq i \leq n.$$

In figure 2.4, we show the number of mutants in each of 4 compartments (assuming  $n = 3$ ) as a function of time, obtained from numerical solution of equations (2.3-2.4). The number of mutants reaches saturation in each compartment; first in the top compartment ( $C_3$ ), followed by compartment  $C_2$  and so on, as clearly seen for  $v = 0.9$  (for  $v = 0.1$  the differences are more subtle and cannot be seen in the logarithmic scale of the figure). The dynamics for two different values of  $v$  are presented. The larger the value of  $v$ , the longer it takes for the lower compartments to reach their equilibrium values. This is because for large proliferation probabilities, long trees are unlikely and divisions rarely happen in the less differentiated compartments. Further details of the deterministic regime are presented in appendix A.

### 2.2.4 Stochastic simulations

The stochastic process is simulated by replacing cells as described in section 2.2.1. We track the numbers of mutants,  $m_i$ , in each of the compartments of constant sizes ( $N_i, i = 0, 1, \dots, n$ ). Let us denote by  $w_i = N_i - m_i$  the number of wild type cells in each compartment.

The initial number of mutants is zero, and the simulation proceeds as a sequence of discrete updates. Each update starts with  $2^n$  cells removed from compartment  $C_n$ . A mutant is discarded with probability  $\frac{m_n}{m_n + w_n}$ , otherwise, the cell discarded is a wild type cell. The next step is to replace the  $2^n$  cells removed in compartment  $C_n$ . Because cells in compartment  $C_n$  can not proliferate,  $2^{n-1}$  cells differentiate out from compartment  $C_{n-1}$ . In each division, a mutant is chosen with probability  $\frac{m_{n-1}}{m_{n-1} + w_{n-1}}$ ,

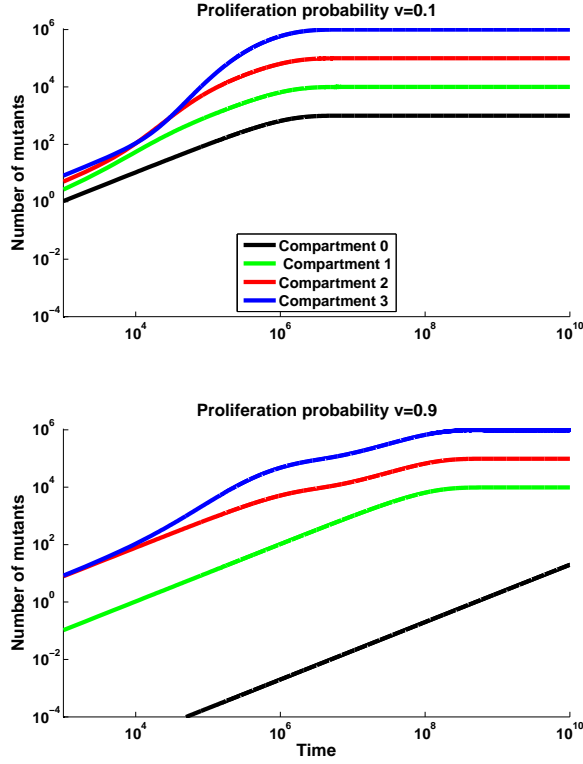


Figure 2.4: The dynamics of the expected number of mutants for a scenario of 4 compartments, comparing behavior for low and high proliferation probabilities. In the top graph,  $v = 0.1$ , and in the bottom graph,  $v = 0.9$ . In this figure we used  $n = 3$ ,  $u = 10^{-3}$ , and the compartment sizes are  $N_0 = 10^3$ ,  $N_1 = 10^4$ ,  $N_2 = 10^5$ ,  $N_3 = 10^6$ .

which increases the number of mutants in compartment  $C_n$  by two while the number of mutants decreases by one in compartment  $C_{n-1}$ . If a wild type cell is chosen for differentiation in compartment  $C_{n-1}$ , a de-novo mutant is produced with probability  $u$ , such that the number of mutants increases by one in  $C_n$ . The number of wild-type cells is decreased by one in  $C_{n-1}$ . There are altogether  $2^{n-1}$  differentiations from  $C_{n-1}$  performed in this way.

Then,  $2^{n-1}$  cells have to be replaced in compartment  $C_{n-1}$ . Each of these cells can be replaced by a proliferation event in  $C_{n-1}$  with probability  $v$ . Cells that are



not replaced by a proliferation event are replaced by a differentiation event from  $C_{n-2}$  with probability  $1 - v$ . If the number of cells to be replaced by differentiation events is odd, we add an extra proliferation event in compartment  $C_{n-1}$  so that the number of remaining openings is even. If the division event is a proliferation, a mutant is chosen with probability  $\frac{m_{n-1}}{m_{n-1} + w_{n-1}}$  which increases the mutant population in compartment  $C_{n-1}$  by one. If the proliferating cell is a wild type cell, it produces a de-novo mutant with probability  $u$  such that the number of mutants in compartment  $C_{n-1}$  increases by one. If the wild type cell did not mutate or a mutant was not chosen for reproduction, the number of wild type cells in compartment  $C_{n-1}$  increases by one. If the event is a differentiation from compartment  $C_{n-2}$ , mutants and wild type cells are updated in the same way as described above for differentiations from compartment  $C_{n-1}$ .

After this, there are a number of cells “missing” from compartment  $C_{n-2}$  that have to be replaced in a similar way. Every time a cell is chosen for division from compartment  $C_i$ , it is a mutant with probability

$$\frac{m_i}{m_i + w_i}. \tag{2.5}$$

The process of cell replacement proceeds until compartment  $C_0$  is reached. Cells “missing” from this compartment are replaced by proliferations in the same compartment with probability 1.

A comparison of the solutions of the ODEs and stochastic simulations is presented in appendix B.

## 2.3 The role of proliferation rates and compartment sizes in mutant generation

The central question we address is what values of the proliferation probability,  $v$ , produce fewer mutants; related to this, we investigate how the length of differen-

tiation chains affects the growth of cancer cells. If low values of  $v$  produce fewer mutants, this would imply that long chains of differentiation are favorable, as they are likely to decrease the number of cancer cells; on the other hand, if high values of  $v$  produce fewer mutants, short chains of differentiation would decrease the number of cancer cells. In addition, we investigate how tissue architecture combined with the proliferation probabilities affects mutant production.

### 2.3.1 De-novo mutant generation

In the ODE model derived here, mutations are generated constantly at a rate  $u$ . This is a correct assumption with high mutation rates and high population numbers. In smaller systems with low mutation rates, the processes of mutant (de novo) generation and their clonal spread can be treated as separate. Mutant generation becomes a rare event, and a single mutant that is generated gives rise to a clone that does not interfere with the creation of other mutant clones. This regime can also be studied with the help of the probabilities calculated above.

The removal of  $2^n$  mature cells from compartment  $C_n$  gives rise to a chain of  $2^n$  cell divisions that replenishes the lost cells. The probability of each such chain is calculated above. Further, every chain gives rise to an expected change in the mutant numbers in each of the compartments. This information can be used to study the de-novo generation of mutants and their subsequent clonal spread. To calculate the probability that a mutant will be generated in each of  $n + 1$  compartments, we evaluate the right hand side of system (2.2) with  $m_i = 0$  for all  $0 \leq i \leq n$  (that is, no prior mutations exist in the system). We obtain a vector proportional to the mutation rate  $u$ . Normalizing this vector to create a probability distribution, we obtain the probability to generate a mutant in each of the compartments. This vector only depends on the quantities  $(v_1, \dots, v_{n-1})$ , and not on the population sizes of individual compartments.

We can study the vector of probabilities of mutant generation by setting  $v_i = v$  for all  $1 \leq i \leq n - 1$  and examining the dependence on  $v$ . Smaller values of  $v$  give rise to longer trees, and consequently higher probabilities of generating mutants in the stem cell compartment. Larger values of  $v$  correspond to shorter trees, such that mutants are not generated in the stem cell compartment. These trends are illustrated in figure 2.5(a).

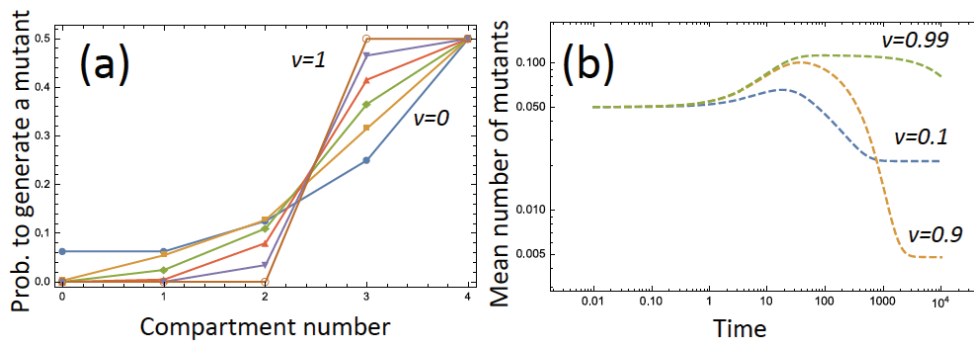


Figure 2.5: The role of the proliferation rate on mutant generation and mutant dynamics (the analytical approach). (a) The probability of generating a mutant in each of the compartments for 6 different values of  $v$ :  $v = 0, v = 0.2, \dots, v = 1.0$ . (b) The expected number of mutants produced from a single mutant cell in the absence of further de-novo mutations, plotted as a function of time for three different values of  $v$ . In this example,  $n = 4$ ,  $u = 10^{-4}$ , and the compartment sizes are, from  $C_0$  to  $C_n$ , 40, 80, 120, 160, 200.

### 2.3.2 Clonal dynamics of mutants

Once generated, a mutant undergoes clonal expansion and is also subject to being flushed out of the system (depending on its location). Let us consider the clonal propagation of mutants, in the absence of new mutations, which is achieved by setting  $u = 0$  in the main system of ODEs, equation (2.2). For simplicity, we first consider the extreme scenario where  $v_i = 0$ , that is, cells do not proliferate in any compartment

except for  $C_0$ , and all trees have length  $n$ . In this case we obtain the following system:

$$\dot{m}_0 = 0, \quad (2.6)$$

$$\dot{m}_1 = 2 \left( \frac{m_0}{N_0} - \frac{m_1}{N_1} \right), \quad (2.7)$$

$$\dot{m}_2 = 4 \left( \frac{m_1}{N_1} - \frac{m_2}{N_2} \right), \quad (2.8)$$

$$\dot{m}_3 = 8 \left( \frac{m_2}{N_2} - \frac{m_3}{N_3} \right), \quad (2.9)$$

...

The structure of this system originates from the fact that in each compartment,  $k$ , mutants can only enter by differentiation out of compartment  $C_{k-1}$ , which is proportional to  $m_{k-1}/N_{k-1}$ , and mutants leave by differentiation from compartment  $C_k$ , which is proportional to  $m_k/N_k$ . In a more general case, we have

$$\dot{m}_k = K_k^{(v)} \left( \frac{m_k}{N_k} - \frac{m_{k+1}}{N_{k+1}} \right), \quad (2.10)$$

for  $k > 0$ , where the constants  $K_k^{(v)}$  depend on the vector  $(v_0, \dots, v_n)$ . To understand why these type of dynamics occur for nonzero values of  $v$ , we note that if  $Q$  cells are removed from compartment  $C_k$  this results in three effects:

- The expected number of mutants removed from  $C_k$  by differentiating out is  $Q\mu_k$ .
- On average,  $Qv_k$  cells will be replaced by proliferations in compartment  $C_k$ , resulting in  $Qv_k\mu_k$  mutants added on average to  $C_k$ .
- The remainder of the cells,  $Q(1 - v_k)$ , will be replaced by differentiations from compartment  $C_{k-1}$ . There will be  $Q(1 - v_k)/2$  such differentiations, resulting in  $Q(1 - v_k)\mu_{k-1}$  mutants added on average to compartment  $C_k$ .

The net change in the mean number of mutants is then given by  $Q(1-v_k)(-\mu_k+\mu_{k-1})$ , which agrees with the above equations. The steady state of system (2.10) is given by

$$m_k = m_0 \frac{N_k}{N_0}. \quad (2.11)$$

The interpretation of this result is quite straightforward: the probability of fixation of the mutant in compartment  $C_0$  is  $m_0/N_0$ , and the expected number of mutants in all the downstream compartments is given by the corresponding compartment size multiplied by this fixation probability.

Depending on the origin of the mutation, the behavior of this system (and therefore, mutant clonal dynamics) will be different. Only in the case where the mutant is introduced at  $C_0$ , is the steady state (2.11) nontrivial, that is, mutations will persist in the system if the stem cell compartment acquires a mutation. If a mutant is introduced in any other compartment, there is transient dynamics, and then the mutation will be flushed out, since  $m_0 = 0$  in (2.11).

The diagonal entries of the lower-triangular matrix in the linear system (2.10) define the time-scale of the transient dynamics. The first diagonal entry is zero and corresponds to the neutrality of the number of mutants in the stem cell compartment.<sup>2</sup> The rest of the diagonal entries of the matrix in system (2.10) have quantities  $N_i$  in the denominators (that is, larger compartments are characterized by slower mutant dynamics), and the numerators are products of powers of  $1 - v_k$ . If all  $v_k$  are equal, then powers of  $(1 - v)$  define the decay of mutants. For small values of the proliferation probabilities, the mutants are flushed out quickly because of a high rate of differentiations leading to upward motion of cells through the compartments. For larger values of  $v$ , mutants are flushed out slowly so they tend to accumulate in compartments, giving rise to very long-lived mutant populated states. In the extreme

---

<sup>2</sup>This is a consequence of modeling the behavior of mutants deterministically. In a stochastic system, the probability of increasing and decreasing the number of mutants in  $C_0$  are equal to each other, leading to a symmetric Markov chain. The mean behavior however is correctly captured by the present system.

case of  $v = 1$ , only compartment  $C_{n-1}$  divides, and mutants accumulate in that compartment (the right hand side of equation (2.10) is zero in this case, except for the equation for  $m_n$ ).

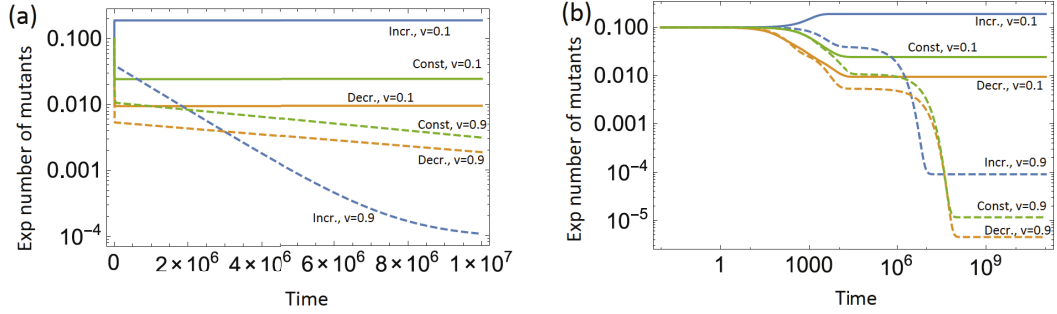


Figure 2.6: Comparison of mutant dynamics for different compartment size arrangements. The expected number of mutants is shown as a function of time for increasing compartment size  $N_i = 80e^{i+1}$  (blue lines), constant compartment size (green lines), and decreasing compartment size  $N_i = 80e^{5-i}$  (yellow lines), for  $0 \leq i \leq n = 4$ . The total population size is the same for all systems. The rare mutation limit is assumed. The probability of proliferation in each compartment is constant,  $v_i = v$  for  $0 < i < n$ , and two values of  $v$  are used:  $v = 0.1$  (solid lines) and  $v = 0.9$  (dashed lines). (a) Shorter time-scales. (b) Longer time-scales (note the log scale on the horizontal axis).

### 2.3.3 The role of proliferation in mutant generation and dynamics

As the value of  $v$  increases, there is a trade-off between two different trends associated with the probability of proliferation: the shortening of the division trees on the one hand, and a decrease in the mutant flush out rate. More precisely, small values of  $v$  imply longer trees and a higher probability of generating mutants in the stem cell compartment. When the mutants arise however, they will be flushed out quickly. On the contrary, large values of  $v$  correspond to shorter trees, such that mutants are not likely to be generated in the stem cell compartment. Once generated, however, the mutants accumulate and persist for longer. The flushing out rate is proportional to

$(1 - v)^b$ , where  $b$  is some large power, so realistically, non-small values of  $v$  result in a very long-lived state populated with mutants.

These trends are illustrated in figure 2.5(b). We observe that for small values of  $v$ , mutant accumulation is initially the least, but for large time, there is a significant expected number of mutants in steady state (that is, a good chance that the mutants fixate). For larger values of  $v$ , mutants tend to accumulate (as shown by the transient increase in the number of mutants), but in the long run, the expected number of mutants is smaller (a smaller chance that there is fixation in the system).

### 2.3.4 The role of compartment sizes

The question of optimal tissue architecture can be addressed in many different ways. If the total number of cells and the number of compartments are fixed, there is a very large number of ways to arrange individual compartment sizes. It is a difficult problem to find the optimum among all possible compartment size arrangements. At the same time, we know that the size distribution of compartments is determined by more than one factor. For example, it would be unrealistic to say that the number of cells in the SC compartment is large and the number of terminally differentiated cells is small, because it is the more mature compartments that are there to perform the function of the cells, and from the functional perspective, it is the numbers of such cells that have to be maximized.

To study the question of mutant generation and the role of the compartment sizes, we will not attempt to consider all possible compartment size arrangements. Instead, we will look for general trends. From equation (2.10) we can see that to increase the outflow of mutants from each compartment, one should decrease the  $N_k/N_{k-1}$  ratio. Basically, the inflow and the outflow of mutants are both proportional to their concentrations, and to increase the relative size of the outflow one should increase the concentration in compartment  $C_k$  and decrease the concentration in compartment

$C_{k-1}$ .

This simple argument provides an important constraint on mutant production and dynamics. To study this constraint, we will consider three types of tissue architecture: increasing compartment sizes, constant compartment sizes, and decreasing compartment sizes. The latter case is clearly unrealistic, and is included for completeness.

In the simplest case, we fix the probability of proliferation to be constant among the compartments (for  $0 < i < n$ ), and compare the expected mutant production following a (rare) mutation event for different arrangements of compartment sizes. Figure 2.6 illustrates three different types of architecture: exponentially increasing from  $N_0$  to  $N_n$  (blue lines), constant (green lines) and exponentially decreasing from  $N_0$  to  $N_n$  (yellow lines). The two panels show the expected number of mutants on different time-scales. In figure 2.6(a), on the time-scale of this plot, for small  $v$ , decreasing compartment size minimizes mutations, and for large  $v$ , increasing size minimizes mutations. In figure 2.6(b), the same plot is shown for longer time-scales. Now decreasing compartment size minimizes mutations for both values of  $v$ . In appendix C we explore a model where the proliferation probability  $v$  is a function of compartment sizes.

### 2.3.5 Stochastic simulations and a summary of trends

In this study, the number of mutants produced by a stem cell lineage system is influenced by different factors. The two factors that we focused our investigation on are the probability of proliferation in the compartments,  $v$  (such that low probability of proliferation translates into having longer division trees), and the size of different compartments. Here we summarize our findings and further illustrate them with stochastic simulations, figure 2.7. In this figure, we present the mean dynamics of mutations in different compartments, corresponding to two different values of  $v$  and two different architectures, increasing and constant. As shown below, the behavior



Chapter 2. Optimal homeostatic cell renewal

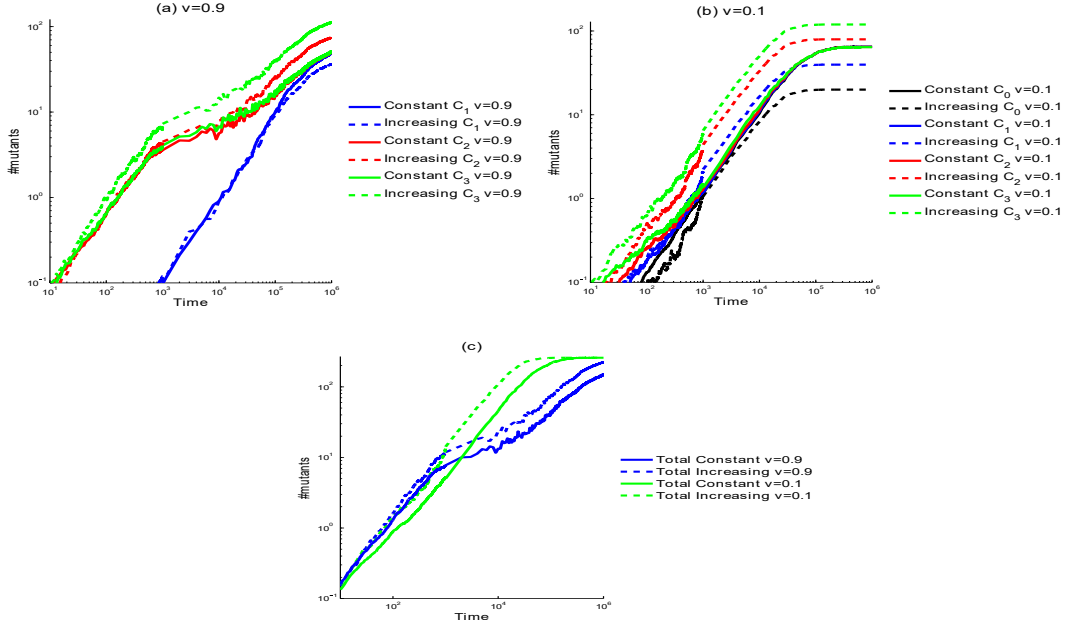


Figure 2.7: Mean number of mutants from 1000 stochastic simulations. We compare two arrangements of the compartment sizes for  $n = 3$ : constant from  $C_0$  to  $C_3$  ( $N_0 = 65, N_1 = 65, N_2 = 65, N_3 = 65$ ) and increasing from  $C_0$  to  $C_3$  ( $N_0 = 20, N_1 = 40, N_2 = 80, N_3 = 120$ ). (a) The mean number of mutants produced in compartments  $C_1$ ,  $C_2$  and  $C_3$  for  $v = 0.9$ . Note that no mutants were produced in compartment  $C_0$  over the time scale shown. (b) The mean number of mutants produced in compartments  $C_0$ ,  $C_1$ ,  $C_2$  and  $C_3$  for  $v = 0.1$ . (c) The mean of the total number of mutants comparing both architectures for  $v = 0.9$  (blue line) and  $v = 0.1$  (green line). For all panels, solid lines correspond to constant architecture and dashed lines to increasing architecture. In these simulations  $u = 0.001$ .

of the stochastic system is consistent with our predictions based on the ODEs, that were described above.

1. In the short term, lower probabilities of cell proliferation (lower values of  $v$ ) tend to be advantageous, as they result in a lower overall number of mutants. Transiently, for larger  $v$  one observes the effect of mutant accumulation, which temporarily increases the number of mutants compared to low- $v$  systems, see figures 2.6 and 2.7(c). As  $v$  increases and the mean tree length decreases, there is a trade-off between decreasing the probability of mutant creation in the SC compartment and also decreasing the flush-out rate. In the long run, however,

we observe that the latter tendency becomes less important, and larger values of  $v$  result in a smaller overall number of mutants. This can be seen in figure 2.6, where the dashed lines corresponding to larger  $v$  are lower than the solid lines (small  $v$ ) for longer times. The same tendency is observed in stochastic simulations of figure 2.7(c), where blue lines ( $v = 0.9$ ) are below green lines ( $v = 0.1$ ) for large times. Note that the larger the value of  $v$ , the longer the mutant accumulation stage persists, thus making values of  $v \approx 1$  unrealistic.

2. Larger values of  $v$  are again advantageous from the viewpoint of minimizing the number of mutants in the stem cell compartment. With a shorter division tree length, divisions in the stem cell compartment happen less often leading to a lower number of mutations. This can be seen for example in figure 2.4 by comparing the black lines (the number of mutants in compartment  $C_0$ ); see also figure 2.7, where for the time-scale of the simulations, no mutants have appeared in  $C_0$  in (a) for  $v = 0.9$ , and there is a nonzero expected number of mutants in  $C_0$  in (b) for  $v = 0.1$  (depicted by black lines).
3. Given that the value of  $v$  is fixed, in the long run, architectures where all compartment sizes are equal (marked “constant” in the figures) produce fewer mutants than increasing architectures, see figure 2.6(b) and figure 2.7(c). Transiently, this trend can be reversed, see figure 2.6(a), for larger values of  $v$ . Another scenario where increasing compartment sizes are advantageous arises if we assume that the proliferation probabilities in compartments are correlated with compartment sizes, such that differentiation from large to small compartments is favored. In this case, increasing architecture may give rise to fewer mutants, see figure C.1(b,c).
4. Increasing architecture always minimizes the number of mutants in the stem cell compartment. This follows from the ODE description, see for example, the equation for the number of mutants in compartment  $C_0$ , equation (2.4). And

the same trend is observed in the stochastic dynamics, see the black lines in figure 2.7(b), where the dashed line corresponding to the increasing architecture shows fewer mutants in  $C_0$  compared to the solid line for constant architecture (please note that in this figure, in the long run, the number of mutants in each compartment in the constant architecture is very similar, such that all the solid lines are superimposed).

### 2.3.6 Generation of two-hit mutants

Stochastic simulations developed here were also used to investigate the dynamics of two-hit mutant generation. In this setting, one-hit mutants were allowed to undergo a secondary mutation process, and the simulations were stopped as soon as the first two-hit mutant was generated. This situation corresponds to the scenario where two-hit mutants are advantageous and do not obey the same homeostatic control as the wild type cells or one-hit mutants. In this section, we used the two-sample  $t$ -test to compare the obtained  $p$ -values. Figure 2.8 shows the histograms of times when the first two-hit mutant was generated under different parameters. It presents a comparison between different tissue architectures, panels (a) and (b), and different proliferation probabilities, panels (c) and (d). In particular we notice that the largest difference in two-hit mutant generation times is experienced when we change  $v$  (figure 2.8(c,d)). For both architecture types, low values of  $v$  lead to longer two-hit mutant generation times. Therefore, we can say that from the viewpoint of two-hit mutant generation, low values of  $v$  are advantageous. This can again be explained by thinking about flush-out rates. Larger  $v$  lead to long-lived (although transient) mutant accumulation in tissue compartments, which in turn results in a higher chance of two-hit mutant generation. As a consequence, having lower proliferation rates and longer differentiation trees results in slower two-hit mutant generation.

The differences in tissue architectures result in smaller differences in two-hit mu-

tant generation time, but the trends we observe coincide with those seen in figure 2.6(a): for small values of  $v$ , increasing architecture leads to a faster production of two-hit mutants (because it results in the fastest accumulation of one-hit mutants), and for larger values of  $v$ , increasing architecture corresponds to the largest delay of two-hit mutant generation, see also figure C.3.

Figure 2.9 further explores the differences between increasing and constant architecture by assuming that the proliferation probability is defined by the compartment sizes according to formula (C.1) with  $\beta = 1$ . We observe that the constant architecture tends to delay the production of two-hit mutants compared to an increasing architecture. This result follows from the fact that lower values of  $v$  slow down two-hit mutant generation, as demonstrated above. Since the constant architecture results in lower values of  $v$ , it results in the longest two-hit mutant generation times. Figure C.3 shows an even stronger trend when the hypothetical, decreasing architecture was investigated.

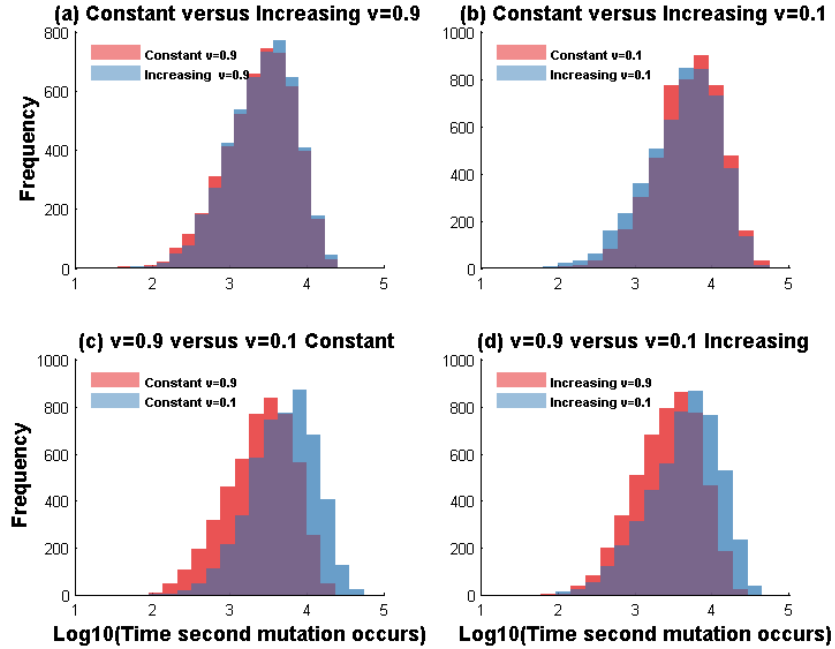


Figure 2.8: Distribution of the generation times to second mutation, obtained from 5000 stochastic simulations. We consider two arrangements of the compartment sizes for  $n = 3$ : constant from  $C_0$  to  $C_3$  ( $N_0 = 65, N_1 = 65, N_2 = 65, N_3 = 65$ ) and increasing from  $C_0$  to  $C_3$  ( $N_0 = 20, N_1 = 40, N_2 = 80, N_3 = 120$ ). (a) The time to observe a second mutant for both architectures and a high value of the proliferation probability,  $v = 0.9$ . The mean time for constant and increasing architectures is 3.38 and 3.41 respectively; the  $p$ -value obtained in the  $t$ -test is  $p = 0.0023$ , indicating that the means are different. (b) Same as (a) with a small value of the proliferation probability,  $v = 0.1$ . The mean time for constant and increasing architectures is 3.68 and 3.61 respectively; the  $p$ -value obtained in the  $t$ -test is  $< 0.001$ , indicating that the means are different. (c) and (d) The time to observe a second mutant for a constant and increasing architecture, respectively, for small and high  $v$ . In these simulations  $u = 0.001$ .

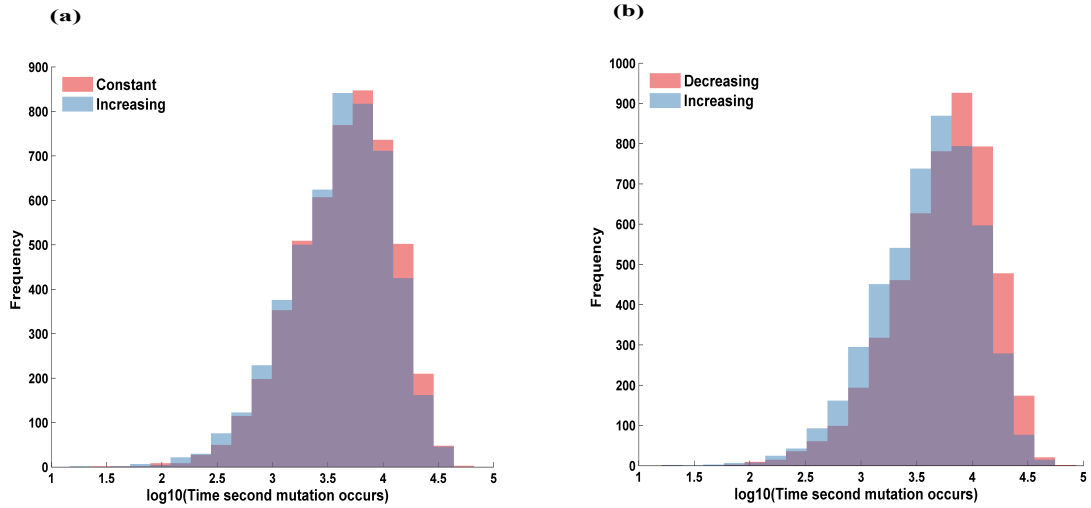


Figure 2.9: Distribution of the generation times to second mutation, obtained from stochastic simulations, in the case where  $v$  depends on the compartment sizes. We perform 5000 stochastic simulations and compare two arrangements of the compartment sizes: (a) constant compartment size (red bars) and increasing (blue bars); (b) decreasing (red bars) and increasing (blue bars). Compartment sizes are as in figure 2.8 and C.3. The proliferation probabilities are  $v_1 = 1, v_3 = 0, v_i = \frac{N_i}{N_i + N_{i-1}}, i = 1, 2$ . We assume  $n = 3$  and  $u = 0.001$ . In part (a), the mean time to a two-hit mutant for constant and increasing architecture is 3.6387 and 3.5997 respectively; the  $p$  value obtained by  $t$ -test is  $p < 0.001$ . In part (b), the mean time to a two-hit mutant for decreasing architecture is 3.7232; the  $p$  value obtained by  $t$ -test is  $p < 0.001$ .

## 2.4 Discussion

In this chapter we considered the dynamics of mutant accumulation in hierarchical tissues under homeostatic turnover. What tissue architecture can be considered optimal from the viewpoint of minimizing mutations? We have focused our attention on two aspects of tissue architecture: (1) probability of proliferations/differentiations of cells in compartments; and (2) compartment size.

The first aspect is the probability of cells in each compartment to proliferate. Proliferation division is one way of replenishing cells that have been removed (by differentiation) from the compartment; the other way is to replace “missing” cells by a differentiation division from an upstream compartment. Therefore, by changing the probability of proliferation (as opposed to differentiation) we change the probability that an upstream compartment will be engaged, thus changing the length of a typical hierarchical division tree. We have found that increasing  $v$  (the probability of proliferation) results in two clear trends: (i) the trees get shorter and it becomes unlikely to acquire a mutation in more primitive compartments, and (ii) mutations that are generated are flushed out more slowly from the non-stem cell compartments, and tend to accumulate (at least, transiently). This interesting trade-off results in different “optimal” solutions, depending on the objective of optimization. If the goal is to minimize the total number of one-hit mutants residing long-term in all compartments, relatively large values of  $v$  are desirable. If on the other hand we want to protect the stem cell compartment, then low values of  $v$  are superior. Finally, from the point of view of two-hit mutant generation, again lower values of  $v$  are advantageous.

The latter result is important in the context of tumor suppressor gene inactivation, which is a common event in carcinogenesis. In tumor suppressor genes, such as the APC gene that is inactivated in a large fraction of colorectal cancers, or Rb gene responsible for retinoblastoma, both copies must be inactivated for the resulting cell to acquire a phenotypic change that eventually may lead to cancer. Tumor

## Chapter 2. Optimal homeostatic cell renewal

suppressor gene inactivation is often considered an early event in cancer progression, and therefore a delay in this event is of crucial importance for evolution. Our analysis indicates that in order to delay tumor suppression gene inactivation in a hierarchical tissue, mitotic activities must be concentrated near the stem cell. This finding coincides with *in vivo* measurements performed in [22, 34], where divisions were more often observed near the bottom of the hierarchical compartment.

Other, indirect pieces of evidence pointing toward the protective potential of cell division regulation come from studies that investigate the connection between loss of differentiation and cancer. Our result that small values of the proliferation probability  $v$  lead to double-hit mutant suppression is consistent with the findings of [35], who reported that overexpression of protein kinase  $C\beta_{II}$  induced colonic hyperproliferation, and thus, increased the risk of colon carcinogenesis. This behavior has also been observed in other types of cancers, where a disruption in differentiation patterns might increase the risk of cancer [33, 36–39]. Tenen [40] explained that the loss of differentiation is an important component of many cancers, specifically, haematopoietic transcription factors are crucial for differentiation to particular lineages, and their disruption is critical in acute myeloid leukemia (AML) development. Researchers have also found that mutations related to brain cancer and leukemia cause the production of an enzyme that can reconfigure on–off switches across the genome and stop cells from differentiating [41–43].

We should also discuss this result in the context of the previous theoretical work by [5] and [8]. In both of these papers, variants of a linear model of the colon were investigated, where individual cells were arranged in a linear array and where dividing cells pushed out their neighbors upstream [44]. Interestingly, while both papers found that divisions near the stem cell compartment (the “bottom-high” division distribution) resulted in lowering the risk of secondary mutations experienced by existing one-hit mutants, the overall two-hit mutant generation was found by [8] to be accelerated in this case (and the “top-high” division distribution, where most divisions happen near



the top, was shown to lead to a delay in two-hit mutant production). This pattern is different from the result reported in the present model, and the difference stems from the modeling assumptions: the linear model was adopted by [5, 8], whereas a model with separate compartments that experience a certain degree of mixing was considered here (similar in spirit to metapopulation models that are often used in population biology, see e.g. [45–48]). In the present model, the linear arrangement is not 1-cell thick, but instead, there is a possibility that mutants can accumulate, or “get stuck”, in a compartment that has a size greater than one cell. This is in contrast to the linear model, where such a possibility does not exist, and each mutant will inevitably be pushed toward death at the top of the crypt in a regular fashion. The tendency of mutants to accumulate in the presence of a large proliferation probability discovered in the present setting, points toward a possibility that is ignored in the linear models. In a sense, this is similar to the differences between one-dimensional spatial population models on the one hand, and two-/three-dimensional population models or metapopulation models on the other, see also [49, 50] for discussion of these issues. Mutant spread is greatly restricted in one-dimensional geometry, whereas there are different ways to spread in higher dimensions or in metapopulations.

The second aspect of architecture investigated here is the arrangement of compartment sizes. It is physiologically determined that the top compartment containing the most mature cells performing their function in the organ, must be the largest. Under this restriction, there is a great variety of ways in which sizes of consecutive compartments can be arranged. In this paper we show that the size of the upstream compartments matter when it comes to delaying mutant production in a hierarchical tissue. We found that the smaller the differences in the relative compartment size, the longer it takes on average to generate a double-hit mutant. This suggests the existence of evolutionary pressure to equalize compartment sizes to facilitate the flushing out of mutant cells.

Next, we would like to interpret our model and its implications in the broader

## Chapter 2. Optimal homeostatic cell renewal

context of tissue architecture and the development of multicellular organisms. We can view tissue as the “functional unit” consisting of the physiologically necessary, fully mature cells, and a “support unit” consisting of less differentiated cells that do not perform the same function but are there to support and replenish the cells from the functional unit. The question then becomes, how to best organize the support unit that maintains a certain number of “functional” cells, see also [11, 51]. As one extreme scenario, one can envisage a great number of very short division trees where more or less each mature cell is replenished by divisions of its own stem cell. At the other extreme, it could happen that all the mature cells are replenished by means of an enormously long division tree, and are all part of the same large lineage stemming from a common SC. Our model is capable of distinguishing between these two extreme possibilities (and the whole range of intermediate possibilities). If  $2^n$  cells are removed, the longest division tree has length  $n$  and the shortest has length 1. If  $v = 0$ , then the longest tree is always utilized. If  $v = 1$ , then only the shortest trees are activated, and only cells in one upstream compartment (compartment  $C_{n-1}$ ) divide. If this was the evolutionarily preferable scenario, this would mean that compartment  $C_{n-1}$  is essentially the SC compartment, and that only one division step separates SCs from fully differentiated cells. If an intermediate value of  $v$  was selected, then the size of stem cell lineage would be defined by the length of a typical division tree corresponding to this value of  $v$ , and the upstream compartments that hardly ever divide would eventually be eliminated. Our results point towards the evolutionary utility of lengthening of stem cell lineages, because decreasing  $v$  leads to an increase in the two-hit mutant generation time. This process of lengthening of stem cell lineages however has to be limited by other factors, such as geometric constraints and the necessity of spatial distribution of lineages (for example colon crypts).

Incidentally, our result whereby lengthening of the SC lineages is preferred, is again different from the previous one obtained in [51], for the same reason that was highlighted above: the present model allows for mixing in the compartments, whereas

the older model of [51] is rigid in the same way as the linear model of [5] (although it is not a linear model but rather a sequence of deterministic divisions on a binary tree, where randomness only comes about when creating de-novo mutations, see [20]).

The hierarchical model considered here, although less rigid in terms of division patterns compared with the linear model of [5] and the binary model of [51], is obviously still a simplification of reality. There are many extensions that can be introduced into this model. Somatic mutations are not necessarily neutral, they might be disadvantageous, or advantageous. In this context, a fitness advantage or disadvantage might be assigned to mutants to study how it impacts the mutant population. Another important feature that could be added to our model is a replication capacity. This could be done by assigning a maximum number of divisions to each compartment, which would definitely have an impact on the type of chains of differentiation observed and therefore, on mutant development. It has been shown that a finite, and relatively small, replication capacity (between 50 and 70 divisions [52]) is a mechanism of protection against cancer in hierarchically organized tissues [32].

Finally, we note that the present model takes the metapopulation approach to spatial relationships among cells. It can be refined by adopting a fully spatial, two- or three-dimensional description, for example, a cellular automaton or a hybrid model with a degree of cell migration included. It will be interesting to see how the properties of this model change under such a refinement. The main finding of the present model is that lowering the probability of proliferation in each compartment and compensating by differentiations in longer division trees leads to a delay in two-hit mutant generation. We predict that this result should continue to hold in the fully spatial case.

# Chapter 3

## Optimal homeostatic cell renewal under a selective pressure

### 3.1 Introduction

During homeostasis, cell replacement in some hierarchically organized tissues is neutral [28, 29]. When mutations arise, they likely confer a fitness advantage or disadvantage to the cells. It is well known that tissues evolve to minimize the risk of accumulation of mutations to prevent cancer [2, 9, 53]. Multiple mechanisms of protection against cancer have been identified such as the hierarchical organization of most tissues, the proliferation patterns for self-renewal, slow division rates, and the type of cell division [1–8].

Most hierarchically organized tissues are composed of a small number of quiescent and active stem cells, a relatively large pool of transit amplifying cells (TACs), and mature differentiated cells. Cells in the mature differentiated part of the hierarchy are constantly discarded and replenished to maintain homeostasis. This is a process carried out by TACs and stem cells which replace those discarded cells via different

### *Chapter 3. Optimal homeostatic cell renewal under a selective pressure*

patterns of cell proliferation and differentiation. The spatial organization of most tissues works together with cell division patterns to delay the onset of cancer [5, 8, 13]. It has been shown that proliferation patterns with division activity near the stem cell compartment are optimal to eliminate single mutants in colonic crypts [5], whereas Shahriyari and colleagues [8] recently showed that proliferation patterns with activity in more mature compartments are optimal to delay the accumulation of double-hit mutants in the colon and the intestinal crypts. How spatial organization, division patterns and selection interact to delay the accumulation of mutations is a question that is far from being fully understood.

Tissues can be suppressors or amplifiers of selection. A suppressor of selection reduces the probability of fixation of advantageous mutations and increases the probability of fixation of disadvantageous mutations [54]; while an amplifier acts in the reverse direction. Hindersin and colleagues [55] showed that in systems that are composed of few cells, amplification or suppression of selection are a result of subtle changes in the tissue architecture. In this context, graph theory has been an important tool to investigate tissue architecture and natural selection [54]. For example, the linear process or directed line where the first cell is the root and every cell can only replace its immediate successor has been shown to be a suppressor of selection [9]. This linear process has been applied to the colon crypts [5], although other directed and undirected graphs have also been investigated in the colonic crypts [55]. Ideally, if most of the mutations are advantageous, the tissue should act as a suppressor of selection to minimize the risk of cancer. On the other hand, if most of the mutations are deleterious, tissues should evolve and act as amplifiers of selection to minimize the accumulation of such mutations, and therefore, the loss of functionality. Whether a tissue should be a suppressor or amplifier of selection is a complex question that does not have a simple answer. It depends on tissue architecture, and we hypothesize that it also depends on the division patterns observed while the tissue is renewing. We consider an optimal strategy as one where the accumulation of one-hit or second-hit

mutants is minimized.

In chapter 2 we propose a model for tissue renewal where a fixed number of cells is discarded in the compartment of mature differentiated cells. This triggers chains of differentiations which can be short, implying that most of the activity is in the more differentiated cells, intermediate, or long, implying that the stem cell compartment participates in cell division more often. In this chapter, we examine whether this model is a suppressor or amplifier of selection. Specifically, we investigate how changes in the organization of compartment size impact the growth of advantageous and disadvantageous mutations. In addition, we study how advantageous and disadvantageous mutations grow under different patterns of proliferation/differentiation. This allows us to study tissue renewal under different proliferation patterns, different tissue architectures and different fitness values, which are key to understanding when tissue renewal becomes an amplifier or suppressor of selection. Thus we investigate biologically relevant scenarios that could put the tissue at risk of failure, which would indicate that the tissue does not evolve accordingly to maintain functionality.

We start by investigating the accumulation of one-hit mutants with a given fitness advantage or disadvantage in large and small systems using an ODE approximation and stochastic simulations. We also explore the time to observe a second-hit mutant. In these investigations, we study the role of tissue architecture and proliferation patterns for different values of the fitness parameter. We find that the hierarchically organized tissue is a strong suppressor of selection. In the context of second-hit mutant production, an architecture with a small number of SCs and larger number of TACs, and long chains of differentiation could be optimal to minimize the risk of cancer by means of minimizing the time for a second mutation to occur.

## 3.2 Methods

We propose a compartmental model to study the role of mutant fitness during homeostatic cell renewal in hierarchically organized tissues. We use the results obtained in chapter 2, where we derived an approximation of the expected number of mutants in compartment  $C_i, i = 0, \dots, n$ , given that  $2^n$  cells are discarded in compartment  $C_n$ . This approximation was derived by adding the expected number of mutants produced by each chain of differentiation to every compartment. The difference with respect to the previous model is that the probability of choosing a mutant for reproduction is proportional to both the frequency of mutants in the population and the fitness of mutants,  $r$ . We assume that neutral mutations have fitness  $r = 1$ , disadvantageous mutations have fitness  $r < 1$  and advantageous mutations have fitness  $r > 1$ . We propose a model where mutants have the same fitness during their entire life span and only one type of mutation can occur. Although this represents a simplification, the approach allows us to study how a specific type of mutation accumulates in a hierarchically organized tissue undergoing cell renewal. For example, for a tissue with 4 compartments, the dynamics of the expected number of mutants,  $m_i$ , in compartment  $i$  are given by

$$\dot{m}_3 = 8(u + \mu_2(1 - u) - \mu_3), \quad (3.1)$$

$$\begin{aligned} \dot{m}_2 = & 4[u(1 - \mu_1 + v(2 - 3v + 4v^2 - 2v^3))(1 + \mu_1 - 2\mu_2)) \\ & + (1 - v)^2(1 + 2v^2)(\mu_1 - \mu_2)], \end{aligned} \quad (3.2)$$

$$\begin{aligned} \dot{m}_1 = & 2(1 - v)^6(u + \mu_0(1 - u) - \mu_1) + 4u(2 - v)(1 - v)^4v(1 - \mu_1) \\ & + 4uv(2 - 3v + v^3)(1 - \mu_1), \end{aligned} \quad (3.3)$$

$$\dot{m}_0 = 2u(1 - v)^6(1 - \mu_0). \quad (3.4)$$

where the probability of choosing a mutant for reproduction is defined as

$$\mu_i = \frac{rm_i}{rm_i + w_i}, \quad i = 0, \dots, n \quad (3.5)$$

where  $w_i = N_i - m_i$  is the number of wild type cells in compartment  $C_i$ .  $N_i$  represents the size of compartment  $i, i = 0, \dots, n$ ,  $v$  is the proliferation probability, and  $u$  is the mutation rate. For this approximation, we use sampling with replacement, a method identical to that utilized when neutral mutations were investigated. Similar to our study in chapter 2, we will apply this approximation to systems with large population sizes where mutants grow in a deterministic fashion, such as the haematopoietic system, and, under certain assumptions, we also apply it to small systems where mutations are rare events.

To investigate the dynamics of disadvantageous and advantageous mutations for systems with small population sizes such as the small intestine, stochastic simulations are also performed. We perform stochastic simulations in scenarios where mutants have an advantage or disadvantage for different values of the proliferation probability. In addition, different arrangements of the population sizes are studied. The stochastic simulations are fully described in chapter 2, section 2.2.4, where the model for optimal tissue renewal in hierarchical tissues was introduced. In the stochastic simulations, sampling without replacement is used, so that the probability to select a mutant with fitness  $r$  in compartment  $i$  during a division event is given by

$$\mu_i = \frac{rm_i}{rm_i + w_i}, \quad i = 0, \dots, n,$$

where  $w_i$  is the number of wild type cells in compartment  $i$ . In this case,  $w_i + m_i$  is different to  $N_i$ , which is observed when sampling is done without replacement.

## 3.3 Results

### 3.3.1 The ODE approximation

Using the ODEs (3.1-3.4), the model is investigated in a scenario where mutants with a fitness advantage or disadvantage are constantly produced, which requires systems



with large population sizes and (or) high mutation rates. We investigate the dynamics of the ODE approximation for advantageous and disadvantageous mutations in a large system. In figure 3.1 we plot the total number of mutants as a function of the fitness parameter  $r$  obtained by solving the ODE approximation for increasing and constant architectures. Initially, for an increasing architecture, the number of advantageous mutations will be larger than the number of disadvantageous mutations (figure 3.1, top panels). However, as time increases, the number of advantageous mutations becomes smaller than the number of disadvantageous mutations. Eventually, all types of mutations will reach similar numbers (figure 3.1, bottom panels). This indicates that the tissue is a strong suppressor of selection because it reduces the probability of fixation of advantageous mutants. This is confirmed by examining the steady state of the ODEs,  $m_i = N_i, i = 0, \dots, n$ , which is independent of the fitness value,  $r$ . Interestingly, we observe that when the population sizes in all 4 compartments are equal ( $N_i = 277750, i = 0, \dots, 3$ ), even for small times, the total number of mutants decays as the fitness parameter  $r$  increases. As time increases, the qualitative behavior of the scenario with constant architecture is identical to the scenario with increasing architecture (figure 3.1).

Although the number of mutants reaches a steady state value that is independent of fitness, we observe that the transient dynamics are greatly influenced by other key components of the model: specifically the proliferation probability,  $v$ , and the tissue architecture. As we found for neutral mutations, the value of  $v$  that minimizes the number of advantageous or disadvantageous mutations is time dependent. As time increases, the optimal  $v$  is shifting towards an intermediate or high value of  $v$ . We observe that in the long run, small values of  $v$  produce the largest number of mutants, which is similar to the result we obtained for neutral mutations (figure 3.2). Regarding the tissue architecture, we observe that the transient dynamics of all mutants is characterized by a greater accumulation of mutations when the compartment sizes increase from the stem cell compartment to the mature compartment. These dynam-

ics are the same as we observed for neutral mutations. In section 3.3.2 we present further details about the role of tissue architecture.

### 3.3.2 Fitness in a stochastic regime

In this section we investigate small systems where mutations with a given fitness are rare events. If we assume that once a mutant is generated, no more mutations occur,  $u = 0$ , we obtain a similar system of ODEs to the one obtained for neutral mutations. If we further assume that  $v_i = 0$ ,  $i = 1, \dots, n - 1$ , we arrive at

$$\begin{aligned} \dot{m}_0 &= 0, \\ \dot{m}_1 &= 2 \left( \frac{rm_0}{rm_0 + N_0 - m_0} - \frac{rm_1}{rm_1 + N_1 - m_1} \right), \\ \dot{m}_2 &= 4 \left( \frac{rm_1}{rm_1 + N_1 - m_1} - \frac{rm_2}{rm_2 + N_2 - m_2} \right), \\ \dot{m}_3 &= 8 \left( \frac{rm_2}{rm_2 + N_2 - m_2} - \frac{rm_3}{rm_3 + N_3 - m_3} \right), \\ &\vdots \end{aligned}$$

The steady states are identical to those found for neutral mutations:

$$m_k = m_0 \frac{N_k}{N_0}. \quad (3.6)$$

Thus, the steady state does not depend on  $r$  as was found for large systems (section 3.3.1), where the number of mutants reached a steady-state value independent of the fitness parameter. This confirms the role of the tissue as a suppressor of selection, because the probability of fixation is independent of the fitness parameter,  $r$ . In general, if the proliferation probabilities  $v_i$  are non-zero, the steady state is unchanged, although the values of  $v_i$  delay or accelerate the growth rate of mutants. High values

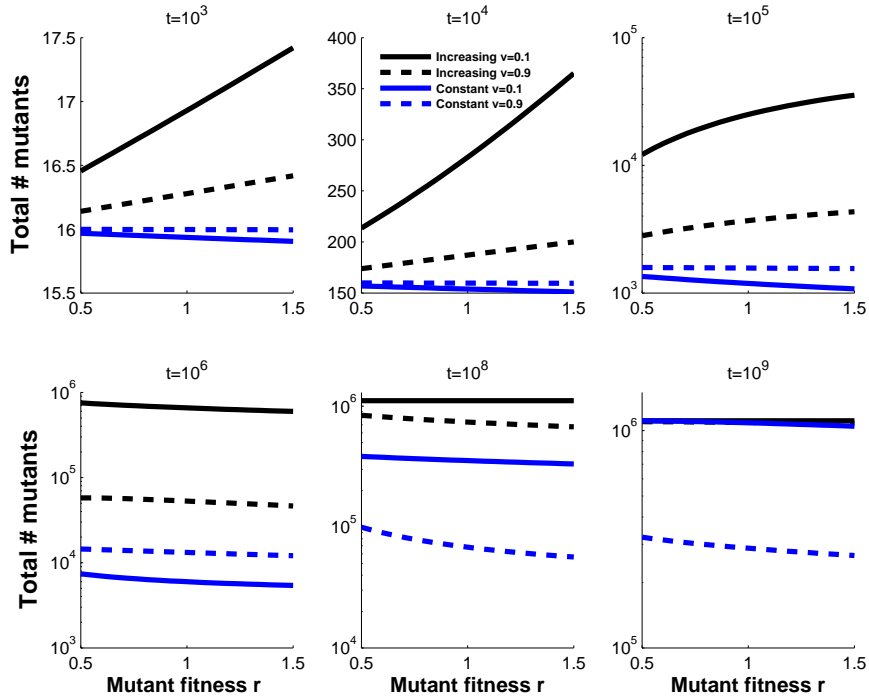


Figure 3.1: The total number of mutants as a function of the fitness parameter  $r$ , obtained from the ODE approximation for different values of the proliferation probability  $v$  and two architectures. We consider a scenario of 4 compartments with populations increasing from compartment  $C_0$  to compartment  $C_n$  ( $N_0 = 10^3, N_1 = 10^4, N_2 = 10^5, N_3 = 10^6$ ) and a tissue architecture with constant compartment sizes ( $N_i = 277750, i = 0, \dots, 3$ ). Each panel represents different time values. The mutation rate is  $u = 10^{-3}$  and  $n = 3$ .

of  $v$  delay the rate at which mutants are flushed out, but eventually fewer mutants are produced; on the other hand, small values accelerate the rate at which mutants are flushed out, although the probability of fixation in all compartments increases. The role of  $v$  is independent of the fitness of the mutants, even though the transient dynamics of mutations with a given fitness advantage or disadvantage are time dependent. Stochastic simulations also reflect the same behavior: eventually high values of  $v$  will accumulate fewer mutants than small values of  $v$  (figure 3.3).

From the stochastic simulations we also find that disadvantageous mutations accumulate slightly more than advantageous mutations. Although, as time increases,

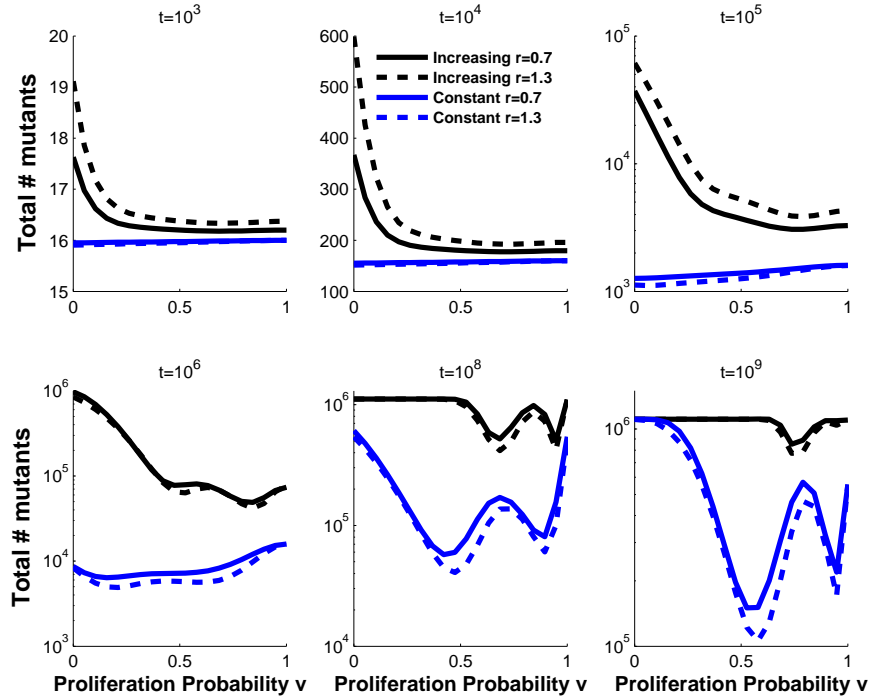


Figure 3.2: The total number of mutants as a function of the proliferation probability  $v$ , obtained from the ODE approximation for different values of the fitness parameter  $r$  and two architectures. We consider a scenario of 4 compartments with populations increasing from compartment  $C_0$  to compartment  $C_n$  ( $N_0 = 10^3, N_1 = 10^4, N_2 = 10^5, N_3 = 10^6$ ), and a tissue architecture with constant compartment sizes ( $N_i = 277750, i = 0, \dots, 3$ ). Each panel represents different time values. The mutation rate is  $u = 10^{-3}$  and  $n = 3$ .

all types of mutation reach similar numbers, as was found in the ODE approximation for the deterministic regime. As we observed in previous chapter, arrangements of the populations where compartment sizes decrease from the stem cell compartment to the top mature differentiated compartments are preferred to delay the accumulation of one-hit mutants (see figure 3.1). These observations are confirmed by the stochastic simulations, where for the two values of  $r$  investigated ( $r = 0.7$  and  $r = 1.3$ ), these patterns hold (figure 3.4).

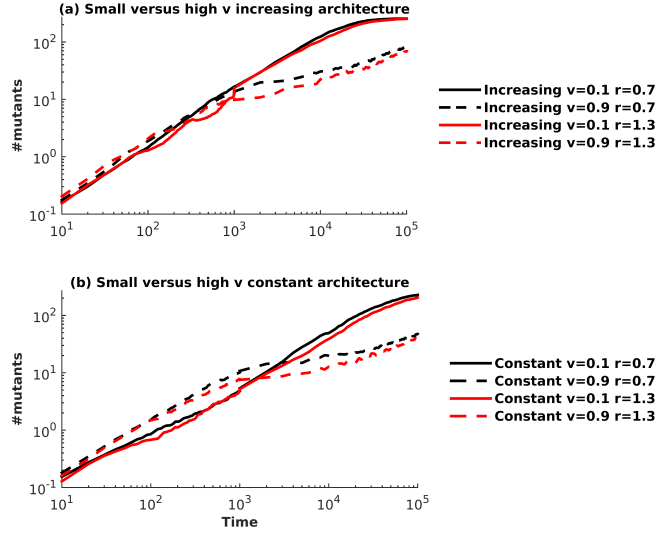


Figure 3.3: Comparing small and high values of  $v$  for increasing and constant architectures, and advantageous and disadvantageous mutants from 1000 stochastic simulations. (a) Small (solid lines) versus high (dashed lines) values of  $v$  for increasing architecture ( $N_0 = 20, N_1 = 40, N_2 = 80, N_3 = 120$ ) and two values of the fitness parameter  $r$ . (b) Small (solid lines) versus high (dashed lines) values of  $v$  for constant architecture ( $N_0 = 65, N_1 = 65, N_2 = 65, N_3 = 65$ ) and two values of the fitness parameter  $r$ . The mutation rate is  $u = 10^{-3}$  and  $n = 3$ .

### 3.3.3 Fitness and second-hit mutants

We now allow for the possibility of a second mutation to occur. We study this scenario via stochastic simulations; we track the time when a second mutation occurs and immediately stop the simulation. We start by comparing different values of  $r$  for a given architecture and proliferation probability  $v$ . In this section, we used the two-sample  $t$ -test to compare the obtained  $p$ -values. Interestingly, we find that with increasing architecture (figure 3.5(a,b)), there is no significant difference in the mean time to observe a second mutation when comparing advantageous and disadvantageous mutations for both high  $v$  ( $p = 0.4314$ ) and small  $v$  ( $p = 0.8231$ ). On the other hand, for constant architecture (figure 3.5(c,d)), advantageous mutations produced second-hit mutants faster than disadvantageous mutants for high  $v$  ( $p = 1.27 \times 10^{-4}$ ).

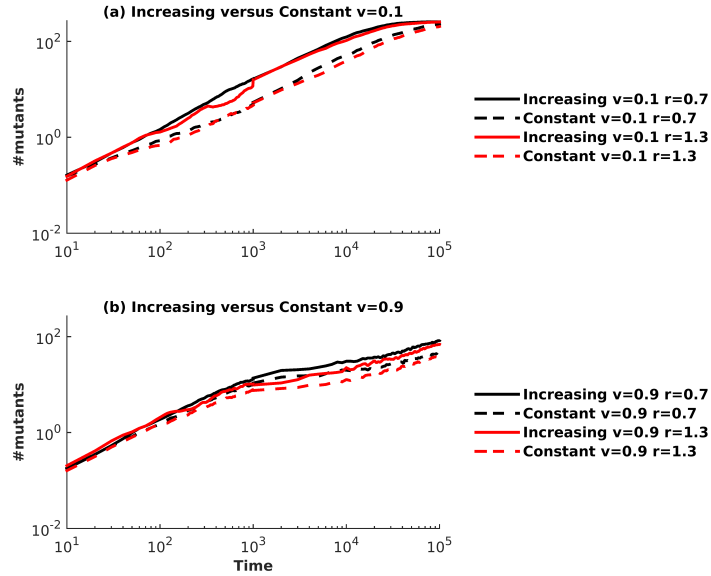


Figure 3.4: Comparing increasing and constant architectures for advantageous and deleterious one-hit mutants. The mean of the total number of mutants from 1000 stochastic simulations. (a) Increasing (solid lines) versus constant architecture (dashed lines) for a small value of  $v$  and two values of the fitness parameter  $r$ . (b) Increasing (solid lines) versus constant architecture (dashed lines) for a high value of  $v$  and two values of the fitness parameter  $r$ . In both panels, black lines correspond to deleterious mutations ( $r = 0.7$ ) and red lines correspond to advantageous mutations ( $r = 1.3$ ). For constant architecture, the compartment sizes are  $N_0 = 65, N_1 = 65, N_2 = 65, N_3 = 65$ , and for increasing architecture, the compartment sizes are  $N_0 = 20, N_1 = 40, N_2 = 80, N_3 = 120$ . The mutation rate is  $u = 10^{-3}$  and  $n = 3$ .

For small  $v$  ( $p = 0.0854$ ) there is no significant difference in the mean time. Significant differences in the mean time to observe a second-hit mutant were also observed when we investigated a decreasing architecture. For small  $v$ , advantageous mutants produced a second-hit mutant faster than deleterious mutants ( $p < 0.0001$ , figure 3.6(b)), and for high  $v$ , disadvantageous mutants produced second-hit mutants faster than advantageous mutants ( $p = 0.0213$ , figure 3.6(a)).

The results described above provide important insights into the role of tissue architecture in minimizing cancer risk. When a second mutation occurs, the increasing

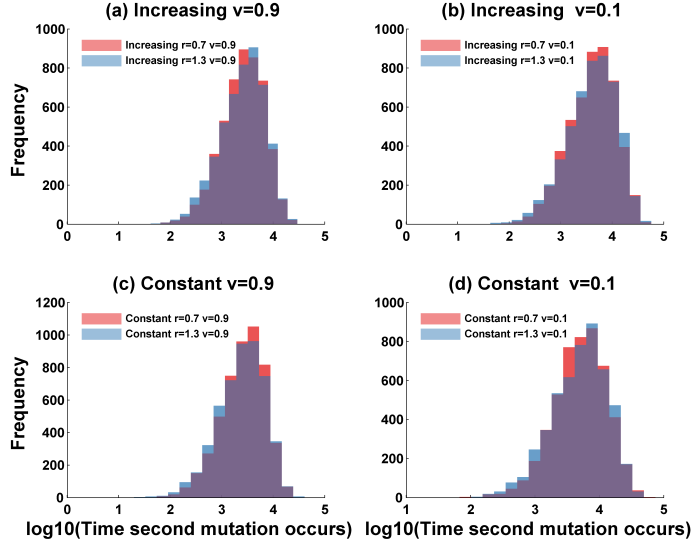


Figure 3.5: Comparing advantageous and disadvantageous mutants. Distribution of the time to observe a second mutation, obtained from 5000 stochastic simulations. (a) and (b) Comparing advantageous and disadvantageous mutations for increasing architecture and high and small  $v$ , respectively. (b) and (d) Comparing advantageous and disadvantageous mutations for constant architecture and high and small  $v$ , respectively. For constant architecture, the compartment sizes are  $N_0 = 65, N_1 = 65, N_2 = 65, N_3 = 65$ , and for increasing architecture, the compartment sizes are  $N_0 = 20, N_1 = 40, N_2 = 80, N_3 = 120$ . The mutation rate is  $u = 10^{-3}$  and  $n = 3$ .

architecture with a small number of stem cells, which is the typical organization of tissues such as the colon and the small intestine, manages to keep the distribution of time to observe a second-hit mutant the same for both advantageous and deleterious mutations. This indicates the robustness of the increasing architecture and its role in minimizing the risk of cancer. On the other hand, when this architecture is altered, so that the stem cell compartments have larger population sizes, then advantageous mutants could increase the time to observe a second mutation compared to disadvantageous mutants, or vice versa depending on the proliferation value and the compartment architecture. Under these circumstances, there would be an increased chance of fixation of advantageous or deleterious mutations, which might put the

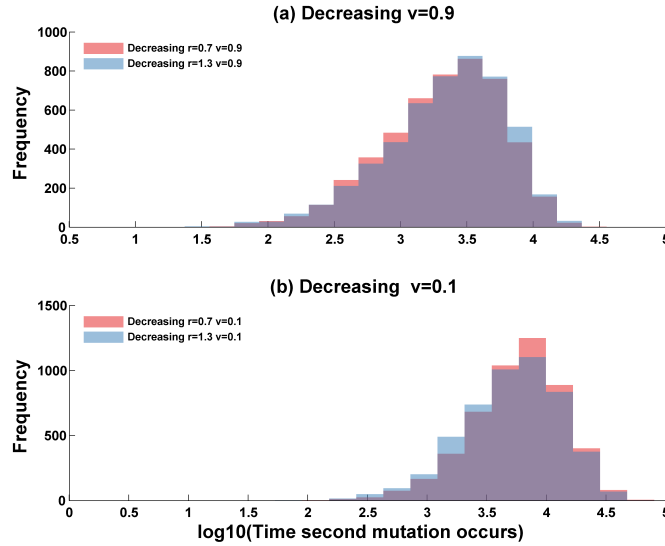


Figure 3.6: Comparing advantageous and disadvantageous mutants for decreasing architecture. Distribution of the time to observe a second mutation from 5000 stochastic simulations. (a) and (b) Comparing advantageous and disadvantageous mutations for decreasing architecture and high and small  $v$ , respectively. The compartment sizes are  $N_0 = 120, N_1 = 80, N_2 = 40, N_3 = 20$ . The mutation rate is  $u = 10^{-3}$  and  $n = 3$ .

tissue at risk. Therefore, an increasing architecture seems to be a good evolutionary strategy, which combined with “the best” proliferation pattern, can minimize the risk of cancer.

Similar to what we found for neutral mutations, small values of  $v$  delay the time to observe a second-hit mutant compared to high values (figure 3.7, for all panels,  $p < 0.05$ ). Importantly, this result holds for all architectures considered, and both advantageous and disadvantageous mutations. Therefore, an optimal strategy to delay the time to observe a second-hit mutant, which would be equivalent to minimizing the risk of cancer, corresponds to long chains of differentiation where the division activity is near the stem cell compartment.



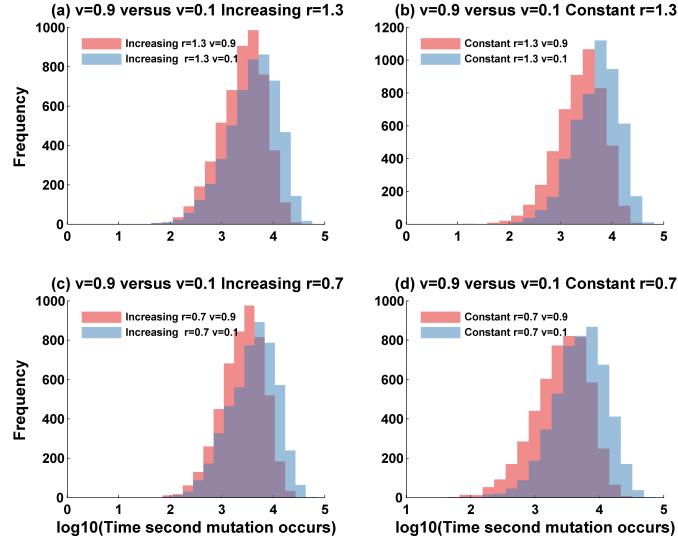


Figure 3.7: Comparing small and high values of  $v$ , for increasing and constant architectures when mutants are advantageous or disadvantageous. Distribution of the time to observe a second mutation from 5000 stochastic simulations. (a) and (b) Comparing small and high values of  $v$  for advantageous mutations and increasing and constant architectures, respectively. (c) and (d) Comparing small and high values of  $v$  for disadvantageous mutations and increasing and constant architectures, respectively. For all panels, the mean time to two-hit mutants is larger for small  $v$  and the  $p$ -values of the t-test performed on the log-transformed data are less than 0.05. For constant architecture the compartment sizes are  $N_0 = 65, N_1 = 65, N_2 = 65, N_3 = 65$  and for increasing architecture,  $N_0 = 20, N_1 = 40, N_2 = 80, N_3 = 120$ . The mutation rate is  $u = 10^{-3}$  and  $n = 3$ .

### 3.4 Discussion

We propose a model to study homeostatic cell renewal under a selective pressure. The model incorporates key variables for cell renewal such as tissue architecture, proliferation patterns and a fitness value. This allows us to study different optimal strategies that delay the accumulation of one- and two-hit mutants when mutations gain a fitness advantage or disadvantage during cell division. During cell renewal, tissues can be suppressors or amplifiers of selection. We find that whether the tissue becomes an

amplifier or suppressor of selection is strictly related to the tissue architecture and the proliferation patterns considered.

First, we discuss the results in terms of accumulation of one-hit mutants. We find that the steady state of the system is independent of the fitness parameter and is identical to the steady state found for neutral mutations, which depends on the probability of fixating the stem cell compartment so that mutations arising in a compartment different to the stem cell compartment are flushed out of the hierarchy. This demonstrates that the tissue is the strongest suppressor of selection in the sense that it reduces the probability of fixation of mutants in the stem cell compartment to a value  $\frac{1}{N_0}$ , where  $N_0$  is the size of the stem cell compartment. Our model is somewhat similar to the linear model proposed by [5], which is a structure that was found to suppress selection [9, 54]. Our model differs from the linear model in the sense that it can be thought of as a metapopulation-style model. In the linear model, cells are arranged in a 1-cell thick chain, in which mutants are pushed toward the top of the hierarchy where they are discarded. In our model, mutants still “travel” from the stem cell compartment to the top compartment, but on the way they can accumulate in all compartments, which is not captured by a one-dimensional array.

The transient dynamics are characterized by greater accumulation of advantageous mutants for early times, and as time increases, deleterious mutants reach similar (or higher) numbers. We interpret this result in terms of cell aging and cancer risk. It is well known that cancer incidence increases with age. As cells age, they lose fitness and are more likely to get damaged, which translates into loss of functionality of the tissue and a higher risk of mutations [56–59]. This indicates that the ability of the tissue to maintain fitness is crucial to minimize cancer risk [59]. Many long-lived multicellular organisms such as large animals like whales and elephants, have evolved highly fit stem cell populations, which leads to lower cancer incidence, despite having larger stem cell pools which makes them a larger target for mutations [59].

When we study second-hit mutants, we observe that tissue architecture plays a key role in delaying the time to observe a second-hit mutant. First, we found that with an increasing architecture, deleterious and advantageous mutations produced two-hit mutants almost at the same times, which indicates that an increasing architecture is a robust evolutionary strategy in terms of minimizing cancer risk. This could be explained by the fact that in an increasing architecture, the stem cell compartment has a small number of cells, which makes it a smaller target for oncogenic mutations. Also, when mutations arise, they are more likely to be pushed toward the top of the hierarchy where they have a higher chance to be eliminated. On the other hand, when we considered a constant architecture (with a larger stem cell pool compared to an increasing architecture), we observed that advantageous mutants could produce a second-hit mutant faster than deleterious mutants when the value of  $v$  was high, indicating an amplification of selection, which could be a dangerous situation for the tissue. When a decreasing architecture was considered, advantageous mutants produced mutants faster than disadvantageous mutants for small values of  $v$ , and the opposite occurred for high values of  $v$ , when disadvantageous mutants produced a second-hit mutant faster. Thus, an increase in the stem cell pool could compromise the functionality of the tissue by making it a larger target for oncogenic mutations. This is emphasized for constant and decreasing architectures, where short chains of differentiation could lead to hyper-proliferation, which is associated with an increased risk of cancer [33, 35–39]. In addition, for all tissue architectures investigated, small values of  $v$  (corresponding to long chains of differentiation) delayed the time to observe a second-hit mutant compared to high values of  $v$  (short chains of differentiation). This suggests that proliferation patterns where the division activity is concentrated near the stem cell compartment are optimal to minimize cancer risk. This is explained by the fact that small values of  $v$  increase the rate at which mutants are flushed out, which reduces the accumulation of mutants.

In the model presented here, mutations are assumed to have a single identical

fitness value for all time. An interesting addition to our model would be to investigate the effects of a fitness parameter that changes as a function of time. This would be a more realistic assumption given that as cells age, their fitness is reduced [59]. We hypothesize that our model would predict an increase in mutant accumulation as fitness decreases with time, as observed in the current model when deleterious mutations were investigated. Again, this would be associated with a higher risk of cell damage, which can make oncogenic mutations more likely to occur. Another feature that could be added is the possibility of having deleterious and advantageous mutants simultaneously, which is not currently allowed in our model. This could be done by assigning a different fitness value to cells, depending on the position in the hierarchy. Stem cells could have the largest fitness value, and the higher the position in the hierarchy is, the less fit cells would be.

Overall, we find that hierarchically organized tissues are suppressors of selection, whereby an increasing architecture (small number of stem cells) and small values of  $v$  (long differentiation trees) are robust evolutionary strategies to minimize the time to observe a second-hit mutant. This can be associated with a reduction in the risk of cancer, given that two mutations are enough to initiate a tumor for certain cancer types such as colon cancer.

# Chapter 4

## A theoretical model of immune checkpoints

### 4.1 Introduction

In the last decade, the immune system has been proven to play a crucial role in the fight against cancer. Cancer immunotherapy, consisting of treatments that stimulate the body's own immune defenses, has become an important alternative and complement to traditional treatments such as chemotherapy. Immunotherapy includes several different types of treatments such as monoclonal antibodies, cancer vaccines and immune checkpoint inhibitors. Despite the success of immunotherapy, the design of these treatments remains challenging, and several situations can lead to failure. Understanding the interactions between the immune system and tumor cells is crucial when designing these types of treatments. In this regard, mathematical modeling is a powerful tool that can help to disentangle this complex process and to design better cancer treatment strategies.

An immune response against cancer is a complex process which requires the co-

operation of different cell types and involves a variety of molecular mechanisms. The immune system deploys an innate immune response that provides an early defense against pathogens but it is the adaptive immune response that is capable of resolving diseases [60]. Cytotoxic T lymphocytes, killer T cells that are part of the adaptive immune system, are able to fight cancer once they are activated. The activation and down regulation of T cells to trigger an immunologic response against cancer cells is orchestrated by several costimulatory and inhibitory signals together with antigen presentation to T cells, which is carried out by antigen presenting cells (APCs) [61–66].

In figure 4.1, we illustrate this process: tumor cells display antigen, and APCs, such as dendritic cells, intake antigen and present it to the T cells in the context of a major histocompatibility complex (MHC) molecule. Then, a costimulatory signal is activated when the ligand B7 in the APC binds the receptor CD-28 in the T cell [61]. Early after activation of T cells, immune checkpoints or negative signals are activated, which downregulate the immunologic response. The most studied immune checkpoints in clinical trials are cytotoxic T lymphocyte antigen 4, CTLA-4 [67–73] and the programmed cell death protein, PD-1 [74–78]. There are other immunologic checkpoints that have been tested and likely many that remain unknown [79–81].

Expression of the CTLA-4 antigen is initiated upon T cell activation, and it traffics to and accumulates in the immunological synapse, eventually attenuating or preventing CD28 costimulation by competition for B7 binding and negative signaling [82–87]. PD-1 is also an inhibitory program of T-cell activity at a variety of stages of the immune response when it interacts with its two ligands PD-L1 and PD-L2 [88–90]. PD-L2 is predominantly expressed in APCs, whereas PD-L1 can be expressed in many cell types, including cells of the immune system, epithelial cells, endothelial cells, and tumor cells. PD-1 does not outcompete CD28 for binding to B7, as CTLA-4 does, but it inhibits T cell responses by interfering with T cell receptor signaling. An extensive review of the immune checkpoints CTLA-4 and PD-1 can be found in [91].

## *Chapter 4. A theoretical model of immune checkpoints*

From a modeling perspective, the immune response can be thought of as a balance between positive and negative signals: positive signals upregulate production of T cells after they encounter APCs, whereas negative signals are initiated after the activation of T cells to downregulate T cells and maintain immunological homeostasis. In previous theoretical studies, little attention has been paid to understanding the interactions between positive and negative signals: it is assumed that tumor cells can impair the immune response, but additional pathways that can lead to its downregulation are ignored. Most of the attention has been focused on understanding the role of antigen presentation by APCs and investigating how dendritic cell vaccination (DCV) can help to stimulate antigen reception by T cells during immunotherapy [92–95]. Wodarz and Jansen [92] found that an immunologic response will be activated and sustained if the rate of antigen presentation/reception is relatively high. The stimulation of antigen presentation by APCs to T cell receptors might be done through a vaccine [96, 97], but if the immune checkpoints are activated, this could potentially result in the increase of an inhibitory signal, as suggested by [98].

Our goal is to describe, with a simple mathematical model, the effects of antigen presentation of APCs to T cells and the interaction of costimulatory and negative signals (immunologic checkpoints). We also investigate the role of the initial number of tumor and immune cells, because, for example, the absolute count of T lymphocytes is regarded as a positive bio marker during immunotherapy. Specifically, we address three broad questions: Under what conditions can an immune response be sustained in the presence of costimulatory and inhibitory signals? Is stimulation of antigen reception signaling beneficial in the presence of inhibitory signals that activate proportionally to the encounter of loaded dendritic cells and T cells? How do initial populations of immune cells and tumor cells affect an immune response in the presence of costimulatory and inhibitory signals?

In this chapter, we first study the system at equilibrium and characterize 3 different types of equilibria. We then investigate how cancer and immune cell dynamics

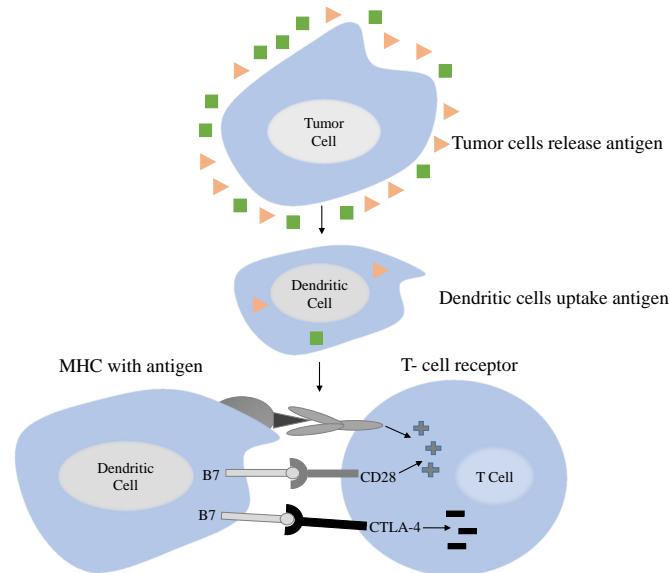


Figure 4.1: T cell activation and immune checkpoints. In order to activate, a T cell requires antigen presentation by antigen presenting cells (APCs) through a major histocompatibility complex (MHC) molecule and a costimulatory signal mediated by B7 molecules in the APCs and the receptor CD-28 in the T cell. Early after activation, several inhibitory pathways are initiated, which downregulate T cell function to maintain immunological homeostasis. The diagram illustrates how the immune checkpoint, CTLA-4, is activated and one of the possible pathways of the immune checkpoint, programmed cell death PD-1. This figure is a combination of figure 1 in [65] and figure 1 in [98].

are affected by the rate of antigen reception and by the presence of costimulatory and inhibitory signals. In addition, we examine how the initial tumor size, the initial number of dendritic cells and the initial count of T cells impact the tumor cell dynamics during an immunologic response in the presence of costimulatory and inhibitory signals. Finally, we perform a sensitivity analysis to investigate the effects of key parameters on our results.



## 4.2 Methods

### 4.2.1 The Model

We construct a system of ordinary differential equations that describes the interactions between a growing tumor cell population and a tumor-specific response by cytotoxic T lymphocytes (CTL) under the action of positive signals and inhibitory signals known as immunologic checkpoints. Our model is similar to that proposed by Wodarz and Jansen [92], and it captures the basic interactions between the immune system and tumor cells represented in other models such as [93]. In [92], it is assumed that tumor cells impair the immune response through an inhibitory signal that occurs after a T cell encounters a tumor cell, but this is only one of the possible ways in which the PD-1 inhibitor might be activated. In our model we also include the effect of an inhibitory signal that might occur after a positive signal is activated when a T cell encounters a loaded APC. This is how the CTLA-4 immunologic checkpoint is activated, and also one of the possible ways in which the immune checkpoint PD-1 protein is activated. We also model the effect of inhibitory signals differently from [92]. In [92], the inhibitory signal activates proportional to the encounter of T cells (T) and cancer cells (C) and directly reduces the population of activated T cells at the rate  $qTC$ , where  $q$  represents the rate at which cancer cells remove T cells. In our model, increasing the inhibitory signal reduces the activation rate of T cells instead of directly reducing the number of activated T cells. This accounts for different effects of inhibitory pathways, such as impairing T cells from recognizing tumor cells or undergoing cell division.

The model consists of 4 variables: tumor cells directly displaying antigen,  $C$ ; antigen-presenting cells (APCs),  $A$ ; loaded APCs,  $D$ ; and activated T lymphocytes,  $T$ , which are able to kill cancer cells. The dynamics of these populations over time is

Chapter 4. A theoretical model of immune checkpoints

described by the following system of differential equations:

$$\begin{aligned}
 \dot{C} &= rC \left(1 - \frac{C}{k}\right) - \gamma TC \\
 \dot{A} &= \lambda - \alpha AC - \delta_1 A \\
 \dot{D} &= \alpha AC - \delta_2 D \\
 \dot{T} &= \frac{psTD}{b_1\beta TC + b_2sTD + n} - uT.
 \end{aligned}
 \tag{4.1}$$

The parameter  $r$  represents the maximum per capita growth rate of tumor cells;  $k$  is the carrying capacity (in the absence of killer T cells); and  $\gamma$  is the killing rate when a killer T cell encounters a tumor cell. APCs are produced at a constant rate  $\lambda$ , they intake antigen and become loaded at rate  $\alpha$  and die at rate  $\delta_1$ . Loaded APCs die at rate  $\delta_2$ . We propose that the rate of activation of T cells is proportional to the ratio of positive to negative signals ( $\frac{psTD}{b_1\beta TC + b_2sTD + n}$ ). After the encounter of an inactivated T cell with loaded APCs, a positive signal is activated. This is represented by term  $psTD$  in system (4.1). Immune checkpoints downregulate T cells proportionally to the encounter of T cells and tumor cells and to the encounter of T cells and APCs, this includes the pathways through which CTLA-4 and PD-1 activate. The parameters  $b_1$  and  $b_2$  represent the strength of the inhibitory signals and the parameter  $p$  represents the strength of the positive signal. The rate of antigen presentation/reception is represented by  $s$  and the rate at which the tumor cells impair the immune response is represented by  $\beta$ . The parameter  $n$  represents an additional inhibitory pathway. T cells die at a rate  $u$ . We estimate some parameter values from the literature, which are based on studies of melanoma in mice. For those parameters for which there is no estimate, we perform a sensitivity analysis over a parameter range that produces biologically relevant values. The description and units of all parameters are in Table 4.1.

## 4.2.2 Equilibria

We investigate the equilibrium points of the system (4.1) as a function of the negative signals  $b_1$  and  $b_2$ , the positive signal  $p$ , and the rate of antigen reception  $s$ , which are the parameters of interest in this investigation because they are the key parameters in the activation/production of killer T cells. There are three biologically relevant equilibrium points obtained by solving the system (4.1): the point

$$E1 = (C^*, A^*, D^*, T^*) = \left(0, \frac{\lambda}{\delta_1}, 0, 0\right) \quad (4.2)$$

corresponds to immunity, an outcome in which tumor cells are cleared. It is straightforward to show that this equilibrium point is always locally unstable when the intrinsic growth rate of the tumor cells is positive ( $r > 0$ ).

One of the outcomes in which tolerance of tumor cells is reached corresponds to the saturation of tumor cells and the disappearance of T cells:

$$E2 = (C^*, A^*, D^*, T^*) = \left(k, \frac{\lambda}{\alpha k + \delta_1}, \frac{\alpha k}{\delta_2} \frac{\lambda}{\alpha k + \delta_1}, 0\right) \quad (4.3)$$

This equilibrium point is stable if

$$D^* = \frac{\alpha k}{\delta_2} \frac{\lambda}{\alpha k + \delta_1} < \frac{un}{ps} \quad (4.4)$$

This condition implies that saturation of tumor cells is stable if the number of loaded APCs remains below a threshold which increases for a small costimulatory signal  $p$  and a small rate of antigen presentation/reception  $s$ .

The other equilibrium points are the solution of a cubic equation (E.4). For more details about the equilibrium points and stability see appendix E. From our simulations, we obtain only one more biologically relevant equilibrium point, in which tumor cells lie between  $C^* = 0$  and the carrying capacity  $C^* = k$ , we name it  $E3$ . The existence and stability of  $E3$  and whether  $E3$  corresponds to saturation of tumor

cells, an intermediate value of tumor cells or immunity depends on the parameter combinations considered.

### 4.2.3 Initial conditions

We investigate the role of initial conditions during an immune response in the presence of costimulatory and inhibitory signals. We start by varying the initial tumor size and compare the tumor dynamics for different values of the inhibitory signals  $b_1$  and  $b_2$  while the positive signal  $p$  is fixed. Then, we vary the initial number of loaded APCs to simulate how dendritic cell vaccination impacts the immune response in the presence of costimulatory and negative signals. Lastly, we investigate how the initial number of activated  $T$  cells affects the tumor dynamics in the presence of costimulatory and inhibitory signals.

### 4.2.4 Sensitivity analysis

We perform a sensitivity analysis in which we simultaneously vary the following key parameters of the model: the net growth rate of tumor cells,  $r$ , the killing rate of tumor cells,  $\gamma$ , the rate of antigen intake,  $\alpha$ , the rate of antigen reception,  $s$ , the negative signals,  $b_1$  and  $b_2$ , the positive signal,  $p$ , and the strength of additional inhibitory pathways,  $n$ . We perform 5000 simulations using latin hypercube sampling within uniform parameter ranges in a logarithmic scale that produce biologically relevant outcomes (see table 4.1). All simulations are performed in MATLAB and Statistics Toolbox Release 2014a, The MathWorks, Inc., Natick, Massachusetts, United States.

Table 4.1: Model parameters

Notation	Description	Value, Units and Reference	Range for Sensitivity Analysis
$r$	Net growth rate of tumor cells	$0.3954 \text{ day}^{-1}$ [93]	$[10^{-6}, 1]$
$k$	Carrying capacity of tumor cells	$10^9 \text{ cells}$ [93]	
$\gamma$	Killing rate when a T cell encounters a tumor cell	$8 \times 10^{-3} \text{ cell}^{-1} \text{ day}^{-1}$ , assumed	$[10^{-3}, 1]$
$\lambda$	Rate of production of dendritic cells	$2.4388 \times 10^4 \text{ cell day}^{-1}$ [93]	
$\alpha$	Rate of antigen uptake	varies, $\text{cell}^{-1} \text{ day}^{-1}$	$[10^{-9}, 1]$
$\delta_1$	Death rate of dendritic cells	$0.2310 \text{ day}^{-1}$ [99]	
$\delta_2$	Death rate of loaded dendritic cells	$0.2310 \text{ day}^{-1}$ [99]	
$u$	Death rate of $T$ cells	$0.1199 \text{ day}^{-1}$ [99]	
$p$	Strength of positive signal	varies, $\text{cell day}^{-1}$	$[10^{-3}, 1]$
$b_1$	Strength of inhibitory signal proportional to encounter of dendritic and T cells	varies, dimensionless	$[10^{-8}, 1]$
$b_2$	Strength of inhibitory signal proportional to encounter of tumor and T cells	varies, dimensionless	$[10^{-8}, 1]$
$s$	Rate of antigen reception	varies, $\text{cell}^{-1} \text{ day}^{-1}$	$[10^{-5}, 1]$
$\beta$	Rate at which tumor cells impair T cells	$9.42 \times 10^{-12} \text{ cell}^{-1} \text{ day}^{-1}$ [100]	
$n$	Additional inhibitory signal	$1 \text{ cell day}^{-1}$ , assumed	$[10^{-1}, 10]$

## 4.3 Results

### 4.3.1 Immune response dynamics at equilibrium

#### Equilibria as a function of positive and negative signals

The equilibrium point  $E1$ , corresponding to immunity, is unstable (for  $r > 0$ ) and exists for all values of the strength of costimulatory and negative signals. The equilibrium point  $E2$ , representing saturation of tumor cells, also exists for all values of the costimulatory and inhibitory signals, and its stability does not depend on  $b_1$  and  $b_2$  (see equation (4.4)). Therefore, we restrict our investigation to the equilibrium  $E3$ , which is the equilibrium value where the number of tumor cells lie between immunity and saturation and whose stability does depend on the inhibitory signals ( $b_1$  and  $b_2$ ), as well as the rate of antigen reception  $s$ , and the costimulatory signal  $p$ , among other parameters.

First, we investigate the strength of the negative signal activated after a T cell encounters a tumor cell ( $b_1$ ) and the strength of the negative signal activated after an APC presents antigen to T cells ( $b_2$ ). In figure 4.2(a), we vary the negative signals  $b_1$  and  $b_2$ , while the positive signal  $p$  is fixed at  $p = 0.1$ . As  $b_1$  and  $b_2$  increase and cross a threshold, tumor cells approach their carrying capacity (figure 4.2(a)). In the parameter region explored, we observe that  $E3$  is unstable for small values of  $b_1$  and  $b_2$ . As  $b_1$  and  $b_2$  increase and cross a threshold,  $E3$  becomes stable. Note that the effect of  $b_1$  on the number of tumor cells is smaller compared to  $b_2$ , which is explained by the assumption that tumor cells impair T cells at a very low rate,  $\beta = 9.42 \times 10^{-12}$ . In the parameter regions investigated in figure 4.2(a), the equilibrium point  $E2$  is unstable.

In figure 4.2(b) we vary the positive signal  $p$  while  $b_1 = b_2$ . By doing this, we study how tumor cells corresponding to  $E3$  vary as function of the positive and

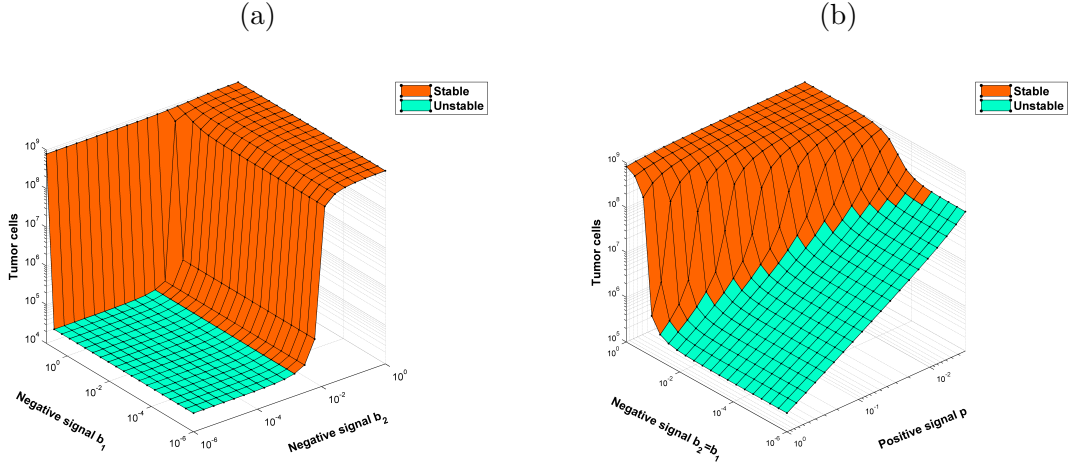


Figure 4.2: Bifurcation diagrams illustrating the number of tumor cells at the equilibrium point  $E3$  as a function of the negative signals  $b_1, b_2$  and the positive signal  $p$ . The orange and green regions represent the parameter values for which the equilibrium point  $E3$  is stable and unstable, respectively. (a) Varying the negative signals  $b_1$  and  $b_2$  while  $p = 0.1, s = 2 \times 10^{-5}, \alpha = 10^{-5}$ . (b) Varying the positive signal  $p$  while  $b_1 = b_2$  and  $s = 10^{-3}, \alpha = 10^{-9}$ . The rest of the parameter values are fixed, see table 4.1.

negative signals, simultaneously. The equilibrium value  $E3$  decreases as we increase the positive signal  $p$  (figure 4.2(b)) when both negative signals  $b_1$  and  $b_2$  are relatively small. Once  $b_1 = b_2$  increases and crosses a threshold, tumor cells reach values close to their carrying capacity despite high values of  $p$ . A similar behavior occurs for stability;  $E3$  is stable provided that  $b_1 = b_2$  is relatively high.

### The rate of antigen presentation/reception and $b_2$

In figure 4.3, we plot a bifurcation diagram of the equilibrium point  $E3$ , as a function of the rate of antigen presentation/reception  $s$  and the strength  $b_2$  of the inhibitory pathway which activates proportional to  $s$  and the encounter of T and loaded APCs. We remark that  $E3$  can get values close to  $E1$  and coincides with  $E2$  depending on the parameter combinations considered. We set  $b_1 = 0$  and  $p = 1$ , so that we can

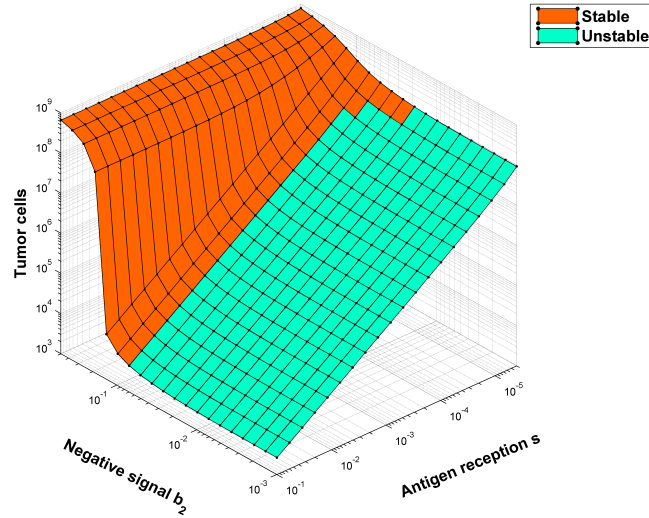


Figure 4.3: Bifurcation diagram of the number of tumor cells corresponding to the equilibrium point  $E3$  lying between saturation and immunity, as a function of the rate of antigen reception  $s$  and the inhibitory signal  $b_2$ . The orange and green regions represent the parameter values for which the equilibrium point  $E3$  is stable and unstable, respectively. Parameters used:  $b_1 = 0, p = 1, \alpha = 10^{-9}$ . The rest of the parameter values are described in table 4.1.

study the joint effect of  $s$  and the negative signal  $b_2$ .

We observe that when  $s$  is near zero, tumor cells reach high values even for a small inhibitory signal  $b_2$ . As  $s$  increases, tumor cells remain at intermediate numbers as long as the inhibitory signal  $b_2$  remains below a threshold. Interestingly, as  $b_2$  increases and crosses a threshold, the number of tumor cells increases approaching saturation very quickly, despite a relatively high rate of antigen reception (figure 4.3). Once  $b_2$  increases and crosses a threshold, the equilibrium  $E3$  becomes stable. Thus, the stimulation of antigen presentation/reception becomes ineffective if the strength of an inhibitory pathway that activates after the encounter of loaded APCs and T cells is relatively high.



### 4.3.2 Dynamics of immune responses as a function of negative and positive signals

We investigate the effects of the costimulatory and inhibitory signals on the type of immunologic responses observed under different scenarios. The initial conditions are taken as follows:  $(C, A, D, T) = (10^6, 10^4, 10, 10)$ . We assume that initially, the number of loaded dendritic cells and activated T cells are small compared to the initial tumor size. In section 4.3.3 we further examine the role of initial conditions during an immunologic response to cancer.

#### How do costimulatory and inhibitory signals shape an immunologic response?

Here, we fix the strength of the positive signal  $p$  and examine the temporal dynamics as we vary the strength of the negative signals  $b_1$  and  $b_2$ . If the inhibitory signals are weak (so that immune checkpoints inhibit T cell activation partially) there is an immune response and the tumor cell population is reduced, then the tumor population grows again, is reduced and the pattern repeats with time (figure 4.4(a)). Tumor cells oscillate and the period of these oscillations increases as we decrease the strength of the negative signals  $b_1$  and  $b_2$ , meaning that tumor cells can remain at small number for longer time periods as long as the inhibitory signals remain small. If we increase the negative signals  $b_1$  and  $b_2$ , the number of cancer cells exhibit damped oscillations that eventually reach high or intermediate values (figure 4.4(b)). If we consider a larger value of the negative signals  $b_1$  and  $b_2$ , cancer cells approach saturation very quickly (figure 4.4(c)). T cells remain at very small numbers when the negative signals are large. Thus, a positive signal is effective as long as the negative signals are small enough, i.e, the immune checkpoints must be blocked in order to clear tumor cells. Notice that in figure 4.4, tumor cells show stable oscillations or tumor cells approach their carrying capacity, which corresponds to a stable equilibrium. This is related

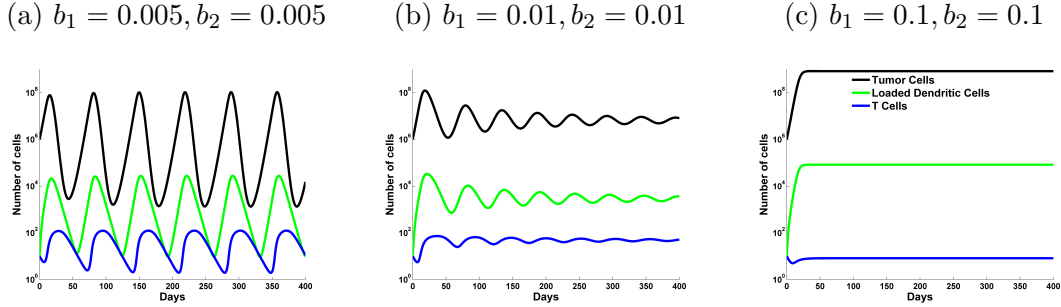


Figure 4.4: The effect of increasing negative signals on the temporal dynamics of tumor and immune cells. In (a)  $b_1 = b_2 = 0.005$ ; (b)  $b_1 = b_2 = 0.01$ ; (c)  $b_1 = b_2 = 0.1$ . The initial population sizes are  $C(0) = 10^6, A(0) = 10^4, D(0) = 10, T(0) = 10$ . Parameters used:  $p = 0.1, s = 10^{-3}, \alpha = 10^{-9}$ . In all panels, the green line corresponds to loaded dendritic cells, the blue line corresponds to T cells, and the black line corresponds to tumor cells. The rest of the parameter values are described in table 4.1.

to the results in section 4.3.1, where we find stable equilibrium points for relatively high values of the strength of the negative signals. As the negative signals decrease, it is possible to find unstable oscillatory solutions, as observed when we investigated the temporal dynamics for smaller values of  $b_1$  and  $b_2$ , and under different initial conditions (see section 4.3.3).

The observations above are also confirmed when we investigate the value of the first peak of tumor cells, the time it takes tumor cells to reach the first peak and the value of the maximum peak of tumor cells as a function of the inhibitory signals  $b_1$  and  $b_2$  in the time interval  $[0, 400]$  days. When the inhibitory signals are small, the value of the first and the maximum peaks of tumor cells are relatively small compared to the high inhibitory signals (figure 4.5, center and bottom panels). Notice that when  $b_2$  is high, tumor cells reach values close to saturation independently of the value of  $b_1$ , while for  $b_1$  tumor cells reach values close to saturation as long as  $b_2$  is also high. As explained earlier, we are assuming that tumor cells impair T cells at a very low rate,  $\beta = 9.24 \times 10^{-12}$ , which diminishes the effect of the negative signal with

Chapter 4. A theoretical model of immune checkpoints

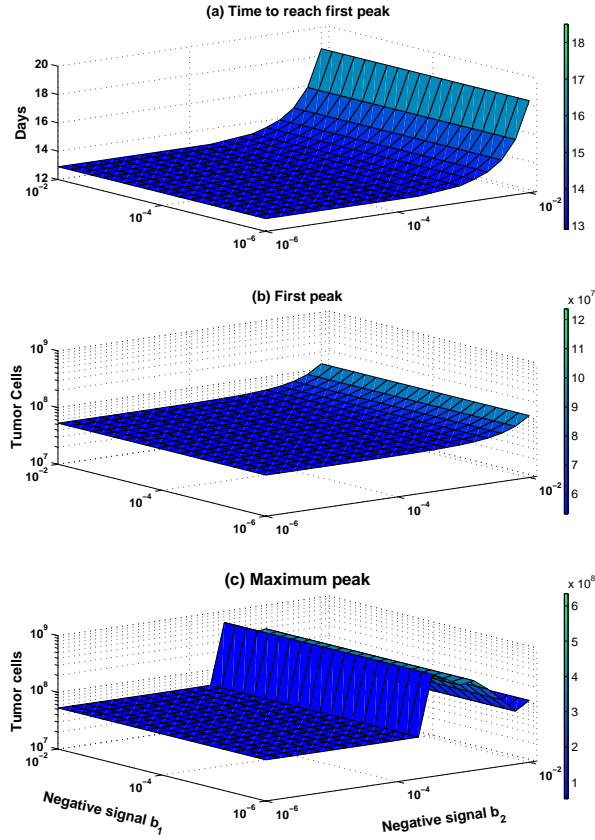


Figure 4.5: The first peak, the time to reach the first peak and the maximum peak as a function of the negative signals  $b_1$  and  $b_2$ . The time interval is  $[0, 400]$  days. The initial population sizes are  $C(0) = 10^6$ ,  $A(0) = 10^4$ ,  $D(0) = 10$ ,  $T(0) = 10$  and the parameters used are  $p = 0.1$ ,  $s = 10^{-3}$ ,  $\alpha = 10^{-9}$ . The rest of parameter values are described in table 4.1.

strength  $b_1$ . In figure 4.4 above, we only observed stable solutions. If we consider smaller values of the negative signals as we did in figure 4.5, we also observe that the maximum peak of tumor cells is a non monotonic function of the negative signals, indicating the existence of unstable oscillatory solutions. These oscillatory solutions are also observed in section 4.3.3 where we investigated the role of initial conditions.

### 4.3.3 The role of initial conditions

In this section, we explore the effects of assuming different initial values of tumor cells, loaded APCs and T cells with varying values of the strengths of costimulatory and inhibitory signals. Overall, we find that the initial sizes of these cell populations alter only the transient dynamics of the immune response, indicating that the signals involved in the activation/downregulation of T cells are more determinant in shaping the long-term immune response to cancer.

#### Tumor size

We investigate the impact of different initial tumor sizes for different values of the negative and positive signals. In figure 4.6 we consider five different initial tumor sizes while we vary the negative signals  $b_1$  and  $b_2$ . Under the action of negative and costimulatory signals, different initial tumor sizes have a similar qualitative behavior. If the negative signals are relatively high and the initial  $T$  cell population is small  $T(0) = 10$ , tumor cells saturate very quickly or remain at an intermediate value for all initial tumor sizes considered (figure 4.6(a), top and center panel). When the negative signals are smaller, tumor cells grow initially, but as time increases they are “cleared out” during a long time period (figure 4.6(a), bottom panel). Tumor cells are not fully eliminated, and eventually they will peak again, but as long as the inhibitory signals remain small, they will not be able to saturate or remain at high numbers.

In figure 4.6(b), we plot the time it takes the number of tumor cells to reach the first peak, the value at the first peak and the maximum value of the peak of tumor cells observed in the time interval  $[0, 400]$  days, as a function of the negative signal  $b_2$  while  $b_1 = 10^{-4}$ . We observe that the value of the first peak of tumor cells increases as we increase the negative signal  $b_2$  for all initial tumor sizes considered (figure 4.6(b), center panel), together with the time to reach the first peak (figure 4.6(b),

Chapter 4. A theoretical model of immune checkpoints

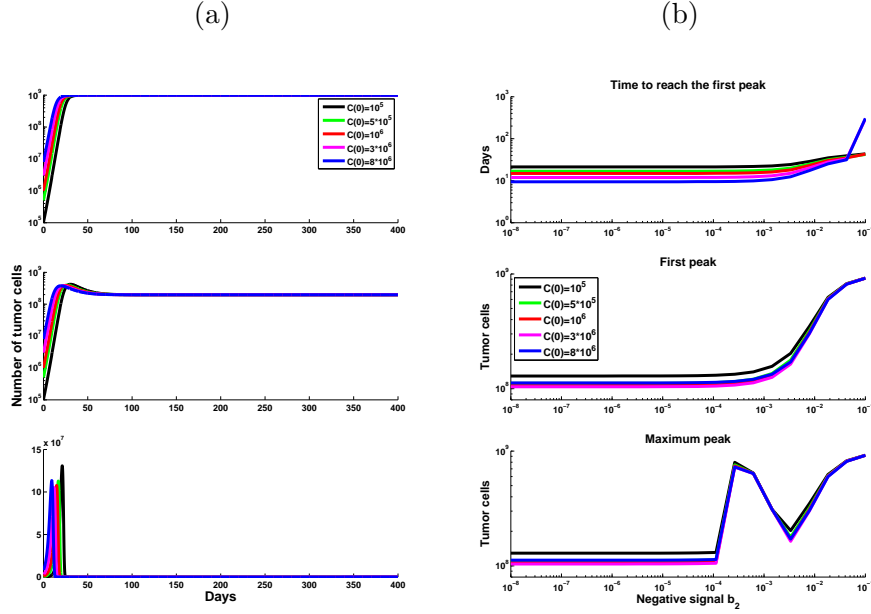


Figure 4.6: Varying the initial tumor size. (a) The top panels, the center panels, and the bottom panels correspond to  $b_1 = b_2 = 0.5$ ,  $b_1 = b_2 = 0.01$  and  $b_1 = b_2 = 10^{-4}$ , respectively. (b) The top panel, the center panel and the bottom panel correspond to the time to reach the first peak, the first peak and the maximum peak of tumor cells, respectively, as a function of the negative signal  $b_2$  while  $b_1 = 10^{-4}$ . The time interval is  $[0, 400]$  days. The initial number of APCs, loaded APCs and T cells are  $A(0) = 10^4$ ,  $D(0) = 10$ ,  $T(0) = 10$ , respectively. Parameters used:  $p = 0.05$ ,  $s = 10^{-3}$ ,  $\alpha = 10^{-9}$ . The rest of the parameter values are described in table 4.1.

top panel). Small initial tumor sizes take longer to reach the first peak (figure 4.6(b), top panel). In general, the maximum peak of tumor cells increases as  $b_2$  increases, although for small values of  $b_2$ , tumor cells can reach large values indicating that even a low inhibitory signal can lead to a high number of tumor cells. Increasing the initial number of tumor cells alters the transient dynamics of the immune response. However, whether the response is sustained is controlled by the signals involved.

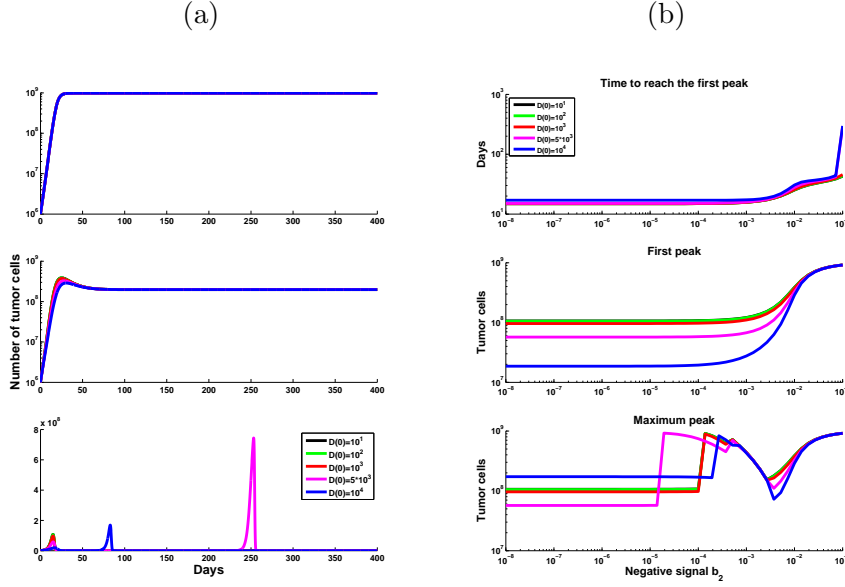


Figure 4.7: Varying the initial number of loaded dendritic cells. (a) The top panels, the center panels and the bottom panels correspond to  $b_1 = b_2 = 0.5$ ,  $b_1 = b_2 = 0.01$  and  $b_1 = b_2 = 10^{-4}$ , respectively. (b) The top panel, the center panel and the bottom panel correspond to the time to reach the first peak, the first peak and the maximum peak, respectively, as a function of the negative signal  $b_2$  while  $b_1 = 10^{-4}$ . The time interval is  $[0, 400]$  days. The initial number of tumor cells, APCs and T cells are  $C(0) = 10^6$ ,  $A(0) = 10^4$ ,  $T(0) = 10$ , respectively. Parameters used:  $p = 0.05$ ,  $s = 10^{-3}$ ,  $\alpha = 10^{-9}$ . The rest of parameter values are described in table 4.1.

### Varying the initial number of loaded APCs

Antigen presenting cells are able to present antigen to T cells so that T cells activate and kill tumor cells. In figure 4.7, we study 5 different values for the initial number of loaded APCs while we vary the inhibitory signals  $b_1$  and  $b_2$ . If the negative signals are relatively high, increasing the number of APCs has no effect; tumor cells reach saturation very quickly or remain at intermediate values (figure 4.7(a), top and center panels). When the negative signals are smaller, even a small number of initial loaded APCs can help to maintain tumor cells at small numbers for long time periods (figure 4.7(a), bottom panel).

In figure 4.7(b), we plot the time it takes for tumor cells to reach the first peak,

the value of the first peak and the value of the maximum peak of tumor cells in the time interval  $[0, 400]$  days as a function of the negative signal  $b_2$  while  $b_1 = 10^{-4}$ . The value of the first peak and the time to reach the first peak increase as  $b_2$  increases (figure 4.7(b), top and center panels); the time to reach the first peak is longer for a larger initial number of loaded APCs. We observe that as  $b_2$  increases and reaches a threshold, all initial numbers of APCs reach similar values for the first peak and the maximum peak of tumor cells (figure 4.7(b), center and bottom panels).

Thus, increasing the initial number of APCs helps to maintain tumor cells at small numbers if the inhibitory signals are small. This is important because it suggests that immunotherapy via dendritic cell vaccination is successful as long as the immune checkpoints are successfully blocked. We remark that under the presence of inhibitory signals, increasing the initial number of dendritic cells is able to modify the transient dynamics of the immune response. The final outcome of the immune response is ultimately controlled by the different signals activating and downregulating T cells.

### **Initial count of activated T cells**

We investigate 5 values of the initial number of T cells for different values of the negative signals while the positive signal  $p$  is fixed. When the strength of the negative signals is relatively high, the outcome is saturation or tumor cells reach an intermediate value (figure 4.8(a), top and center panels). We observe that a larger initial number of T cells delays the time for tumor cells to reach saturation or an intermediate value. When the strength of the negative signals are smaller, even a relatively small number of T cells is able to maintain tumor cells at very small numbers for long periods of time (figure 4.8(a), bottom panel).

When we examine the first peak of tumor cells and the time to reach it, we find that a relatively large initial number of T cells significantly delays the time to reach the first peak, which holds independently of the value of the inhibitory signal  $b_2$

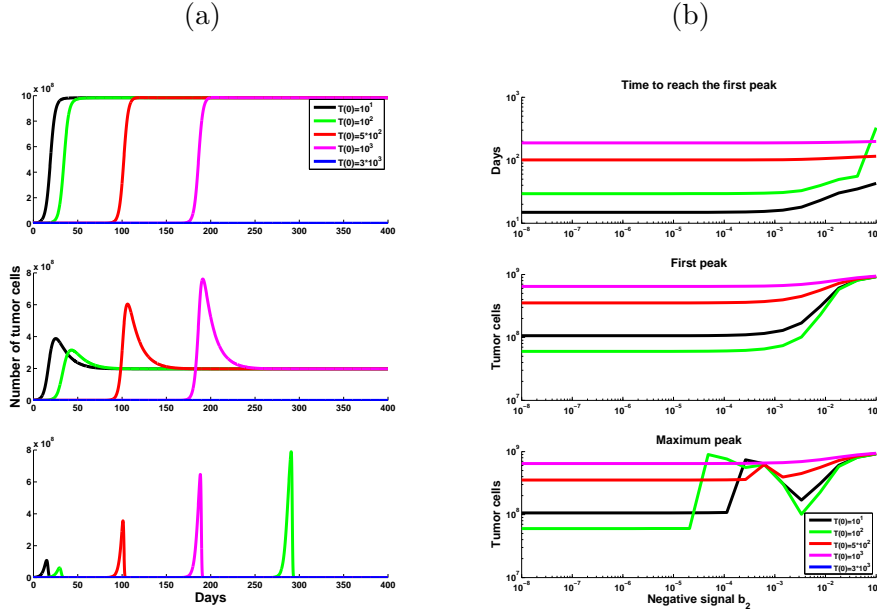


Figure 4.8: Varying the initial number of T cells. (a) The top panel, the center panel and the bottom panels correspond to  $b_1 = b_2 = 0.5$ ,  $b_1 = b_2 = 0.01$  and  $b_1 = b_2 = 10^{-4}$ , respectively. (b) The top panel, the center panel and the bottom panel correspond to the time to reach the first peak, the first peak and the maximum peak of tumor cells, respectively, as a function of the negative signal  $b_2$  while  $b_1 = 10^{-4}$ . The time interval is  $[0, 400]$  days. Parameters used:  $p = 0.05$ ,  $s = 10^{-3}$ ,  $\alpha = 10^{-9}$ . The rest of parameter values are described in table 4.1. The remaining initial populations are  $C(0) = 10^6$ ,  $A(0) = 10^4$ ,  $D(0) = 10$ .

(figure 4.8(b), top panel), in fact, for the largest value of the initial number of T cells considered,  $T(0) = 3 \times 10^3$ , a peak was not observed in the parameter region explored in the time interval  $[0, 400]$  days. For small values of  $b_2$ , a small initial number of T cells can reach the highest peak; as  $b_2$  increases, tumor cells reach a similar value of the highest peak for all initial values of T cells considered.

Therefore, an effective immunologic response is more likely if the initial count of activated T cells is relatively large. In fact, when the inhibitory signals are small, tumor cells can be cleared for long time periods, which could mean an increase in survival times of a patient with cancer. This reveals the role of the absolute T



lymphocyte count as a bio marker associated with immunotherapy success.

## 4.4 Assessing parameter uncertainty

We perform a sensitivity analysis in which we simultaneously vary the key parameters of the model. Specifically, we vary the net growth rate of tumor cells  $r$ , the killing rate of tumor cells  $\gamma$ , the rate of antigen intake  $\alpha$ , the rate of antigen reception  $s$ , the strength of the negative signals  $b_1$  and  $b_2$ , the strength of the positive signal  $p$ , and the strength of the additional inhibitory signals  $n$ . We perform 5000 calculations using latin hypercube sampling. The parameter ranges are given in table 4.1.

In figure 4.9, we plot the resulting distribution of the number of tumor cells at equilibrium  $E3$ , which lies between immunity and saturation (it can reach saturation ( $E2$ ) and values close to immunity ( $E1$ ), as observed before). We investigate combinations of parameter sets that produced biologically relevant outcomes (non-negative number of cells). Approximately 32% of these parameter combinations resulted in a number of tumor cells below one, and only 6% resulted in values above  $10^8$ , so there is approximately 62% percent of intermediate values. We found that 80% of the simulations producing biologically relevant outcomes resulted in an unstable equilibrium, and thus, 20% in a stable one. Most of the unstable solutions correspond to an intermediate or a small number of tumor cells. In addition, we find that all values above  $10^8$  are stable, indicating that once the tumor reaches high values, it will remain there. We also mention that 15% of the 5000 parameter sets produced a number of tumor cells greater than their carrying capacity, which is associated with the lowest values of the positive signal  $p$  and the rate of antigen reception  $s$ . These simulations were not considered given that they correspond to a negative number of T cells.

Overall, we observe that if we allow all important parameters in the model to

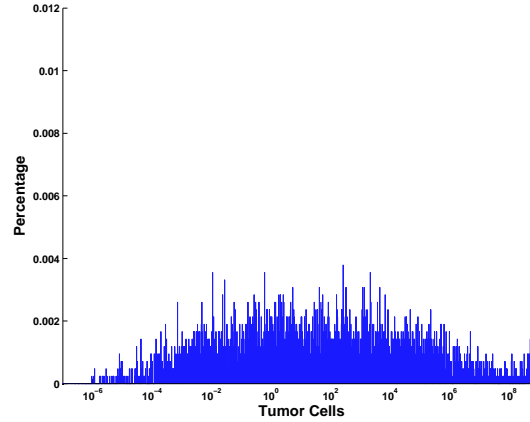


Figure 4.9: Sensitivity analysis. Histogram of the number of tumor cells for the equilibrium value  $E3$ . We simultaneously vary the net growth rate of the tumor,  $r$ , the killing rate of tumor cells,  $\gamma$ , the rate of antigen intake,  $\alpha$ , the rate of antigen reception,  $s$ , the strength of the negative signals,  $b_1$  and  $b_2$ , the positive signal,  $p$ , and the strength of additional inhibitory signals,  $n$ . The parameter ranges and the values of the fixed parameters are presented in table 4.1.

vary in a broad range, the number of tumor cells at equilibrium  $E3$  varies from small values (immunity), through intermediate values to values close to saturation. Most of the intermediate and small values of tumor cells are unstable, while all values close to saturation are stable.

## 4.5 Discussion

We propose a model that describes the role of antigen presentation, costimulatory (positive) signals, and inhibitory (negative) signals during the activation of T cells capable of killing tumor cells. There are two key differences between the model presented here and most of the previous work that has modeled an immunologic response to cancer. First, we assume that tumor cells are not the only cells capable of impairing an immunologic response. Thus, we include a term in which the encounter of APCs with T cells also activates an immune checkpoint. Second, we propose that

killer T cells increase at a rate determined by a balance between positive and negative signals, so that the regulatory feedback upregulates or downregulates the activation of new killer T cells.

We find that the relative strength of positive and negative signals plays a crucial role when triggering T cells to fight tumor cells. When the strength of the costimulatory signal is low, we observe that even a low inhibitory signal can lead to tumor cells remaining at relatively large numbers. This is consistent with the finding that the stimulation of molecules providing positive signals for T cell activation is crucial in the modulation of an immune response [63, 101–104]. When the strength of the costimulatory signal is high enough, T cells are able to trigger and sustain an immunologic response, but this depends on the strength of the inhibitory signals, because tumor cells can remain at high numbers when the inhibitory pathways are also high. Therefore, if a positive signal is maintained and the inhibitory pathways are successfully blocked, T cells can trigger and sustain an immunologic response, which is consistent with the increasing survival rates achieved by blocking immune checkpoints [68, 70, 105–109].

T cells require antigen presentation to activate. The question is how much antigen presentation is optimal given that an inhibitory pathway activates after APCs present antigen to T cells. We observe that increasing the rate of antigen reception is not effective when the strength of this inhibitory pathway is high. This might explain why immunotherapy via stimulation of antigen receptor signaling can fail in sustaining an immunologic response to cancer over longer time periods. Our finding agrees with Sharma and Allison who suggest that over-stimulation of antigen reception signaling might be counter-productive to T cell activation if it is administered when the immune checkpoints are activated [98]. This challenges one of the premises under which antigen stimulation is currently deployed, and suggests that stimulation of antigen reception and blockade of immune checkpoints can be more effective if both are targeted simultaneously.

#### *Chapter 4. A theoretical model of immune checkpoints*

In addition, we studied the role of the initial sizes of immune and tumor cells on the dynamics of the immunologic response. Specifically, we investigated dendritic cell vaccination (DCV) by varying the initial number of loaded APCs. We found that DCV has an effect on the transient dynamics of an immune response if it is administered when the strength of the inhibitory signals is low. This suggests that immunotherapy via DCV can be successful if immune checkpoints are blocked, otherwise, DCV could be counterproductive because it will enhance the strength of the inhibitory pathway initiated after the antigen presentation by dendritic cells to T cells. The initial count of activated T cells also plays an important role in the transient dynamics of an immune response. We found that a relatively large initial number of activated T cells can significantly delay tumor cell growth, even in the presence of inhibitory signals. In fact, when the inhibitory signals are low, a small initial number of activated T cells can keep tumor cells at very small numbers. This is consistent with findings from clinical studies that the absolute lymphocyte count is a positive biomarker associated with longer survival rates during immune checkpoint blockade [69, 110]. Overall, varying the initial number of tumor, dendritic and T cells altered only the transient dynamics of the immune response, indicating that costimulatory and inhibitory signals are the key determinants for the final outcome of an immunologic response against cancer.

Finally, we discuss the limitations and potential extensions of our model. In our study, we used parameter estimates from melanoma in mice (for those parameters for which there is information in the literature, see table 4.1 for more details). The appropriate time scale is days, which would likely be different for data from human patients because many biological processes occur faster in mice than in humans. In order to account for the uncertainty in the model parameters, which could reflect tumor and patient variability, we perform a sensitivity analysis. This analysis lead to a variety of outcomes: from a small number of tumor cells, to intermediate values and finally tumor cells reaching their carrying capacity. Particularly, we notice that when

#### *Chapter 4. A theoretical model of immune checkpoints*

tumor cells reach high numbers close to saturation, the equilibrium  $E3$  was stable, which indicates that once tumor cells reach high numbers, they will remain there. When we investigated the temporal dynamics of immune responses for small values of the strength of the negative signals  $b_1$  and  $b_2$ , in certain scenarios we observed that tumor cells oscillated between high and very small values. Perhaps, in a stochastic framework, once tumor cells reach very small values, these scenarios would correspond to full clearance of tumor cells which is not captured in our deterministic model. This reveals the need for stochastic models that can capture other features of an immune response against cancer, which are not observed under a deterministic framework. Our model does not include all types of immune cells in an attempt to keep the model analysis tractable, but it does include the main interactions between tumor cells and immune cells. In practice, the success of an immunologic response to cancer depends on other factors and it varies from patient to patient and between tumor types. The expression of bio markers in addition to the absolute T lymphocyte count, might be important to investigate. It has been suggested that the T cell receptor repertoire is an important bio marker that could be associated with immunotherapy success [111].

Overall, our model offers potential explanations as to why some immunotherapy treatments cannot sustain an immunologic response to cancer; it suggests that immunotherapy treatments that stimulate antigen reception signaling (up to a certain rate) can maintain a response for longer time periods if the immune checkpoints are blocked. Overstimulation might be counterproductive if the immune checkpoints are activated.

# Chapter 5

## Conclusions

We have used mathematical modeling to gain insight into key mechanisms that shape cancer dynamics. In chapter 2, we derived a compartmental model of homeostatic cell renewal in hierarchical tissues described by a system of differential equations, which predicts the expected number of mutants in each compartment by adding the contributions of different chains of differentiation observed while a number of mature cells is discarded in the top of the hierarchy. This allowed us to investigate the role of different proliferation patterns and tissue architecture in the accumulation of one-hit mutants. Overall, we find that if the optimization task is to delay the accumulation of one-hit mutants, short chains of differentiation are better in the long run; on the other hand, if the optimization task is to delay the time to observe a second-hit mutant, long chains of differentiation are preferred, which is a more realistic measure of cancer risk, given that for some cancers two mutations could be enough to initiate a tumor. In chapter 3 we extend the model proposed in chapter 2 by adding a fitness advantage/disadvantage to mutants. We find that the hierarchical tissue acts as a suppressor of selection during homeostatic cell renewal. In addition, we found that the combination of an increasing architecture and long chains of differentiation provides a robust strategy when it comes to delaying the time to observe a second-hit mutant.

## *Chapter 5. Conclusions*

Particularly, we found that increasing the stem cell pool could decrease the time to observe a second-hit mutant, which can translate into a higher risk of cancer.

Finally, we proposed a model of an immune response to cancer where we show the key role of costimulatory and inhibitory signals. The model allowed us to investigate different immunotherapy treatments and to study under which conditions immunotherapy could succeed/fail. Overall, we find that treatments based on stimulation of antigen reception signaling could be counterproductive if they are administered when the immune checkpoints (inhibitory signals) are not blocked.

# Appendices

A Further analysis of the deterministic mutant dynamics	82
B Comparison of the ODEs and stochastic simulations for large systems	86
C Further notes on the role of the compartment size	88
D Further notes on tissue architecture, division patterns and fitness	93
E Equilibria and stability for the immune response model	97



# Appendix A

## Further analysis of the deterministic mutant dynamics

Here we provide some analysis of the large mutation rate, large population regime ( $Nu \gg 1$ ). We investigate the total number of mutants as a function of the proliferation probability  $v$ . As time increases, the total number of mutants decays with  $v$  (figure A.1) but for some times, the total number of mutants is a non-monotonic function of  $v$ . We observe that small values of the proliferation probability and values close to one produce the largest number of mutants. This might be explained by the fact that when  $v$  is small, cell division occurs in more compartments due to longer chains of differentiation, and thus, more compartments get saturated with mutants, which becomes a permanent state of the system. For large values of  $v$ , the division activity is concentrated in a single top compartment or in a small number of top compartments with relatively large population sizes which leads to the rapid accumulation of mutants in the top part of the tissue. These dynamics are transient because as time increases the remaining compartments saturate, thus, small values will eventually produce more mutants.

It appears that there is an optimal value of the proliferation probability  $v$  that

Appendix A. Further analysis of the deterministic mutant dynamics

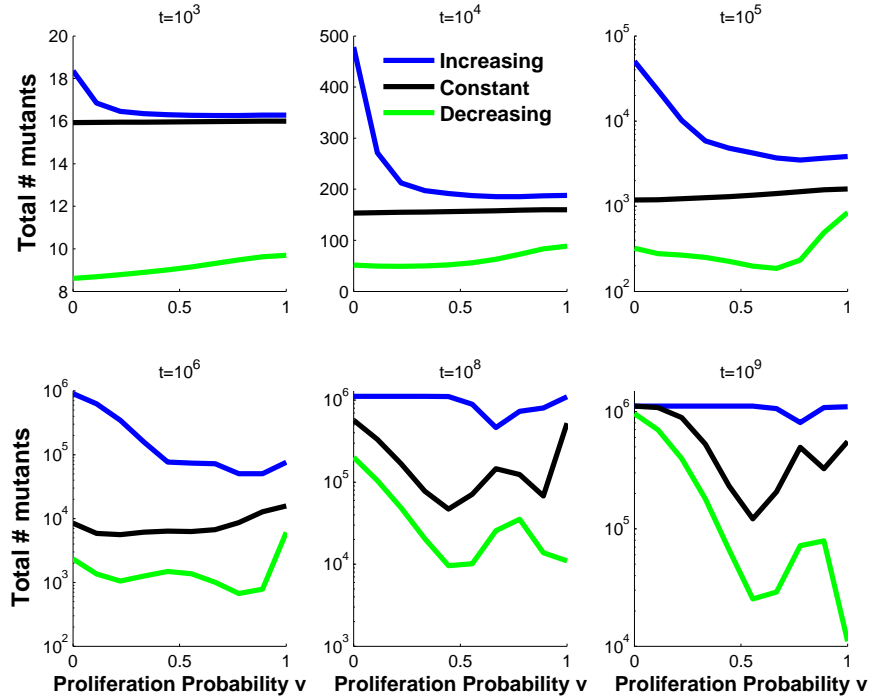


Figure A.1: The total number of mutants as a function of the proliferation probability  $v$  from the ODE approximation. The total population size is assumed to be 1,111,000 cells, the mutation rate is  $u = 10^{-3}$ , and  $n = 3$  (four compartments). We compare the following architectures: increasing compartment sizes ( $N_0 = 10^3, N_1 = 10^4, N_2 = 10^5, N_3 = 10^6$ , corresponds to the blue line), equal population sizes ( $N_i = \frac{\text{Total Population}}{4} = 277750, i = 0, \dots, 3$ , corresponds to the black line), and decreasing compartment sizes ( $N_0 = 10^6, N_1 = 10^5, N_2 = 10^4, N_3 = 10^3$ , corresponds to the green line). We plot the total number of mutants as a function of the proliferation probability  $v$  at different times.

delays the accumulation of mutations and it seems to be time dependent. We observe that as time increases, the optimal value of  $v$  is shifting toward an intermediate or higher value, figure A.1.

In figure A.1, we further investigate three types of tissue architecture as a function of the proliferation probability. We find that a scenario of 4 compartments with populations decreasing from compartment  $C_n$  to the stem cell compartment ( $N_0 = 10^3, N_1 = 10^4, N_2 = 10^5, N_3 = 10^6$ ), accumulated more mutants than a scenario

Appendix A. Further analysis of the deterministic mutant dynamics

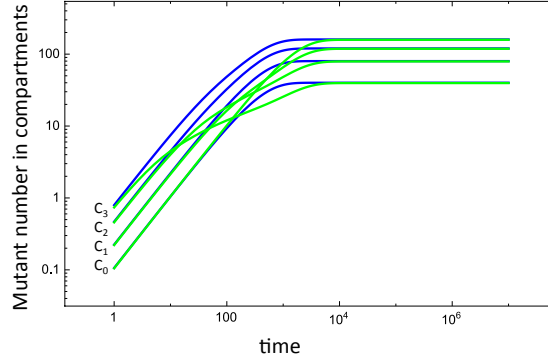


Figure A.2: The ODE mutant dynamics for 4 compartments, under two architectures. Blue lines correspond to increasing compartment size:  $N_0 = 40, N_1 = 80, N_2 = 120, N_3 = 160$ , and green lines to the decreasing compartment sizes,  $N_0 = 160, N_1 = 120, N_2 = 80, N_3 = 40$ . The compartments are labeled  $C_1, \dots, C_4$  to the left of the lines. The other parameters are  $v = 0.1$  and  $u = 0.1$ .

of 4 compartments with equal population sizes ( $N_i = 277750, i = 0, \dots, 3$ ) or a scenario where the population sizes decrease from the stem cell compartment to the compartment with mature cells ( $N_0 = 10^6, N_1 = 10^5, N_2 = 10^4, N_3 = 10^3$ ). This dynamic is transient because the systems eventually reach the same steady-state value, as observed in figure A.2.

Figure A.2 shows details of mutant accumulation dynamics for two opposing tissue architectures: increasing compartmental sizes (blue) and decreasing compartmental sizes (green). One can see that at first, the linear growth of mutants in each compartment is the same for both models; the stem cell compartment has the smallest number of mutants while the mature compartment has the largest because of the larger number of divisions in that compartment. Later on, however, differences in the behavior of the two architecture types appear. In the system where the compartment size increases from the stem cell compartment to the mature cell compartment (blue), the smallest compartment is the most “protected” (has fewer divisions), and the largest compartment has the easiest time accumulating mutations, therefore such

*Appendix A. Further analysis of the deterministic mutant dynamics*

a system is relatively efficient in mutation accumulation. In the opposite case (green), the largest number of mutations has to accumulate in the most protected (stem cell) compartment, and this naturally takes longer. While at the steady state, both systems have the same number of mutations, the transient behavior is characterized by a smaller number of mutations in the architecture where compartment size increases from  $C_n$  to  $C_0$ .

# Appendix B

## Comparison of the ODEs and stochastic simulations for large systems

The stochastic and deterministic models coincide in the regime where  $uN \gg 1$ , as demonstrated in figure B.1. We compare the expected number of mutants predicted by the ODEs with the mean number of mutants obtained from the simulations in a deterministic regime and found that they both predict the qualitative behavior of the model very well. The comparison was made for a scenario with 4 compartments where the population sizes increase from the stem cell compartment to the fully differentiated cell compartment ( $N_0 = 10^3, N_1 = 10^4, N_2 = 10^5, N_3 = 10^6$ ).

Appendix B. Comparison of the ODEs and stochastic simulations for large systems

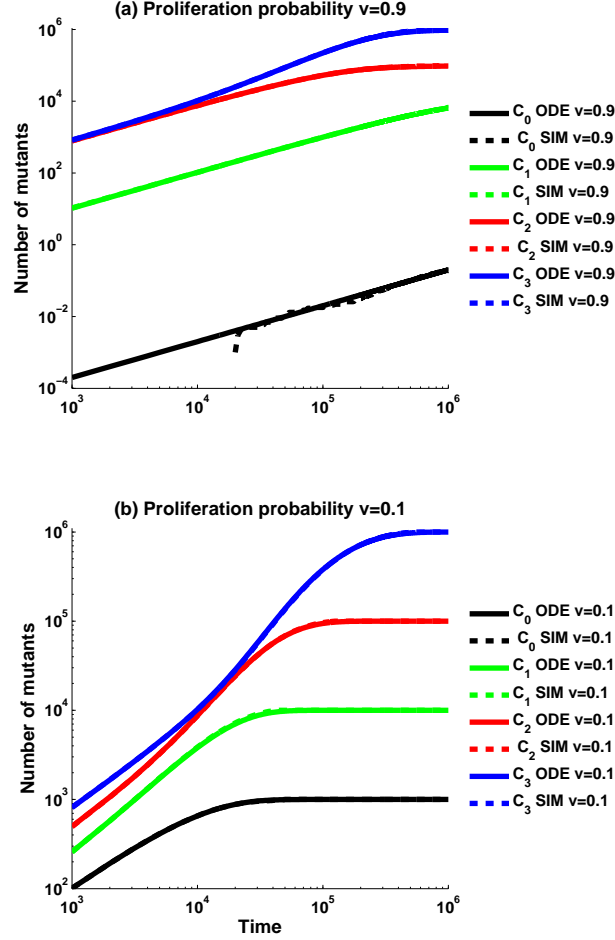


Figure B.1: Comparison between the average number of mutants from 1000 stochastic simulations without replacement and the expected number of mutants predicted by the ODE approximation. (a) Comparing the number of mutants for a high value of the proliferation probability,  $v = 0.9$ . (b) Comparing the number of mutants when the proliferation probability is small,  $v = 0.1$ . Solid lines correspond to the number of mutants in compartment  $C_i, i = 1, \dots, 3$ , predicted by the ODE approximation ( $C_i$  ODE  $v = 0.1$ , for small  $v$  and  $C_i$  ODE  $v = 0.9$  for high  $v$ ) and dashed lines correspond to the mean number of mutants in compartment  $C_i$  from the stochastic simulations ( $C_i$  SIM  $v = 0.1$ , for small  $v$  and  $C_i$  SIM  $v = 0.9$  for high  $v$ ). We assume  $n = 3$ , a mutation rate of  $u = 10^{-1}$ , and the compartment sizes are  $N_0 = 10^3, N_1 = 10^4, N_2 = 10^5, N_3 = 10^6$ .

# Appendix C

## Further notes on the role of the compartment size

In section 2.3.4,  $v$  and the compartment sizes are assumed independent, which might be an over-simplification. Suppose that a number of cells differentiated out of the  $C_k$  compartment. Then compartments  $C_k$  and  $C_{k-1}$  might “compete” to fill the empty spaces. It is possible that compartment  $C_k$  is small and  $C_{k-1}$  is large (and crowded?). In this case, differentiations from  $C_{k-1}$  to  $C_k$  are preferred, and the probability of proliferation,  $v_k$ , is relatively low. One possibility is to set  $v_k = N_k/(N_k + N_{k-1})$ , or, more generally,

$$v_0 = 1, \quad v_k = \frac{N_k^\beta}{N_k^\beta + N_{k-1}^\beta}, \quad 1 \leq k \leq n-1, \quad v_n = 0. \quad (\text{C.1})$$

Again, the optimization task is to arrange the populations in the different compartments to minimize mutation production. Figure C.1 illustrates some of the patterns we have observed. It compares two opposite arrangements of compartment sizes, increasing from  $N_0$  to  $N_n$  (blue lines), and decreasing from  $N_0$  to  $N_n$  (yellow lines). In the example provided, the increase or decrease is exponential, but other laws have also been investigated and give qualitatively similar results. According to formula (C.1),

Appendix C. Further notes on the role of the compartment size

the increasing compartment architecture leads to higher values of  $v$  than decreasing architecture.

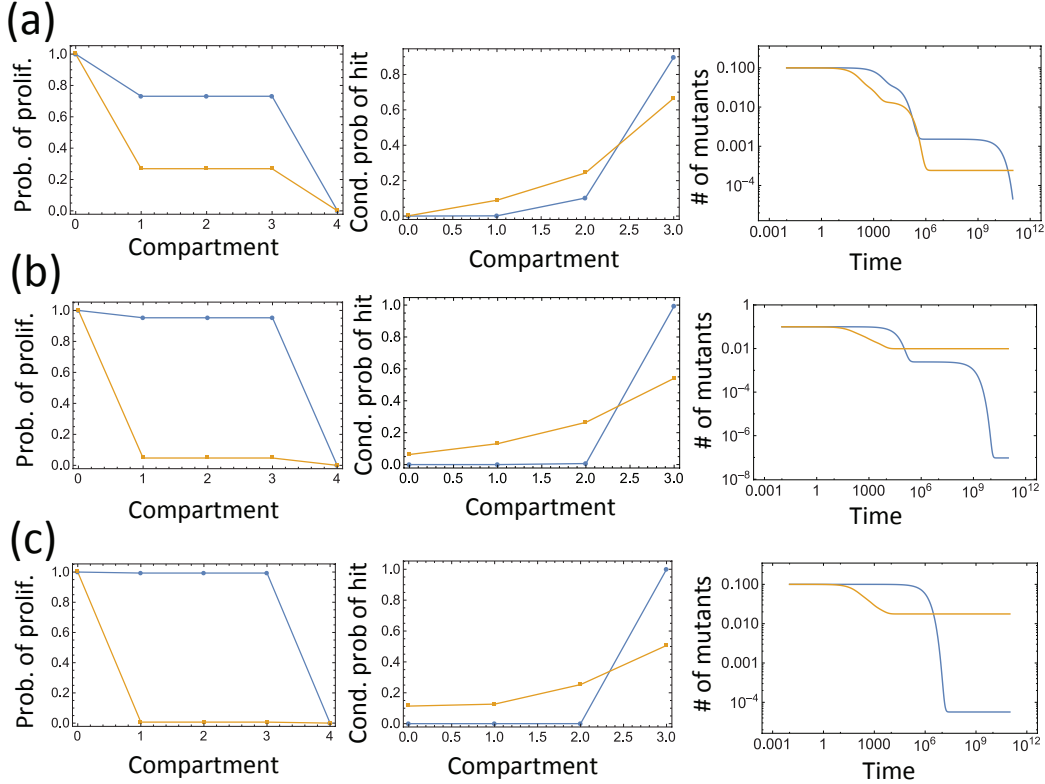


Figure C.1: Comparison of mutant dynamics for two different compartment size arrangements: increasing compartment size  $N_i = 80e^{i+1}$  (blue lines), and decreasing compartment size  $N_i = 80e^{5-i}$  (yellow lines), for  $0 \leq i \leq n = 4$ ,  $m_0 = 0.1$ . The rare mutation limit is assumed. The probability of proliferation in each compartment,  $v_k$ , is determined by equation (C.1), where (a)  $\beta = 1$ , (b)  $\beta = 3$ , and (c)  $\beta = 5$ . The values of  $v_k$  are shown in the leftmost plots. The conditional probability that a mutant is generated in each compartment (given that a mutant is generated) is plotted in the middle graphs. The rightmost graphs show the relative number of mutants in both systems as functions of time. Note that these graphs can only be interpreted for purposes of comparison, not as absolute numbers.

Consider an extreme scenario where  $\beta \rightarrow \infty$  in (C.1). If the compartment size grows from  $C_0$  to  $C_n$ , we have  $v_k = 1$  for  $0 \leq k \leq n - 1$ , and only trees of length 1 exist. If the compartment size decreases from  $C_0$  to  $C_n$ , we have  $v_k = 0$  for  $1 \leq k \leq n$ ,



*Appendix C. Further notes on the role of the compartment size*

and all the trees have length  $n$ .

For increasing compartment sizes, mutants can only appear in compartment  $C_{n-1}$ , and they fixate with probability  $m_0/N_{n-1}$  (where  $m_0$  is the initial number of mutants), such that the expected colony size is given by  $m_0$ . For decreasing sizes, mutants can appear in all compartments, but they are flushed out from any compartment except from  $C_0$ , where they fixate with probability  $1/N_0$ . So, only mutants that originate in  $C_0$  can give rise to fixation in the state

$$\frac{m_0}{N_0} \sum_{k=0}^{n-1} N_k. \quad (\text{C.2})$$

The probability that a mutation occurs in compartment  $C_0$  (given that a mutation occurs) is

$$\frac{1}{1 + \sum_{i=0}^{n-2} 2^i} = 2^{1-n}. \quad (\text{C.3})$$

The product of factors (C.2) and (C.3) defines the long time behavior of the mutant numbers for the decreasing compartment sizes in figure C.1, as  $\beta$  increases. In the limit where  $\beta \rightarrow \infty$ , the increasing compartment system is characterized by a constant (and equal to  $m_0$ ) number of mutants.

Finally, for completeness, we present stochastic simulations addressing the differences between the behavior of increasing and decreasing architecture structures. In figure C.2, one-hit mutants are studied. This figure shows the same trends as figure 2.7, where increasing and constant architectures are compared; in figure 2.7, the differences are more pronounced.

Figure C.3 studies two-hit mutant generation, and includes increasing and decreasing architectures. It should be compared with figure 2.8 (increasing and constant architectures). Again, the same trends are observed, but the differences are larger in the case of figure C.3.

Appendix C. Further notes on the role of the compartment size

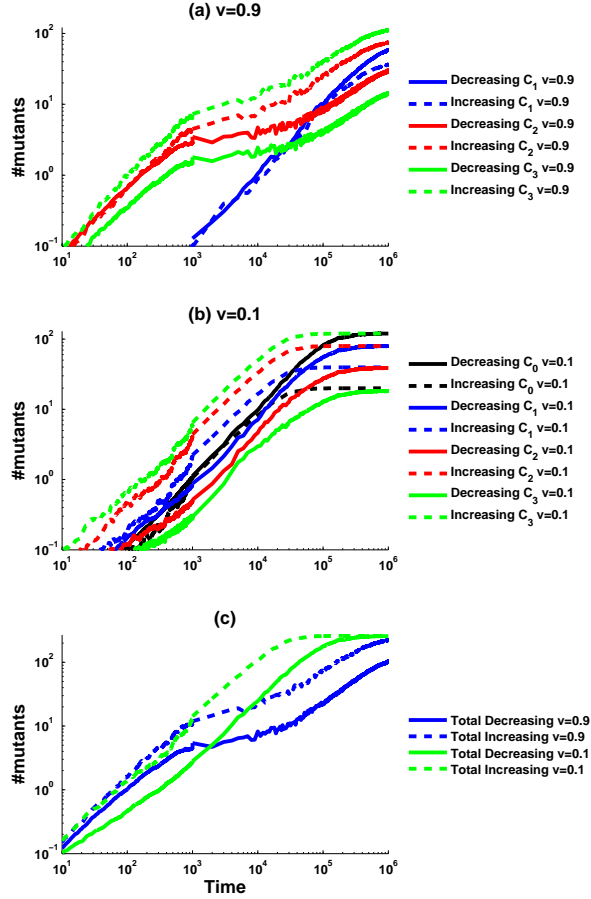


Figure C.2: Mean number of mutants from 1000 stochastic simulations. We compare two arrangements of the compartment sizes: decreasing from  $C_0$  to  $C_3$  ( $N_0 = 120, N_1 = 80, N_2 = 40, N_3 = 20$ ) and increasing from  $C_0$  to  $C_3$  ( $N_0 = 20, N_1 = 40, N_2 = 80, N_3 = 120$ ). (a) The mean number of mutants produced in compartments  $C_0, C_1, C_2$  and  $C_3$  for  $v = 0.9$  (b) The mean number of mutants produced in compartments  $C_0, C_1, C_2$  and  $C_3$  for  $v = 0.1$ . (c) The mean of the total number of mutants comparing both architectures for  $v = 0.9$  (blue line) and  $v = 0.1$  (green line). For all panels, solid lines correspond to decreasing architecture and dashed lines to increasing architecture. We assume  $n = 3$  and  $u = 0.001$ .

Appendix C. Further notes on the role of the compartment size

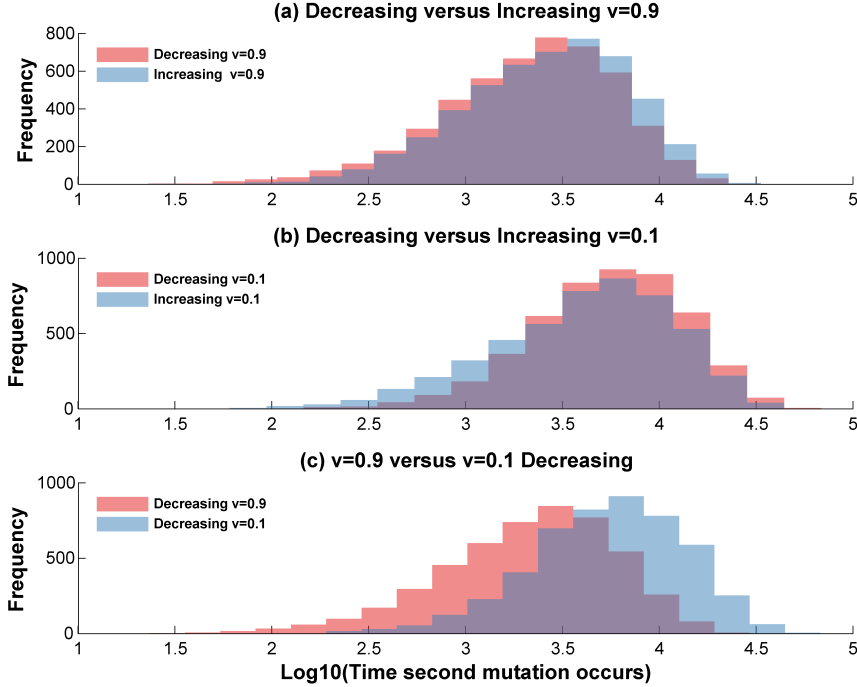


Figure C.3: Distribution of the time to observe a second mutation from 5000 stochastic simulations. We consider two arrangements of the compartment sizes: decreasing from  $C_0$  to  $C_3$  ( $N_0 = 120, N_1 = 80, N_2 = 40, N_3 = 20$ ) and increasing from  $C_0$  to  $C_3$  ( $N_0 = 20, N_1 = 40, N_2 = 80, N_3 = 120$ ). (a) The time to observe a second mutant for both architectures and a high value of the proliferation probability,  $v = 0.9$ . The mean time for decreasing and increasing architectures is 3.32 and 3.41 respectively ( $p < 0.001$ ). (b) The time to observe a second mutant for both architectures and a small value of the proliferation probability,  $v = 0.1$ . The mean time for decreasing and increasing architectures is 3.73 and 3.51 respectively ( $p < 0.001$ ). (c) The time to observe a second mutant for a decreasing architecture for both small and high  $v$ . We assume  $n = 3, u = 0.001$ .

# Appendix D

## Further notes on tissue architecture, division patterns and fitness

We observe in the stochastic simulations that advantageous and disadvantageous one-hit mutants reached similar numbers when a decreasing architecture was investigated, with disadvantageous mutations accumulating slightly more mutants, specially for high values of  $v$  (figure D.1(b)). This is similar to what we observed when we use the ODE approximation for large systems, see figure 3.1. For small  $v$ , all types of mutations reached identical numbers (figure D.1(a)). Clearly, a decreasing architecture accumulates less mutants than an increasing architecture, similar to what was observed for the ODE approximation (figure 3.1).

For second-hit mutants, increasing architecture did better delaying the time for second-hit mutant compared to either constant or decreasing architecture for short chains of differentiation (high values of  $v$ ). In figure D.2 we compare increasing and constant architectures. We find that for small values of  $v$  (panels c and d), constant is better than increasing architecture for both advantageous and disadvantageous mu-

Appendix D. Further notes on tissue architecture, division patterns and fitness

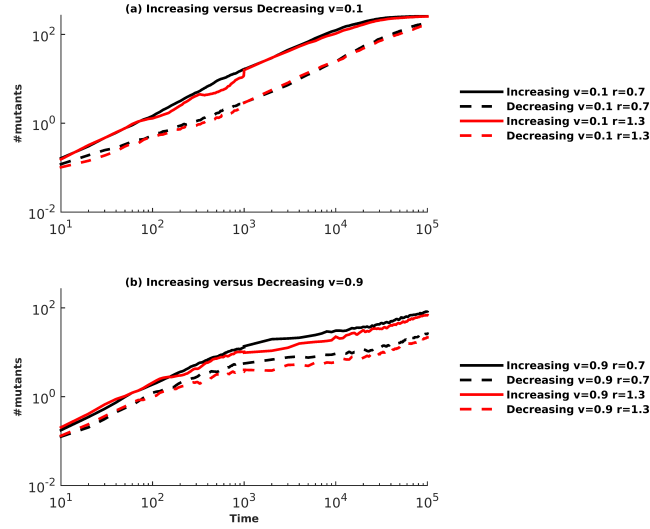


Figure D.1: The mean of the total number of mutants that occur in increasing versus decreasing architectures for different fitness values, based on 1000 stochastic simulations. (a) Increasing architecture ( $N_0 = 20, N_1 = 40, N_2 = 80, N_3 = 120$ , solid lines) versus decreasing architecture ( $N_0 = 120, N_1 = 80, N_2 = 40, N_3 = 20$ , dashed lines), for small values of  $v$  and 2 values of the fitness parameter  $r$ . (b) Same as in (a) but for a high value of  $v$ . The mutation rate is  $u = 10^{-3}$  and  $n = 3$ .

tants. For advantageous mutants, the mean times to a two-hit mutant for constant and increasing architectures are 3.6798 and 3.5929, respectively, and for deleterious mutants, the mean times for constant and increasing architectures are 3.6945 and 3.5948, respectively. For both panels, figure D.2(c,d), the  $p$ -value is less than 0.05, which means that there is a significant difference in the mean times to observe a second-hit mutant. Conversely, for high values of  $v$ , increasing architecture is better than constant architecture only for advantageous mutations (figure D.2(a): the mean times to a two-hit mutant for constant and increasing architectures are 3.3690 and 3.3953, respectively). For disadvantageous mutants there is no significant difference, (figure D.2(b),  $p = 0.9235$ ).

Appendix D. Further notes on tissue architecture, division patterns and fitness

A similar result was observed when we compared increasing and decreasing architectures. In this scenario, increasing was better than decreasing only for high values of  $v$  for both advantageous and disadvantageous mutants (figure D.3). High values of  $v$  can lead to hyperproliferation of cells, which can be a dangerous scenario. In this context, an increasing architecture does a better job delaying the time to a second mutation for high values of  $v$  and advantageous mutations. This can be interpreted as an optimal evolutionary strategy to minimize cancer risk when differentiation is lost.

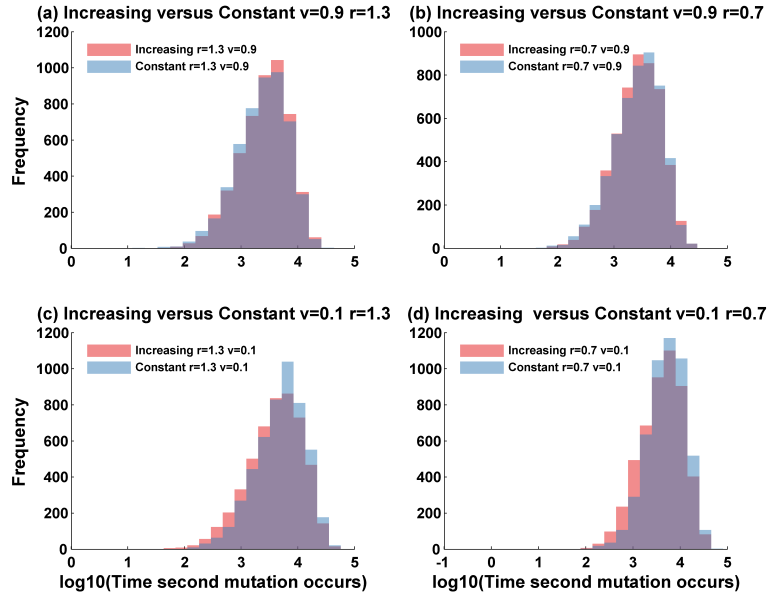


Figure D.2: Comparing increasing and constant architectures for advantageous and disadvantageous mutants. Distribution of the time to observe a second mutation from 5000 stochastic simulations. (a) and (b) Comparing increasing and constant architectures for high  $v$  and advantageous and disadvantageous mutants, respectively. (c) and (d) Comparing increasing and constant architectures for small  $v$  and advantageous and disadvantageous mutants, respectively. For constant architecture, the compartment sizes are  $N_0 = 65, N_1 = 65, N_2 = 65, N_3 = 65$  and for increasing architecture,  $N_0 = 20, N_1 = 40, N_2 = 80, N_3 = 120$ . The mutation rate is  $u = 10^{-3}$  and  $n = 3$ .

Appendix D. Further notes on tissue architecture, division patterns and fitness

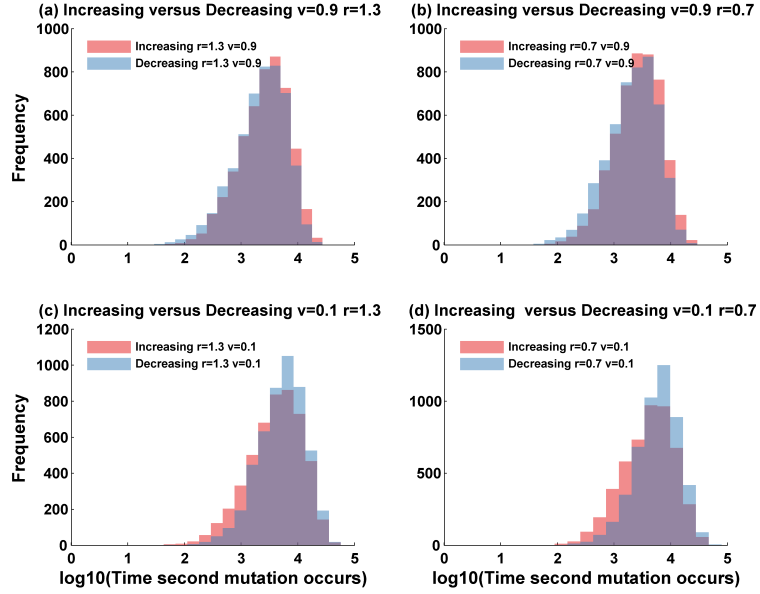


Figure D.3: Comparing increasing and decreasing architectures for advantageous and disadvantageous mutants. Distribution of the time to observe a second mutation from 5000 stochastic simulations. (a) and (b) Comparing increasing and decreasing architectures for high  $v$  and advantageous and disadvantageous mutants, respectively. (c) and (d) Comparing increasing and decreasing architectures for small  $v$  and advantageous and disadvantageous mutants, respectively. For decreasing architecture, compartment sizes are  $N_0 = 120, N_1 = 80, N_2 = 40, N_3 = 20$  and for increasing architecture,  $N_0 = 20, N_1 = 40, N_2 = 80, N_3 = 120$ . The mutation rate is  $u = 10^{-3}$  and  $n = 3$ .

# Appendix E

## Equilibria and stability for the immune response model

The Jacobian of system (4.1) is given by

$$J = \begin{pmatrix} r - \frac{2rC}{k} - \gamma T & 0 & 0 & -\gamma C \\ -\alpha A & -\alpha C - \delta_1 & 0 & 0 \\ \alpha A & \alpha C & -\delta_2 & 0 \\ \frac{-psb_1\beta DT^2}{(b_1\beta TC + b_2sTD + n)^2} & 0 & \frac{psT(b_1\beta TC + n)}{(b_1\beta TC + b_2sTD + n)^2} & \frac{psnD}{(b_1\beta TC + b_2sTD + n)^2} - u \end{pmatrix} \quad (\text{E.1})$$

One of the equilibrium values obtained by setting system (4.1) equal to zero corresponds to immunity,  $(C, A, D, T) = (0, \frac{\lambda}{\delta_1}, 0, 0)$ . If we plug these values into equation (E.1), we obtain

$$J(0, \frac{\lambda}{\delta_1}, 0, 0) = \begin{pmatrix} r & 0 & 0 & 0 \\ -\alpha \frac{\lambda}{\delta_1} & -\delta_1 & 0 & 0 \\ \alpha \frac{\lambda}{\delta_1} & 0 & -\delta_2 & 0 \\ 0 & 0 & 0 & -u \end{pmatrix}. \quad (\text{E.2})$$

The eigenvalues of this matrix are the diagonal entries, therefore, the equilibrium value corresponding to immunity is unstable if  $r > 0$ .



Appendix E. Equilibria and stability for the immune response model

The equilibrium value corresponding to saturation of tumor cells is given by

$$(C, A, D, T) = \left(k, \frac{\lambda}{\alpha k + \delta_1}, \frac{\alpha k}{\delta_2} \frac{\lambda}{\alpha k + \delta_1}, 0\right).$$

If we plug these values into equation (E.1), we get

$$J\left(k, \frac{\lambda}{\alpha k + \delta_1}, \frac{\alpha k}{\delta_2} \frac{\lambda}{\alpha k + \delta_1}, 0\right) = \begin{pmatrix} -r & 0 & 0 & -\gamma k \\ -\alpha \frac{\lambda}{\alpha k + \delta_1} & -\alpha k - \delta_1 & 0 & 0 \\ \alpha \frac{\lambda}{\alpha k + \delta_1} & \alpha k & -\delta_2 & 0 \\ 0 & 0 & 0 & \frac{ps}{n} \frac{\alpha k}{\delta_2} \frac{\lambda}{\alpha k + \delta_1} - u \end{pmatrix} \quad (\text{E.3})$$

The eigenvalues of this matrix are all negative except for the eigenvalue

$$e = \frac{ps}{n} \frac{\alpha k}{\delta_2} \frac{\lambda}{\alpha k + \delta_1} - u,$$

which is negative if

$$D = \frac{\alpha k}{\delta_2} \frac{\lambda}{\alpha k + \delta_1} < \frac{un}{ps}.$$

This is the stability condition for the equilibrium point where tumor cells reach saturation.

The other equilibrium values are given by

$$A = \frac{\lambda}{\alpha C + \delta_1}, D = \frac{\alpha \lambda C}{\delta_2(\alpha C + \delta_1)}, T = \frac{r}{\gamma} \left(1 - \frac{C}{k}\right),$$

where  $C$  is a solution of the equation

$$f(C) = \frac{ub_1\beta r\alpha}{\gamma k} C^3 + \left(\frac{ub_2sr\alpha\lambda}{\gamma\delta_2 k} - \frac{ub_1\beta r}{\gamma} \left(\alpha - \frac{\delta_1}{k}\right)\right) C^2 + \left(\frac{ps\alpha\gamma}{\delta_2} - \frac{ub_1\beta r\delta_1}{\gamma} - \frac{ub_2r\alpha\lambda}{\gamma\delta_2} - un\alpha\right) C - un\delta_1 = 0. \quad (\text{E.4})$$

This is a cubic equation as a function of  $C$  and solutions are obtained numerically. The function  $f(C)$  must always have at least one real positive solution because  $f(0) < 0$  and  $f \rightarrow +\infty$  as  $C \rightarrow \infty$  (the coefficient of  $C^3$  is positive for all positive values of the parameters). The solution could be larger than  $k$ , in which case,  $T$  would be negative, which is not biologically relevant. It is also straightforward to obtain conditions that guarantee the

*Appendix E. Equilibria and stability for the immune response model*

existence of a single real positive solution by inspecting the curvature of  $f$ . In general, if  $f''(C) > 0$  for all  $C \geq 0$ , a single positive-valued solution always exists.

We find that

$$f''(C) = \frac{6ub_1\beta r\alpha}{\gamma k}C + 2\left(\frac{ub_2sr\alpha\lambda}{\gamma\delta_2k} - \frac{ub_1\beta r}{\gamma}\left(\alpha - \frac{\delta_1}{k}\right)\right) \quad (\text{E.5})$$

Given that the first term in equation E.5 is always positive or zero when  $C \geq 0$ , one condition that guarantees the existence of a single real positive solution occurs when the constant term is greater than zero, which implies that

$$sb_2\alpha\lambda - b_1\beta k\alpha\delta_2 + b_1\beta\delta_1\delta_2 > 0. \quad (\text{E.6})$$

# References

- [1] Komarova NL. Spatial interactions and cooperation can change the speed of evolution of complex phenotypes. *Proceedings of the National Academy of Sciences*. 2014;111:10789–10795. doi:10.1073/pnas.1400828111.
- [2] Komarova NL, Cheng P. Epithelial tissue architecture protects against cancer. *Mathematical Biosciences*. 2006;200(1):90–117. doi:10.1016/j.mbs.2005.12.001.
- [3] Dingli D, Traulsen A, Michor F. (A)symmetric stem cell replication and cancer. *PLoS Computational Biology*. 2007;3(3):0482–0487. doi:10.1371/journal.pcbi.0030053.
- [4] Komarova NL. Principles of Regulation of Self-Renewing Cell Lineages. *PLoS ONE*. 2013;8(9):1–12. doi:10.1371/journal.pone.0072847.
- [5] Zhao R, Michor F. Patterns of Proliferative Activity in the Colonic Crypt Determine Crypt Stability and Rates of Somatic Evolution. *PLoS Computational Biology*. 2013;9(6):1–15. doi:10.1371/journal.pcbi.1003082.
- [6] Rodriguez-Brenes IA, Wodarz D, Komarova NL. Minimizing the risk of cancer: tissue architecture and cellular replication limits. *Journal of the Royal Society*. 2013;10(86):1–12. doi:10.1098/rsif.2013.0410.
- [7] Shahriyari L, Komarova NL. Symmetric vs. asymmetric stem cell divisions: an adaptation against cancer? *PLoS One*. 2013;8(10):1–16. doi:10.1371/journal.pone.0076195.
- [8] Shahriyari L, Komarova NL, Jilkine A. The role of cell location and spatial gra-

## REFERENCES

- dients in the evolutionary dynamics of colon and intestinal crypts. *Biology Direct*. 2016;11(42):1–17. doi:10.1186/s13062-016-0141-6.
- [9] Nowak MA, Michor F, Iwasa Y. The linear process of somatic evolution. *Proceedings of the National Academy of Sciences*. 2003;100(25):14966–14969.
- [10] Michor F, Iwasa Y, Nowak MA. Dynamics of cancer progression. *Nature Reviews Cancer*. 2004;4:197–205. doi:10.1038/nrc1295.
- [11] Komarova NL. Cancer, aging and the optimal tissue design. *Seminars in Cancer Biology*. 2005;15(6):494–505. doi:10.1016/j.semcancer.2005.07.003.
- [12] Dingli D, Traulsen A, Pacheco JM. Compartmental architecture and dynamics of hematopoiesis. *PLoS One*. 2007;(4):2–5. doi:10.1371/journal.pone.0000345.
- [13] Werner B, Dingli D, Traulsen A. A deterministic model for the occurrence and dynamics of multiple mutations in hierarchically organized tissues. *Journal of the Royal Society*. 2013;10:1–9.
- [14] Reya T, Morrison SJ, Clarke MF, Weissman IL. Stem cells, cancer, and cancer stem cells. *Nature*. 2001;414:105–111.
- [15] Barker N, van Es JH, Kuipers J, Kujala P, van den Born M, Cozijnsen M, et al. Identification of stem cells in small intestine and colon by marker gene *Lgr5*. *Nature*. 2007;449:1003–1007. doi:10.1038/nature06196.
- [16] Sangiorgi E, Capecchi M. *Bmi1* is expressed in vivo in intestinal stem cells. *Nature Genetics*. 2010;40(7):915–920. doi:10.1038/ng.165.*Bmi1*.
- [17] Wright NA. Epithelial stem cell repertoire in the gut: clues to the origin of cell lineages, proliferative units and cancer. *Journal of Experimental Pathology*. 2000;181:117–143.
- [18] Brittan M, Wright NA. Stem cell in gastrointestinal structure and neoplastic development. *Gut*. 2004;53:899–910. doi:10.1136/gut.2003.025478.

## REFERENCES

- [19] Werner B, Dingli D, Lenaerts T, Pacheco JM, Traulsen A. Dynamics of mutant cells in hierarchical organized tissues. *PLoS Computational Biology*. 2011;7(12):1–9. doi:10.1371/journal.pcbi.1002290.
- [20] Komarova NL, Wang L. Initiation of colorectal cancer: Where do the two hits hit? *Cell Cycle*. 2004;3(12):1558–1565. doi:10.4161/cc.3.12.1186.
- [21] Dunn SJ, Appleton PL, Nelson SA, Näthke IS, Gavaghan DJ, Osborne JM. A two-dimensional model of the colonic crypt accounting for the role of the basement membrane and pericryptal fibroblast sheath. *PLoS Computational Biology*. 2012;8(5):1–20. doi:10.1371/journal.pcbi.1002515.
- [22] Buske P, Galle J, Barker N, Aust G, Clevers H, Loeffler M. A comprehensive model of the spatio-temporal stem cell and tissue organisation in the intestinal crypt. *PLoS Computational Biology*. 2011;7(1):1–13. doi:10.1371/journal.pcbi.1001045.
- [23] van der Wath RC, Gardiner BS, Burgess AW, Smith DW. Cell Organisation in the colonic crypt: a theoretical comparison of the pedigree and niche concepts. *PLoS ONE*. 2013;8(9):1–15. doi:10.1371/journal.pone.0073204.
- [24] Bravo R, Axelrod DE. A calibrated agent-based computer model of stochastic cell dynamics in normal human colon crypts useful for in silico experiments. *Theoretical biology and medical modelling*. 2013;10(66):1–24. doi:10.1186/1742-4682-10-66.
- [25] Traulsen A, Lenaerts T, Pacheco JM, Dingli D. On the dynamics of neutral mutations in a mathematical model for a homogeneous stem cell population. *Journal of the Royal Society*. 2012;10:1–8. doi:10.1098/rsif.2012.0810.
- [26] Pepper JW, Sprouffske K, Maley CC. Animal Cell Differentiation Patterns Suppress Somatic Evolution. *PLoS Computational Biology*. 2007;3(12):2532–2545. doi:10.1371/journal.pcbi.0030250.
- [27] Sprouffske K, Aktipis CA, Radich JP, Carroll M, Nedelcu AM, Maley CC. An evolutionary explanation for the presence of cancer nonstem cells in neoplasms. *Evolutionary Applications*. 2012;6:92–101. doi:10.1111/eva.12030.

## REFERENCES

- [28] Lopez-Garcia C, Klein AM, Simons BD, Winton D. Intestinal stem cell replacement follows a pattern of neutral drift. *Science*. 2010;330:822–825. doi:10.1126/science.1196236.
- [29] Snippert HJ, Van Der Flier LG, Sato T, Van Es JH, Van Den Born M, Kroon-Veenboer C, et al. Intestinal crypt homeostasis results from neutral competition between symmetrically dividing Lgr5 stem cells. *Cell*. 2010;143(1):134–144.
- [30] Simons BD, Clevers H. Strategies for homeostatic stem cell self-renewal in adult tissues. *Cell*. 2011;145(6):851–862.
- [31] Klein AM, Simons BD. Universal patterns of stem cell fate in cycling adult tissues. *Development*. 2011;138(15):3103–3111.
- [32] Rodriguez-Brenes IA, Komarova NL, Wodarz D. Cancer-associated mutations in healthy individuals: assessing the risk of carcinogenesis. *Cancer Research*. 2014;74(6):1661–1669. doi:10.1158/0008-5472.CAN-13-1452.
- [33] Merritt AJ, Potten CS, Watson AJ, Loh DY, Nakayama Ki, Nakayama K, et al. Differential expression of bcl-2 in intestinal epithelia. Correlation with attenuation of apoptosis in colonic crypts and the incidence of colonic neoplasia. *Journal of Cell Science*. 1995;108:2261–2271.
- [34] Potten CS, Kellett M, Rew D, Roberts SA. Proliferation in human gastrointestinal epithelium using bromodeoxyuridine in vivo: data for different sites, proximity to a tumour, and polyposis coli. *Gut*. 1992;33(4):524–529.
- [35] Murray NR, Davidson LA, Chapkin RS, Gustafson WC, Schattenberg DG, Fields AP. Overexpression of protein kinase C  $\beta$ II induces colonic hyperproliferation and increased sensitivity to colon carcinogenesis. *Journal of Cell Biology*. 1999;145(4):699–711.
- [36] Pabst T, Mueller BU, Harakawa N, Schoch C, Haferlach T, Behre G, et al. AML1 ETO downregulates the granulocytic differentiation factor C/EBP  $\alpha$  in t (8;21) myeloid leukemia. *Nature Medicine*. 2001;7(4):444–451.

## REFERENCES

- [37] Pabst T, Mueller BU, Zhang P, Radomska HS, Narravula S, Behre G, et al. Dominant-negative mutations of CEBPA, encoding CCAAT/enhancer binding protein- $\alpha$  (C/EBP  $\alpha$ ), in acute myeloid leukemia. *Nature Genetics*. 2001;27:263–270.
- [38] Pabst T, Mueller BU. Complexity of CEBPA dysregulation in human acute myeloid leukemia. *Clinical Cancer Research*. 2009;15(17):5303–5307. doi:10.1158/1078-0432.CCR-08-2941.
- [39] Van Der Flier L, Clevers H. Stem cells, self-Renewal, and differentiation in the intestinal epithelium. *Annual Review of Physiology*. 2009;71:241–260. doi:10.1146/annurev.physiol.010908.163145.
- [40] Tenen DG. Disruption of differentiation in human cancer: AML shows the way. *Nature Reviews Cancer*. 2003;3:89–101. doi:10.1038/nrc989.
- [41] Koivunen P, Lee S, Duncan CG, Lopez G, Lu G, Ramkissoon S, et al. Transformation by the (R)-enantiomer of 2-hydroxyglutarate linked to EGLN activation. *Nature*. 2012;483:484–488. doi:10.1038/nature10898.
- [42] Turcan S, Rohle D, Goenka A, Walsh LA, Fang F, Yilmaz E, et al. IDH1 mutation is sufficient to establish the glioma hypermethylator phenotype. *Nature*. 2012;483:479–483. doi:10.1038/nature10866.
- [43] Lu C, Ward PS, Kapoor GS, Rohle D, Turcan S, Abdel-wahab O, et al. IDH mutation impairs histone demethylation and results in a block to cell differentiation. *Nature*. 2012;483:474–478. doi:10.1038/nature10860.
- [44] Michor F, Iwasa Y, Rajagopalan H, Lengauer C, Nowak MA. Linear model of colon cancer initiation. *Cell cycle*. 2004;3(3):356–360.
- [45] Levins R. Some demographic and genetic consequences of environmental heterogeneity for biological control. *Bulletin of the Entomological Society of America*. 1969;15(3):237–240.

## REFERENCES

- [46] Hanski I. Single-species metapopulation dynamics: concepts, models and observations. *Biological Journal of the Linnean Society*. 1991;42(1-2):17–38.
- [47] Hanski I. *Metapopulation ecology*. Oxford University Press; 1999.
- [48] Gilpin M. *Metapopulation dynamics: empirical and theoretical investigations*. Academic Press; 2012.
- [49] Wodarz D, Sun Z, Lau JW, Komarova NL. Nearest-neighbor interactions, habitat fragmentation, and the persistence of host-pathogen systems. *The American Naturalist*. 2013;182(3):E94–E111.
- [50] Komarova NL, Shahriyari L, Wodarz D. Complex role of space in the crossing of fitness valleys by asexual populations. *Journal of The Royal Society Interface*. 2014;11(95):20140014.
- [51] Komarova NL, Cheng P. Epithelial tissue architecture protects against cancer. *Mathematical biosciences*. 2006;200(1):90–117.
- [52] Huffman KE, Levene SD, Tesmer VM, Shay JW, Wright WE. Telomere shortening is proportional to the size of the G-rich telomeric 3-overhang. *The Journal of Biological Chemistry*. 2000;275(26):19719–19722. doi:10.1074/jbc.M002843200.
- [53] Bozic I, Nowak MA. Unwanted evolution. *Science*. 2013;342(6161):938–939. doi:10.1126/science.1247887.
- [54] Lieberman E, Hauert C, Nowak MA. Evolutionary dynamics on graphs. *Nature*. 2005;433:312–316. doi:10.1038/nature03211.1.
- [55] Hindersin L, Werner B, Dingli D, Traulsen A. Should tissue structure suppress or amplify selection to minimize cancer risk? *Biology Direct*. 2016;11(41):1–11. doi:10.1186/s13062-016-0140-7.
- [56] Casas-Selves M, DeGregory J. How cancer shapes evolution, and how evolution shapes cancer. *Evolution*. 2013;4(4):624–634. doi:10.1007/s12052-011-0373-y.



## REFERENCES

- [57] Henry CJ, Marusyk A, Zaberezhnyy V, Adane B, Degregori J. Declining lymphoid progenitor fitness promotes aging-associated leukemogenesis. *Proceedings of the National Academy of Sciences*. 2010;107(50):21713–21718. doi:10.1073/pnas.1005486107.
- [58] Marusyk A, Degregori J. Declining cellular fitness with age promotes cancer initiation by selecting for adaptive oncogenic mutations. *Biochimica et Biophysica Acta*. 2007;1785:1–11. doi:10.1016/j.bbcan.2007.09.001.
- [59] Degregori J. Evolved tumor suppression: Why are we so good at not getting cancer? *Cancer Research*. 2011;71(11):3739–3744. doi:10.1158/0008-5472.CAN-11-0342.
- [60] Janeway C, P T, Walport M, Schlomchik MJ. *Immunobiology: the immune system in health and disease*. Garland Science, New York; 2005.
- [61] Greenwald RJ, Freeman GJ, Sharpe AH. The B7 Family Revisited. *Annual Review of Immunology*. 2005;23(1):515–548. doi:10.1146/annurev.immunol.23.021704.115611.
- [62] Foell J, Hewes B, Mittler RS. T cell costimulatory and inhibitory receptors as therapeutic targets for inducing anti-tumor immunity. *Current Cancer Drug Targets*. 2007;7:55–70.
- [63] Driessens G, Kline J, Gajewski T. Costimulatory and coinhibitory receptors in anti-tumor immunity. *Immunology Reviews*. 2009;229(1):126–144. doi:10.1111/j.1600-065X.2009.00771.x.
- [64] Pardoll DM. The blockade of immune checkpoints in cancer immunotherapy. *Nature Reviews Cancer*. 2012;12:252–264. doi:10.1038/nrc3239.
- [65] Postow MA, Callahan MK, Wolchok JD. Immune checkpoint blockade in cancer therapy. *Journal of Clinical Oncology*. 2015;33(17):1–10. doi:10.1200/JCO.2014.59.4358.
- [66] Littman DR. Releasing the brakes on cancer immunotherapy. *Cell*. 2015;162(6):1186–1190. doi:10.1016/j.cell.2015.08.038.

## REFERENCES

- [67] Yang JC, Hughes M, Kammula U, Royal R, Sherry RM, Topalian SL, et al. Ipilimumab (anti-CTLA4 antibody) causes regression of metastatic renal cell cancer associated with enteritis and hypophysitis. *Journal of Immunotherapy*. 2007;30(8):825–830.
- [68] Hodi FS, Butler M, Oble Da, Seiden MV, Haluska FG, Kruse A, et al. Immunologic and clinical effects of antibody blockade of cytotoxic T lymphocyte-associated antigen 4 in previously vaccinated cancer patients. *Proceedings of the National Academy of Sciences*. 2008;105(8):3005–3010. doi:10.1073/pnas.0712237105.
- [69] Carthon BC, Wolchok JD, Yuan J, Kamat A, Tang DS, Sun J, et al. Preoperative CTLA-4 blockade: tolerability and immune monitoring in the setting of a presurgical clinical trial. *Clinical Cancer Research*. 2010;16(10):2861–2871. doi:10.1158/1078-0432.CCR-10-0569.
- [70] Hodi FS, O’Day SJ, McDermott DF, Weber RW, Sosman JA, Haanen JB, et al. Improved survival with ipilimumab in patients with metastatic melanoma. *The New England Journal of Medicine*. 2010;363(8):711–723.
- [71] van den Eertwegh A, Versluis J, van den Berg P, Santegoets SJ, Van Moorselaar J, Van der Sluis T, et al. Combined immunotherapy with granulocyte-macrophage colony-stimulating factor-transduced allogeneic prostate cancer cells and ipilimumab in patients with metastatic castration-resistant prostate cancer: a phase 1 dose-escalation trial. *The Lancet Oncology*. 2012;13(5):509–517. doi:10.1016/S1470-2045(12)70007-4.
- [72] Robert C, Thomas L, Bondarenko I, O’Day S, Weber J, Garbe C, et al. Ipilimumab plus dacarbazine for previously untreated metastatic melanoma. *The New England Journal of Medicine*. 2011;364(26):2517–2526. doi:10.1056/NEJMoa1104621.
- [73] Kwon ED, Drake CG, Scher HI, Fizazi K, Bossi A, Van den Eertwegh AJM, et al. Ipilimumab versus placebo after radiotherapy in patients with metastatic castration-resistant prostate cancer that had progressed after docetaxel chemotherapy (CA184-

## REFERENCES

- 043): a multicentre, randomised, double-blind, phase 3 trial. *The Lancet Oncology*. 2014;15(7):700–712. doi:10.1016/S1470-2045(14)70189-5.
- [74] Brahmer J, Tykodi S, Chow L, Hwu W, Topalian S, Hwu P, et al. Safety and activity of anti-PD-L1 antibody in patients with advanced cancer. *New England Journal of Medicine*. 2012;366(26):2455–2465. doi:10.1016/j.juro.2012.08.169.
- [75] Topalian S, Hodi S, Brahmer J, Gettinger S, Smith DC, Powderly JD, et al. Safety, activity, and immune correlates of anti-PD-1 antibody in cancer. *The New England Journal of Medicine*. 2012;366(26):2443–2454.
- [76] Powles T, Eder JP, Fine GD, Braiteh FS, Loriot Y, Cruz C, et al. MPDL3280A (anti-PD-L1) treatment leads to clinical activity in metastatic bladder cancer. *Nature*. 2014;515:558–562. doi:10.1038/nature13904.
- [77] Ansell SM, Lesokhin AM, Borrello I, Halwani A, Scott EC, Gutierrez M, et al. PD-1 Blockade with nivolumab in relapsed or refractory hodgkin’s lymphoma. *The New England Journal of Medicine*. 2015;372(4):311–319. doi:10.1056/NEJMoa1411087.
- [78] Robert C, Long GV, Brady B, Dutriaux C, Maio M, Mortier L, et al. Nivolumab in previously untreated melanoma without BRAF mutation. *The New England Journal of Medicine*. 2015;372(4):320–30. doi:10.1056/NEJMoa1412082.
- [79] Triebel F, Jitsukawa S, Baixeras E, Roman-Roman S, Genevee C, Viegas-Pequignot E, et al. LAG-3, a novel lymphocyte activation gene closely related to CD4. *The Journal of Experimental Medicine*. 1990;171:1393–1405.
- [80] Wang L, Rubinstein R, Lines JL, Wasiuk A, Ahonen C, Guo Y, et al. VISTA, a novel mouse Ig superfamily ligand that negatively regulates T cell responses. *The Journal of Experimental Medicine*. 2011;208(3):577–92. doi:10.1084/jem.20100619.
- [81] Sakuishi K, Apetoh L, Sullivan JM, Blazar BR, Kuchroo VK, Anderson AC. Targeting Tim-3 and PD-1 pathways to reverse T cell exhaustion and restore anti-tumor immunity. *The Journal of Experimental Medicine*. 2010;207(10):2187–2194. doi:10.1084/jem.20100643.

## REFERENCES

- [82] Linsley PS, Brady W, Urnes M, Grosmaire LS, Damle NK, Ledbetter JA. CTLA-4 is a second receptor for the B cell activation antigen B7. *Journal of Experimental Medicine*. 1991;174:561–569.
- [83] Krummel MF, Allison JP. CD28 and CTLA-4 have opposing effects on the response of T cells to stimulation. *Journal of Experimental Medicine*. 1995;182:329–375. doi:10.1210/me.2014-1154.
- [84] Krummel MF, Allison JP. CTLA-4 engagement inhibits IL-2 accumulation and cell cycle progression upon activation of resting T cells. *Journal of Experimental Medicine*. 1996;183:2533–2540.
- [85] Riley JL, Mao M, Kobayashi S, Biery M, Burchard J, Cavet G, et al. Modulation of TCR-induced transcriptional profiles by ligation of CD28, ICOS, and CTLA-4 receptors. *Proceedings of the National Academy of Sciences*. 2002;99(18):11790–11795.
- [86] Qureshi OS, Zheng Y, Nakamura K, Attridge K, Manzotti C, Schmidt EM, et al. Trans-endocytosis of CD80 and CD86: a molecular basis for the cell extrinsic function of CTLA-4. *Science*. 2011;332(6029):600–603. doi:10.1126/science.1202947.
- [87] Walunas TL, Lenschow DJ, Christina Y, Linsley PS, Freeman GJ, Jonathan M, et al. CTLA-4 can function as a negative regulator of T cell activation . *The Journal of Immunology*. 2013;1:405–413.
- [88] Freeman GJ, Long A, Iwai Y, Bourque K, Chernova T, Nishimura H, et al. Engagement of the PD-1 immunoinhibitory receptor by a novel B7 family member leads to negative regulation of lymphocyte activation. *The Journal of Experimental Medicine*. 2000;192(7):1027–1034. doi:10.1084/jem.192.7.1027.
- [89] Ishida Y, Agata Y, Shibahara K, Honjo T. Induced expression of PD-1, a novel member of the immunoglobulin gene superfamily, upon programmed cell death. *The EMBO Journal*. 1992;11(11):3887–3895.

## REFERENCES

- [90] Keir ME, Liang SC, Guleria I, Latchman YE, Qipo A, Albacker LA, et al. Tissue expression of PD-L1 mediates peripheral T cell tolerance. *Journal of Experimental Medicine*. 2006;203(4):883–895. doi:10.1084/jem.20051776.
- [91] Baumeister SH, Freeman GJ, Dranoff G, Sharpe AH. Coinhibitory pathways in immunotherapy for cancer. *Annual Review of Immunology*. 2016;34:539–573. doi:10.1146/annurev-immunol-032414-112049.
- [92] Wodarz D, Jansen V. A dynamical perspective of CTL cross-priming and regulation: implications for cancer immunology. *Immunology Letters*. 2003;86(3):213–227. doi:10.1016/S0165-2478(03)00023-3.
- [93] dePillis L, Gallegos A, Radunskaya A. A model of dendritic cell therapy for melanoma. *Frontiers in oncology*. 2013;3(56):1–14. doi:10.3389/fonc.2013.00056.
- [94] dePillis L, Eladdadi A, Radunskaya A. Modeling cancer-immune responses to therapy. *Journal of Pharmacokinetics and Pharmacodynamics*. 2014;41(5):461–478. doi:10.1007/s10928-014-9386-9.
- [95] Castillo-Montiel E, Chimal-Eguía JC, Tello JI, Piñon-Zaráte G, Herrera-Enríquez M, Castell-Rodríguez AE. Enhancing dendritic cell immunotherapy for melanoma using a simple mathematical model. *Theoretical biology and medical modelling*. 2015;12(11):1–14. doi:10.1186/s12976-015-0007-0.
- [96] Nestle FO. Dendritic cell vaccination for cancer therapy. *Oncogene*. 2000;19(56):6673–6679.
- [97] Palucka K, Banchereau J. Cancer immunotherapy via dendritic cells. *Nature Reviews Cancer*. 2012;12:265–277. doi:10.1038/nrc3258.
- [98] Sharma P, Allison JP. Immune checkpoint targeting in cancer therapy: toward combination strategies with curative potential. *Cell*. 2015;161(2):205–214. doi:10.1016/j.cell.2015.03.030.

## REFERENCES

- [99] Ludewig B, Krebs P, Junt T, Metters H, Ford NJ, Anderson RM, et al. Determining control parameters for dendritic cell-cytotoxic T lymphocyte interaction. *European Journal of Immunology*. 2004;43:2407–2418. doi:10.1002/eji.200425085.
- [100] dePillis L, Gu W, Radunskaya A. Mixed immunotherapy and chemotherapy of tumors: modeling, applications and biological interpretations. *Journal of Theoretical Biology*. 2006;238:841–862. doi:10.1016/j.jtbi.2005.06.037.
- [101] Ward RC, Kaufman HL. Targeting costimulatory pathways for tumor immunotherapy. *International Reviews of Immunology*. 2007;26:161–196. doi:10.1080/08830180701365941.
- [102] Song J, Lei FT, Xiong X, Haque R. Intracellular signals of T cell costimulation. *Cellular and Molecular Immunology*. 2008;5(4):239–247.
- [103] Capece D, Verzella D, Fischietti M, Zazzeroni F, Alesse E. Targeting costimulatory molecules to improve antitumor immunity. *Journal of Biomedicine and Biotechnology*. 2012;2012:1–17. doi:10.1155/2012/926321.
- [104] van de Ven K, Borst J. Targeting the T-cell co-stimulatory CD27/CD70 pathway in cancer immunotherapy: rationale and potential. *Immunotherapy*. 2015;7(6):655–667.
- [105] Chung KY, Gore I, Fong L, Venook A, Beck SB, Dorazio P, et al. Phase II study of the anti-cytotoxic T-Lymphocyte associated antigen 4 monoclonal antibody, tremelimumab, in patients with refractory metastatic colorectal cancer. *Journal of Clinical Oncology*. 2010;28(21):3485–3490. doi:10.1200/JCO.2010.28.3994.
- [106] Calabrò L, Morra A, Fonsatti E, Cutaia O, Amato G, Giannarelli D, et al. Tremelimumab for patients with chemotherapy-resistant advanced malignant mesothelioma: an open-label, single-arm, phase 2 trial. *Lancet Oncology*. 2013;14:1004–1011. doi:10.1016/S1470-2045(13)70381-4.
- [107] Sangro B, Gomez-Martin C, Mata MD, Iñarrairaegui M, Garralda E, Barrera P, et al. A clinical trial of CTLA-4 blockade with tremelimumab in patients with hepa-

## REFERENCES

- tocellular carcinoma and chronic hepatitis C. *Journal of Hepatology*. 2013;59:81–88. doi:10.1016/j.jhep.2013.02.022.
- [108] Robert C, Long GV, Brady B, Dutriaux C, Maio M, Mortier L, et al. Nivolumab in previously untreated melanoma without BRAF mutation. *The New England Journal of Medicine*. 2015;372(4):320–30. doi:10.1056/NEJMoa1412082.
- [109] Schadendorf D, Hodi FS, Robert C, Weber JS, Margolin K, Hamid O, et al. Pooled analysis of long-term survival data from phase II and phase III trials of ipilimumab in unresectable or metastatic melanoma. *Journal of Clinical Oncology*. 2015;33(17):1889–1894. doi:10.1200/JCO.2014.56.2736.
- [110] Delyon J, Mateus C, Lefeuvre D, Lanoy E, Zitvogel L, Chaput N, et al. Experience in daily practice with ipilimumab for the treatment of patients with metastatic melanoma: an early increase in lymphocyte and eosinophil counts is associated with improved survival. *Annals of Oncology*. 2013;24(6):1697–1703. doi:10.1093/annonc/mdt027.
- [111] Postow MA, Manuel M, Wong P, Yuan J, Dong Z, Liu C, et al. Peripheral T cell receptor diversity is associated with clinical outcomes following ipilimumab treatment in metastatic melanoma. *Journal for Immunotherapy of Cancer*. 2015;3(23):3–7. doi:10.1186/s40425-015-0070-4.